MICROFLUIDICALLY ENABLED BIOLOGICAL AND PHOTONIC SYSTEMS

A Dissertation

Presented to the Faculty of the Graduate School

of Cornell University

In Partial Fulfillment of the Requirements for the Degree of

Doctor of Philosophy

by

Aram Jongnam Chung

August 2011

MICROFLUIDICALLY ENABLED BIOLOGICAL AND PHOTONIC SYSTEMS

Aram Chung, Ph. D.

Cornell University 2011

The theme of my Ph.D. research is the integration of microscale fluid mechanics with two fields: biology and optics to solve problems at the interface between life and physical sciences. In detail, my graduate work revolves around the use *microfluidics* and focuses on creating "Rapid drug delivery devices for insect biorobots, and Optofluidic reconfigurable photonic systems". The first major thrust of my research has been in the development of a method to directly and reversibly control insect (*Manduca sexta* moth) flight using implanted microfluidics. The idea is to fuse a living system with a rapid drug delivery component which releases chemical stimulants on command to exert control over the level of neuromuscular activity. More recently, I established a novel hybrid control approach for the insect biorobot manipulation that simultaneously employs both electrical and chemical stimulation signals to generate integrated biorobotic systems that can perform an array of flight maneuver operations. Along with working on the insect cyborg projects, my graduate work has expanded into the field of *optofluidics*. I have developed a reconfigurable photonic system which allows me to take advantage of the chemical and physical adaptability of liquid state photonics with the robustness and speed available from traditional solid state photonics. Basically, by combining liquid and planar solid state components on a chip, I was able to establish a novel optical switching platform which is not only tunable and adaptive, but also fast, stable and user-friendly.

BIOGRAPHICAL SKETCH

Aram Chung was born in 1979 in Tuscaloosa, AL and grew up in Cambridge, MA. After spending five years in U.S. Aram moved to Korea and he completed his Bachelor's degree in 2006 from the Department of Mechanical and Aerospace Engineering at Seoul National University (SNU) with Distinction in the Major. During that time, he worked in Digital Automotive Laboratory in SNU, Samsung Electronics, and SK Computer & Communication. Aram then moved back to U.S. for his graduate studies and joined Prof. David Erickson's "Integrated Micro- and Nanofluidic Systems Laboratory" in the Department of Mechanical and Aerospace Engineering at Cornell University. He was awarded a Master of Science in Mechanical Engineering in August 2009, and currently he is a Ph.D. candidate in the same department. His work revolves around the use microfluidics and focuses on creating "Rapid microfluidic drug delivery devices for autonomous microsystems, and Optofluidic reconfigurable photonic systems".

To my lovely wife, Ahra

ACKNOWLEDGMENTS

First of all, I would like to thank Prof. David Erickson, my advisor and mentor, for the guidance and endless support that I have received for last five years. I still clearly remember when I first met Prof. Erickson, having lunch with him. Only with one meeting, I knew I wanted to join his group since I could see he was a pure embodiment of passion and devotion with a great personality. Five years from that one particular lunch, now I can surely say that my decision was so correct. I have received so far and he has been a real role model for me as an advisor and a scientist. I am grateful that I had a chance to spend my graduate span with him that has been one of the most rewarding times in my life.

I would like to acknowledge my committee members: Prof. Abraham D. Stroock and Prof. Ephrahim Garcia. I truly appreciate all of their support and insight throughout my graduate studies. They have provided me invaluable advice on my research and post graduate career planning as well.

I would also like to thank all of the members of the Erickson group members. Especially I would like to thank Bernardo Cordovez, my best non-Korean friend and colleague for always being there for me. I have learned a lot from him especially my first year at Cornell and received so much from him. Thank him again and very best wishes for his start-up company in Philly. I would also like to thank Mekala Krishnan and Yun Suk Huh, both of which are great friends and researchers who have helped me tremendously whenever I was in a dead end in my research. Finally, I would like to thank the people who I worked together particularly Erica Jung, Donn Kim, Toby Huang, Nipun Jasuja, Daniel Lee and Likun Chen for their hard work. Erica in particular was of great support in the Reconfigurable photonics project, and all her inputs were immensely helpful.

I would like to thank my colleagues and friends at Cornell notably Sudeep Mandal, Julie Goddard, Pilgyu Kang, and Sung-Ju Park for your great support. I hopefully will see them in near future wherever we are.

Last but not least, to my family. My mom, I know I never have come to this point without her pray and encouragement. Just her existence always becomes a great strength to me throughout my graduate span. My Dad… Over the course of my entire life, I have been witness to him who has devoted his entire life to being a true scientist. And I truly appreciate that he has instilled in me a lot great values that a good scientist must have. I would also like to thank my sister because I have received tremendously from her, and I hope to see her in Boston or LA soon this fall. I should thank to my two lovely princesses, Hayoon and Gahyoon also. They are indeed my everything and their lovely smiles always make me happy.

Finally to my wife, Ahra. She has sacrificed a lot of her own just for me. I do not have a clue how I should appreciate for her devotion seriously. Ahra, thank you so much. You complete me. I love you more than anything.

TABLE OF CONTENTS

Biographical Sketch iii
Dedication iv
Acknowledgements v
Table of Contents vii
List of Figures viii
List of Tables x
List of Symbols xi
Chapter 1. Introduction 1
Chapter 2. Electrokinetic microfluidic devices for rapid, low power drug delivery in autonomous microsystems 23
Chapter 3. Engineering insect flight metabolics using immature stage implanted microfluidics 50
Chapter 4. A robust, electrochemically driven microwell drug delivery system for controlled vasopressin release 75
Chapter 5. Hybrid techniques for modulating insect flight activity and longevity 93
Chapter 6. Optofluidic waveguides for reconfigurable photonic systems 111
Chapter 7. Conclusions 128

LIST OF FIGURES

Figure 1.1 Schematic view of electrical double layer and electroosmotic flow 7
Figure 1.2 Schematic view of electrophoresis 9
Figure 2.1 Microfluidic Drug Delivery Device Layout 27
Figure 2.2 Schematic Views of the Device Operation and Images of the Devices 30
Figure 2.3 Time Lapse Images Illustrating the Ejection of Fluorescent Particles from an Electroactive Microwell 32
Figure 2.4 Device Characterization Plots for Dispersion Radius and Instantaneous Front Velocity 34
Figure 2.5 Plot of Time Required to Empty the Electroactive Microwell 35
Figure 2.6 Plots of Average Power Load during Ejection Process and Total Energy .. 36
Figure 2.7 Computed Electric Field Lines in Electroactive Microwell 39
Figure 2.8 Finite Element Simulations of the Transport Process 41
Figure 2.9 Finite Element Analysis of Time-Dependent Species Transport 42
Figure 2.10 Comparison of Experimental and Numerical Results 43
Figure 3.1 Images of the Developmental Stages of a M. Sexta Moth, Device Insertion and Successfully Emerged Insect-MAVs 39
Figure 3.2 Microfluidic Device Layout 40
Figure 3.3 Injection Procedure 60
Figure 3.4 Finite Element Simulations of the Transport Process 61
Figure 3.5 Demonstration of Microfluidically Modulated Insect Activity 65
Figure 3.6 Quantification of the Metabolic Rate 68
Figure 4.1 Electrochemical Microfluidic Device Layout 77
Figure 4.2 Device Operation Scheme 80
Figure 4.3 Ejection of Vasopressin with Fluorescent Particles 82
Figure 4.4 Plots of Release Rate of Vasopressin and Concentration Profile 83
Figure 4.5 Power Load during Ejection Process 86
Figure 4.6 Ejection Efficiency 87
Figure 5.1 Combined Electrical and Chemical Modulation of Insect Flight Power and Speed 96
Figure 5.2 Wireless Hybrid System for Manduca Sexta Flight Control 98

Figure 5.3 Wireless Hybrid Flight Operation and Flight Tracking 101
Figure 5.4 Comparison of Mechanical and Electrical Flight Duration Enhancement Techniques 103
Figure 6.1 Schematic Views of Optofluidic Reconfigurable Photonics Systems and Its Experimental Setup 114
Figure 6.2 Optofluidic Tunable Attenuator 116
Figure 6.3 Optofluidic Tunable Attenuator Power Characterization 117
Figure 6.4 Optofluidic Switch 119
Figure 6.5 Output Power vs. Switching Period 120
Figure 6.6 Bandwidth Characterization 121

LIST OF TABLES

Table 2.1 Comparison of Power Consumption of Dosing Systems 37
Table 3.1 Comparison of Survivability Rate Depending on the Implantation Date 58
Table 3.2 List of Chemicals Injected into the Thorax for Immobilization..... 61

LIST OF SYMBOLS

ρ	=	mass density
ρ_E	=	volumetric charge density
$\boldsymbol{v}$	=	flow velocity
η	=	dynamic viscosity
Re	=	Reynolds number
p	=	pressure
$\boldsymbol{E}$	=	electrical field
$\boldsymbol{E_{ext}}$	=	external electrical field
$\boldsymbol{B}$	=	magnetic flux density
$\boldsymbol{D}$	=	electric flux density
$\boldsymbol{H}$	=	magnetic field
$\boldsymbol{J}$	=	current density
c	=	local species concentration
D	=	diffusion coefficient
ϕ	=	electric potential
ε	=	permittivity of the medium
ζ	=	surface (zeta) potential
v_{eo}	=	electroosmotic velocity
μ_{eo}	=	electroosmotic mobility
v_{ep}	=	electrophoretic velocity
μ_{ep}	=	electroophoretic mobility
F	=	flight trust
F_{ref}	=	flight trust before injection of chemical
m	=	mass

θ = displacement angle

$\boldsymbol{F_E}$ = electrophoretic force

e = electron charge

z = ion valence

k_o = free space wave vector

β = transverse wave vector

n_i = refractive index of the medium

CHAPTER 1
INTRODUCTION

1.1 Research Scope

In this research I developed new ways that how microfluidics can be integrated with biology and optics. Through the use of electrokinetically and electrochemically induced flows in small microchannels, I have been able to demonstrate an implantable, low power and rate controllable drug delivery systems for living insects and autonomous microsystems. I have also demonstrated the implementation of liquid-core / liquid-cladding waveguides into a conventional solid-state optics intended use for reconfigurable photonics.

The first contribution from this research is the ability to create an electrokinetic rapid drug delivery system with an energy consumption of as little as 20 mJ. Compared to the diffusion based system, the rapid drug delivery system developed here shows with an improvement on the order of approximately 130-fold. My second contribution is the demonstration of a method of exerting chemical control over insect flight activity and longevity, exploiting the use of immature stage implanted microfluidics to reversibly control the rate of metabolic output. This was the first step towards to create an artificial insect nervous system where the controlled release of inhibitory or excitatory neurotransmitters could be accomplished in response to external stimuli. Third, I developed the electrochemically induced rapid drug delivery system for *in vitro* vasopressin release. Electrolysis based ejection builds up the pressure in the reservoir which then forces the contents out of the well, independent of the external environmental conditions. My fourth contribution is the demonstration of

the integrated microsystem that uses both chemical and electrical methods to modulate the flight activity of *Manduca sexta* moths for the first time. 35-fold improvement (on average 3 hours continuous flight) in flight longevity compared to mechanical stimulation has presented and 50% mean flight power output reduction can be achieved with the proper neurotransmitter dose. Lastly, new approach to reconfigurable photonics which couples the physical adaptability of microfluidic waveguides to fiber-in and fiber-out optical systems has been demonstrated. Two components that could form the basis of a more complex reconfigurable photonic system: a signal attenuator and a 1x2 optical switch have been shown.

In the remainder of this chapter, I present a brief introduction to microfluidics and how it can be adopted into other fields. I will motivate and explain why this field is important and what kind of useful toolbox can be made to answer complex problems especially in the interface between biology and physics. I then present my accomplishments in Chapters 2 through Chapter 6 and conclude my findings for my work in Chapter 7.

1.2 Microfluidics: Motivation

Microfluidics is as it says a field of studying and investigating small scale fluid mechanics whose channel size is smaller than millimeter. Researchers have already investigated how the fluids flow in small channel [1], mix [2] and the fluids and wall interfacial phenomena [3]. With regards to its applications, to date DNA, protein and cellular scale using microfluidic platform, mostly biological studies, have been paid a lot of attentions since fundamental spatial dimensions allow tremendous advantages [4]. For example, small dimension, thus small sensing volume (reduced to the same scale order as that of target [5]) requires extremely little quantities of samples and

analytes to perform biochemical reactions with high detection sensitivity [6]. Ideally, microfluidic platforms fundamentally can provide low cost with short time analyzing systems which are extremely attractive for many of the biological sensing applications [7].

As briefly mentioned above, in the aspect of the biological application one of the main streams of the use of microfluidic devices is to interrogate biological events [8] or reconstitute the biological functions in a centimeter scale lab-on-a-chip devices [9, 10]. For DNA analysis using microfluidic platforms, polymerase chain reaction (PCR), separation [11, 12], hybridization [13, 14], monitor [15] and detection [16, 17] methods have been extensively explored. Protein analysis through microfluidics also have been studied including digestion [18, 19], identification and synthesis [20]. Lastly, in cellular scale, microfluidics also have been integrated to cell handling [21], cytometry [22], manipulation [21] and sorting [23-25]. While such technology is extremely successful and useful, rarely has the extension been made to exerting active control over a living system. The idea is that through microfluidic devices I tried to exert control over the biological system as a whole, yielding a microfluidically enabled biological system (Chap. 2-5). In addition, this idea can be applied to other fields as well and I investigated microfluidics for optical systems that will be discussed below in Chap. 6.

1.3 Microfluidic Applications Enabled Through My Work

1.3.1: Chemical and electrical control over flying bio-robotic systems

Microairvehicles are small unmanned aircrafts with a maximal wingspan of approximately 15 cm and flight speed below 10 m/s [26]. Such systems are of interest

[27] due to their capabilities to remote surveillance [28] and power harvesting [29, 30]. Progress in micro-electro-mechanical-systems (MEMS) [31, 32] technology has enabled further miniaturization and improved control schemes in MAVs. Wood *et al.* [33] reported small flying robots, flapping *Diptera* insects, however the downscaling of traditional air vehicles [34] is still a great challenges. Particularly, through downsizing of the wing size compromises complex vehicle aerodynamics and most importantly the lack of a compact and lightweight high-density power source with a sufficiently long lifetime [34, 35] becomes the most challenging issue.

Recently, in the name of "bio-inspired" engineering, researchers have been trying to overcome the power supplying concerns [36], for instance mimicking the body shapes, wing morphology and flapping motions that are present in nature [37-42]. Bio-inspired MAVs have shown great possibility to solve the power supplying problems through emulating the complexity of nature however it is true that still they cannot outperform natural flyers in the near future. On the other hand, living flyers, for example insects, have evolved perfectly in terms of flight dynamics and power efficiency. In the aspect of the power supplying, many insects feed themselves tremendously a lot during pre-adult stage in the form of caterpillar (pre-adult stage) to store sufficient energy for their adult stage (*i.e. Manduca sexta* moths can live approximately two weeks with no food). There is no doubt that these insect are of the best fliers however it is also reported that they are extremely difficult to be trained to perform useful flight [43].

Rather than depending on pure MAVs or natural flyers, there have been efforts to form insect-MAVS as a revolutionary notion to create MAVs that exceed the flying performance. Basically, the idea is that harnessing the living insects' great flying capabilities and exerting flight control over flying insects through MEMS technologies. Bozkurt *et al.* [44] have reported aerodynamic operations including liftoff, yaw control

and landing and similar operations using *Cotinis texana* beetles were demonstrated by Sato *et al.* [45, 46] but all these works to are based on electrical stimulations.

In this section of my work, I demonstrated a more localized method of exerting control over insect flight using chemical (implanted microfluidics) while taking advantage of electrical (implanted electrodes) control as well. Microfluidic control can be the ideal method to modulate moths' flight behavior since it can offers localized chemical release precisely that could mimic the actual chemical signal processes occurring inside of the body. I demonstrated a drug delivery system (Chap. 2 and 4 for device aspect and Chap. 3 and 5 for actual moth controls via microfluidics) affecting the insect nervous system and the flight activity and longevity of *Manduca sexta* moths.

1.3.2: Optofluidics for reconfigurable photonics

Field Programmable Gate Array (FPGA) [47] is a representative example of the on-the-fly reconfigurable system in electronics via reprogramming the hierarchy of interconnections among logic blocks. Users can easily re-program and engineer its output performance rapidly with low cost. Interestingly, it is extremely hard to find the equivalent system or technology that has demonstrated near the level of reconfigurability of the FPGAs in other fields. Especially in optics, in order to provide analogous tunability commonly two methods have been applied (1) varying the physical layout or (2) changing the refractive indices. The recent advancements in MEMS also has benefited optics to dynamically vary the physical layout [48-50] though still relatively limited tunability has been provided. With regards to the latter, various technologies have been reported including electro-optic [51, 52], magneto-optic [53], acousto-optic [54, 55], thermo-optic [56], and carrier injection [57]. All of

these techniques however are limited by the achievable Δn/n, occasionally requiring either a longer interaction optical path length which is not desirable for miniaturized systems.

Recent developments in optofluidics [58, 59] have demonstrated much higher Δn/n and been regarded as an alternative approach for higher reconfigurability. For example, a number of pure liquid state photonic elements have been demonstrated such as waveguides [60, 61], microlenses [62, 63], and dye lasers [64, 65]. Liquid based photonic components have shown great tunability throughout flow rate adjustments, however little work has been reported that they can directly be incorporated into conventional solid-state photonic systems to be more practical. In particular, the liquid-core and liquid-cladding waveguide system was reported by Wolfe *et al.* [60] but because of its innately high loss nature (diffusion between core and cladding fluids), liquid waveguide system has not been regarded as a practical optical element.

I addressed mentioned problems by integrating the liquid-core / liquid-cladding waveguide into a fiber-in and fiber-out system. In short, the liquid waveguide interconnects the optical fibers and through dynamic modulation of its shape via microfluidic flow controls I was able to develop a practical new type of photonic element for use in reconfigurable photonic and optical communication systems.

1.4 Key Concepts and Background Theory

1.4.2: Electrokinetic flow

Most of the flows in microfluidic channel are dominated by viscous effect ($Re << 1$), thus, flows are considered under Stokes regime. With this assumption, the Navier-Stokes equation (in steady-state) can be simplified to Stokes equation as shown below.

$$\nabla p - \eta \nabla^2 \boldsymbol{v} = 0 \tag{1.1}$$

where, p is pressure, η is dynamic viscosity and $\boldsymbol{v}$ is flow velocity. Also we assume the fluid medium is incompressible (Eq. 1.2). The electric field is applied across microfluidic channel in order to induce the flow so that an electrostatic $\rho_E \boldsymbol{E}$ term has been added as a body force to Eq.1.1 yielding Eq. 1.3.

$$\nabla \cdot \boldsymbol{v} = 0 \tag{1.2}$$

$$\nabla p - \eta \nabla^2 \boldsymbol{v} = \rho_E \boldsymbol{E} \tag{1.3}$$

where ρ_E is the volumetric charge density and $\boldsymbol{E}$ is external electrical field. Conventionally electrokinetic flow is mainly due to the combination of electroosmosis and electrophoresis (species) effects in response to the external electric field and I will mainly discuss electroosmosis and electrophoresis that are specifically used in my drug delivery device described in Chap. 2.

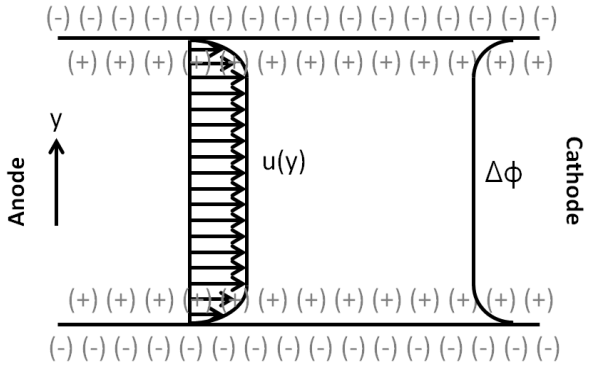

Figure 1.1. Schematic view of electrical double layer (EDL) and electroosmotic flow.

1.4.2a: Electroosmosis

As illustrated in Fig. 1.1, electroosmosis is referred to a plug type flow motion of the liquid in the microfluidic channel with an external electric field ($\boldsymbol{E}_{\text{ext}}$). Normally the surface of the microfluidic channel is charged (here negatively) and due to Coulomb force the opposite charge ions form a thin cloud layer that we call the electrical double layer (EDL) [66]. In the bulk solution, the net charge is neutral but the near the wall (in the EDL) small net charge exists. The potential difference between the wall and the bulk solution is defined as zeta potential (ζ). With a uniform external electrical field and assumption of steady and isobaric flow Eq. 1.3 can be reduced to

$$\eta\nabla^2 v + \rho_E \boldsymbol{E}_{ext} = 0 \tag{1.4}$$

By coupling Eq. 1.4 with the uniform permittivity (ε) and Poisson equation (shown below) in one dimensional configuration (see Fig. 1.1) we obtain,

$$-\varepsilon\nabla^2\phi = \rho_E \tag{1.5}$$

and we can derive the bulk fluid flow velocity profile, v_{EO} with assuming very thin EDL as follows.

$$\boldsymbol{v}_{EO} = -\varepsilon\zeta/\eta\boldsymbol{E}_{\text{ext}} \tag{1.6}$$

The term $\varepsilon\zeta/\eta$ is called as the electroosmotic mobility, μ_{eo}.

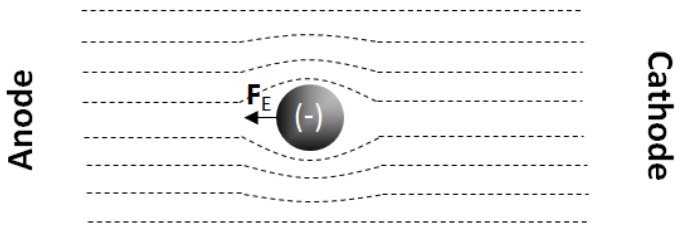

Figure 1.2. Schematic view of electrophoresis (regenerated from Dr. Bernardo Cordovez's original work). No flow drag is shown.

1.4.2b: Electrophoresis

Chemical species can be migrated through fluid systems due to the presence of electrical fields. Charged ions are transported in response to the Coulomb force and qualitatively this process is called electrophoresis. The electrophoretic force is shown below.

$$\boldsymbol{F}_E = ze\boldsymbol{E}_{\text{ext}} \tag{1.6}$$

where e is the electron charge and z is the valence of the ion.

1.4.3: Electrolysis

Electrolysis of water is the breakdown of the H_2O into oxygen (O_2) and hydrogen gas (H_2) through an oxidation and reduction reactions induced by DC potentials [67]. Equations 1.7-9 show the detailed chemical reactions.

$$\textit{Anode (oxidation)}: 2H_2O\,(l) \rightarrow O_2\,(g) + 4H^+\,(aq) + 4e^- \quad (1.7)$$

$$\textit{Cathode (reduction)}: 2H_2O\,(g) + 2e^- \rightarrow H_2\,(g) + 2OH^-\,(aq) \quad (1.8)$$

$$\textit{Overall reaction}: 2H_2O\,(l) \rightarrow 2\,H_2\,(g) + O_2\,(g) \quad (1.9)$$

Electrolysis has been introduced in this study as a pumping mechanism through building up a pressure in a confined reservoir to expel the liquid contents out through the dissolved membrane (see Chap. 4 for more details). Occasionally, i*n vivo* electrolysis is not desired for biomedical applications because that could possibly change the local pH changes, however in this study most of the electrolysis based ejection experiments were operated to avoid the pH changes. In addition, the generated gases escape through internal insects' gas expelling system [68].

1.4.4: Light propagation in waveguides

It is almost impossible to obtain analytical solutions of how light propagates in the liquid-core / liquid-cladding waveguide however through overviewing the conventional solid-state waveguide case qualitative light transmission physics can be understood. Starting from Maxwell's equations,

$$\nabla \times \boldsymbol{E} = -\frac{\partial \boldsymbol{B}}{\partial t} \tag{1.8}$$

$$\nabla \times \boldsymbol{H} = \boldsymbol{J} + \frac{\partial \boldsymbol{P}}{\partial t} \tag{1.9}$$

$$\nabla \cdot \boldsymbol{B} = 0 \tag{1.10}$$

$$\nabla \cdot \boldsymbol{D} = \rho_E \tag{1.11}$$

where $\boldsymbol{B}$ is the magnetic flux density, $\boldsymbol{D}$ is the electric flux density, $\boldsymbol{H}$ is the magnetic field, $\boldsymbol{J}$ is the current density and we can derive wave equation as follows,

$$\nabla^2 \boldsymbol{E} - \mu_0 \varepsilon \frac{\partial^2 \boldsymbol{E}}{\partial t^2} = 0 \tag{1.12}$$

and this can be solved using the method of separation of variables,

$$\nabla^2 \boldsymbol{E} + (k_o^2 n_i^2 - \beta)\boldsymbol{E} = 0 \tag{1.13}$$

where $\boldsymbol{E}$, k_o, n_i and β are the electric field, the free-space wavenumber, the refractive index of the medium and the propagation constant respectively. For simplified 1D case, we can obtain a sinusoidal solution in the core (which determines mode profile) and an exponential decay solution in the claddings. Numerically once the refractive index profile is obtained, light propagation within the waveguide can be solved [69]. With the help of my colleague Erica Jung, we reported a numerical study [69] on a hybrid system for coupling light between liquid- and solid-state waveguides, and I expanded this technique experimentally to develop two liquid

waveguide based photonic elements for use in reconfigurable photonic systems which are discussed in detail in Chap. 6.

1.5 Research Overview and Dissertation Breakdown

Chapter 2 is the demonstration of a rapid, low power and implantable drug delivery system, intended for use with autonomous microsystems. To date most of the current drug delivery devices or systems rely on the diffusion based chemical delivery but the drug release mechanism developed in my graduate work utilizes the electrokinetic effects (discussed in Section 1.4.1-2) to control both the release time and rate of chemicals. The fundamental advantage of the system is that this can rapid deliver the drugs from hours to second over previous diffusion based approaches with energy consumption of as little as 20 mJ. Furthermore, the device can be applied to the situation where rapid dosage or pulsatile manner release are needed for biomedical applications that are discussed in Chap. 4.

Chapter 3 presents the direct application of the electrokinetic drug delivery device for autonomous systems. I developed, for the first time, a method that directly and reversibly engineers insect flight metabolics using implanted microfluidics. Detailed injection and implantation experiments are also presented in this chapter. This chapter also explores how injected chemicals can modulate the internal level of moths' metabolic rates by monitoring respiratory CO_2 output. Throughout chemical injection, behaviors ranging from retarded motion to complete, reversible paralysis, are presented. This work shows the possibility of a new paradigm for insect flight control alongside established electrical techniques.

Chapter 4 presents a next generation version of the electrolysis based drug delivery systems for biomedical use presented in Chapter 2. In this chapter, I developed and

discussed an implantable microreservoir based devices that enable delivery of 15 μl of vasopressin using an electrochemically based transport mechanism. Administration of vasopressin release plays a crucial role in compensatory mechanism for restoring blood pressure during hemorrhagic shock [70, 71]. Characterizations of vasopressin delivery via electrochemical transport mechanism are explored and the device was directly implemented into insect-MAVs that are presented in Chap 5.

Chapter 5 discusses an integrated microsystem that uses both chemical and electrical methods to modulate the flight activity and longevity of *Manduca sexta* moths. The electrical component of the system initiates and maintains tetherless flight by applying electrical pulses to an antenna lobe and an implanted microfluidic component modulates flight speed and output power by administering a neurotransmitter dose to the central nervous system. In short, the implanted microfluidic device was used to eject a neurotransmitter solution into a *Manduca sexta* moth's thorax resulting in a reversible and chemically induced mid-flight flight control. Furthermore, in this chapter I presented that the electrical stimulation provides as much as 35-fold enhancement in flight duration with respect to mechanical approach and that a 50% mean flight power output reduction can be achieved with the proper neurotransmitter dose.

In Chap. 6, I shifted the topics from microfluidically enabled biology to optics. The developments of two liquid-core / liquid-cladding waveguide based photonic elements: an optical switch or signal attenuator, are presented for use in reconfigurable photonic systems. In this work, I was able to demonstrate the ability to couple light between conventional optical fibers through interconnecting them with the liquid waveguide. Small scale flow control enabled the reconfigurable shape and position of the liquid waveguide yielding an attenuation range of 3.1-10.7 dB and a 1x2 sub-second switching system with a maximum coupling efficiency of 3.87 dB.

Chapter 7 concludes the work presented by summarizing my research contributions to microfluidics and their impacts with additional remarks.

REFERENCES

1. Happel, J. and H. Brenner, *Low Reynolds Number Hydrodynamics*. 1965, NJ: Englewood Cliffs, Prentice-Hall.
2. Stroock, A.D., S.K.W. Dertinger, A. Ajdari, I. Mezic, H.A. Stone, and G.M. Whitesides, *Chaotic mixer for microchannels.* Science, 2002. **295**(5555): p. 647-651.
3. Hunter, R.J., *Zeta potential in colloid science: principles and applications*. 1981, London and New YorK: Academic Press.
4. Stone, H.A., A.D. Stroock, and A. Ajdari, *Engineering flows in small devices: Microfluidics toward a lab-on-a-chip.* Annual Review of Fluid Mechanics, 2004. **36**: p. 381-411.
5. Erickson, D., S. Mandal, A.H.J. Yang, and B. Cordovez, *Nanobiosensors: optofluidic, electrical and mechanical approaches to biomolecular detection at the nanoscale.* Microfluidics and Nanofluidics, 2008. **4**(1-2): p. 33-52.
6. Dawson, E.D., C.L. Moore, J.A. Smagala, D.M. Dankbar, M. Mehlmann, M.B. Townsend, C.B. Smith, N.J. Cox, R.D. Kuchta, and K.L. Rowlen, *MChip: A tool for influenza surveillance.* Analytical Chemistry, 2006. **78**(22): p. 7610-7615.
7. Whitesides, G.M., *The origins and the future of microfluidics.* Nature, 2006. **442**(7101): p. 368-373.
8. Erickson, D. and D. Li, *Integrated microfluidic devices.* Analytica Chimica Acta, 2004. **507**(1): p. 11-26.

9. Huh, D., B.D. Matthews, A. Mammoto, M. Montoya-Zavala, H.Y. Hsin, and D.E. Ingber, *Reconstituting Organ-Level Lung Functions on a Chip.* Science, 2010. **328**(5986): p. 1662-1668.

10. Jang, K.-J. and K.-Y. Suh, *A multi-layer microfluidic device for efficient culture and analysis of renal tubular cells.* Lab on a Chip, 2010. **10**(1): p. 36-42.

11. Kopp, M.U., A.J. de Mello, and A. Manz, *Chemical amplification: Continuous-flow PCR on a chip.* Science, 1998. **280**(5366): p. 1046-1048.

12. Burns, M.A., C.H. Mastrangelo, T.S. Sammarco, F.P. Man, J.R. Webster, B.N. Johnson, B. Foerster, D. Jones, Y. Fields, A.R. Kaiser, and D.T. Burke, *Microfabricated structures for integrated DNA analysis.* Proceedings of the National Academy of Sciences of the United States of America, 1996. **93**(11): p. 5556-5561.

13. Lagally, E.T., I. Medintz, and R.A. Mathies, *Single-molecule DNA amplification and analysis in an integrated microfluidic device.* Analytical Chemistry, 2001. **73**(3): p. 565-570.

14. Khandurina, J., T.E. McKnight, S.C. Jacobson, L.C. Waters, R.S. Foote, and J.M. Ramsey, *Integrated system for rapid PCR-based DNA analysis in microfluidic devices.* Analytical Chemistry, 2000. **72**(13): p. 2995-3000.

15. Schena, M., D. Shalon, R.W. Davis, and P.O. Brown, *Quantitative Monitoring of Gene Expression Patterns with a Complementary DNA Microarray.* Science, 1995. **270**(5235): p. 467-470.

16. Foquet, M., J. Korlach, W. Zipfel, W.W. Webb, and H.G. Craighead, *DNA fragment sizing by single molecule detection in submicrometer-sized closed fluidic channels.* Analytical Chemistry, 2002. **74**(6): p. 1415-1422.

17. Auroux, P.A., Y. Koc, A. deMello, A. Manz, and P.J.R. Day, *Miniaturised nucleic acid analysis.* Lab on a Chip, 2004. **4**(6): p. 534-546.

18. Gao, J., J.D. Xu, L.E. Locascio, and C.S. Lee, *Integrated microfluidic system enabling protein digestion, peptide separation, and protein identification.* Analytical Chemistry, 2001. **73**(11): p. 2648-2655.

19. Wang, C., R. Oleschuk, F. Ouchen, J. Li, P. Thibault, and D.J. Harrison, *Integration of immobilized trypsin bead beds for protein digestion within a microfluidic chip incorporating capillary electrophoresis separations and an electrospray mass spectrometry interface.* Rapid Communications in Mass Spectrometry, 2000. **14**(15): p. 1377-1383.

20. Yamamoto, T., T. Nojima, and T. Fujii, *PDMS-glass hybrid microreactor array with embedded temperature control device. Application to cell-free protein synthesis.* Lab on a Chip, 2002. **2**(4): p. 197-202.

21. Skelley, A.M., O. Kirak, H. Suh, R. Jaenisch, and J. Voldman, *Microfluidic control of cell pairing and fusion.* Nature Methods, 2009. **6**(2): p. 147-152.

22. Gawad, S., L. Schild, and P. Renaud, *Micromachined impedance spectroscopy flow cytometer for cell analysis and particle sizing.* Lab on a Chip, 2001. **1**(1): p. 76-82.

23. Fu, A.Y., H.-P. Chou, C. Spence, F.H. Arnold, and S.R. Quake, *An Integrated Microfabricated Cell Sorter.* Analytical Chemistry, 2002. **74**(11): p. 2451-2457.

24. Chou, H.P., C. Spence, A. Scherer, and S. Quake, *A microfabricated device for sizing and sorting DNA molecules.* Proceedings of the National Academy of Sciences of the United States of America, 1999. **96**(1): p. 11-13.

25. Wolff, A., I.R. Perch-Nielsen, U.D. Larsen, P. Friis, G. Goranovic, C.R. Poulsen, J.P. Kutter, and P. Telleman, *Integrating advanced functionality in a*

microfabricated high-throughput fluorescent-activated cell sorter. Lab on a Chip, 2003. **3**(1): p. 22-27.

26. Shyy, W., M. Berg, and D. Ljungqvist, *Flapping and flexible wings for biological and micro air vehicles.* Prog in Aero Sci, 1999. **35**(5): p. 455-505.
27. Weinberger, S., *Defence research: Still in the lead?* Nature, 2008. **451**: p. 390-393.
28. Lian, Y.S., W. Shyy, D. Viieru, and B.N. Zhang, *Membrane wing aerodynamics for micro air vehicles.* Prog. Aerosp. Sci., 2003. **39**(6-7): p. 425-465.
29. Jeon, Y.B., R. Sood, J.h. Jeong, and S.G. Kim, *MEMS power generator with transverse mode thin film PZT.* Sensor. Actuat. A, 2005. **122**(1): p. 16-22.
30. Wickenheiser, A.M., T. Reissman, W.J. Wu, and E. Garcia, *Modeling the Effects of Electromechanical Coupling on Energy Storage Through Piezoelectric Energy Harvesting.* Ieee-Asme Transactions on Mechatronics, 2010. **15**(3): p. 400-411.
31. Gad-el-Hak, M., *MEMS: Design and Fabrication*. 2006, Boca Raton, FL: CRC/Taylor & Francis Group.
32. Tanaka, M., *An industrial and applied review of new MEMS devices features.* Microelectron. Eng., 2007. **84**(5-8): p. 1341-1344.
33. Wood, R.J., *The first takeoff of a biologically inspired at-scale robotic insect.* Ieee Transactions on Robotics, 2008. **24**(2): p. 341-347.
34. Wootton, R., *Aerodynamics: From insects to microvehicles.* Nature, 2000. **403**(6766): p. 144-145.
35. Ellington, C.P., *The novel aerodynamics of insect flight: Applications to micro-air vehicles.* Journal of Experimental Biology, 1999. **202**(23): p. 3439-3448.

36. Dudley, R., *BIOMECHANICS:Enhanced: Unsteady Aerodynamics.* Science, 1999. **284**(5422): p. 1937-1939.

37. Franceschini, N., F. Ruffier, and J. Serres, *A bio-inspired flying robot sheds light on insect piloting abilities.* Curr Bio, 2007. **17**(4): p. 329-335.

38. Wood, R.J., *Liftoff of a 60mg flapping-wing MAV.* Proc IEEE/RSJ Int Conf Intelli Rob Sys, 2007: p. 1889-1894.

39. Wood, R.J., *The first takeoff of a biologically inspired at-scale robotic insect.* IEEE Trans Robotics, 2008. **24**(2): p. 341-347.

40. Wood, R.J., S. Avadhanula, R. Sahai, E. Steltz, and R.S. Fearing, *Microrobot design using fiber reinforced composites.* J Mech Design, 2008. **130**(5).

41. Tanaka, H., K. Hoshino, K. Matsumoto, and I. Shimoyama, *Flight dynamics of a butterfly-type ornithopter.* Proc IEEE/RSJ Int Conf Intelli Rob Sys, 2005: p. 2706- 2711.

42. Steltz, E., S. Avadhanula, and R.S. Fearing, *High lift force with 275 Hz wing beat in MFI.* Proc IEEE/RSJ Int Conf Intelli Rob Sys, 2007: p. 3987-3992.

43. Helm, B., *Finding Land Mines by Following a Bee*, in *Business Week*. 2005.

44. Bozkurt, A., A. Lal, and R. Gilmour, *Aerial and terrestrial locomotion control of lift assisted insect biobots.* Conf. Proc. IEEE. Eng. Med. Biol. Soc., 2009. **2009**: p. 2058-61.

45. Sato, H., C.W. Berry, Y. Peeri, E. Baghoomian, B.E. Casey, G. Lavella, J.M. Vandenbrooks, J.F. Harrison, and M.M. Maharbiz, *Remote radio control of insect flight.* Front. Integr. Neurosci., 2009. **3**: p. 24.

46. Daly, D.C., P.P. Mercier, M. Bhardwaj, A.L. Stone, Z.N. Aldworth, T.L. Daniel, J. Voldman, J.G. Hildebrand, and A.P. Chandrakasan, *A Pulsed UWB Receiver SoC for Insect Motion Control.* Ieee Journal of Solid-State Circuits, 2010. **45**(1): p. 153-166.

47. Strukov, D.B. and K.K. Likharev, *CMOL FPGA: a reconfigurable architecture for hybrid digital circuits with two-terminal nanodevices.* Nanotechnology, 2005. **16**(6): p. 888-900.

48. Lin, L.Y. and E.L. Goldstein, *Opportunities and challenges for MEMS in lightwave communications.* IEEE Journal of Selected Topics in Quantum Electronics, 2002. **8**(1): p. 163-172.

49. Lyshevski, S.E., *MEMS and NEMS : systems, devices, and structures*, ed. C. Press. 2002, Boca Raton, Fl.

50. Gad-el-Hak, M., *MEMS : design and fabrication*. 2006, Boca Raton: CRC Press.

51. Roussey, M., M.P. Bernal, N. Courjal, and F.I. Baida, *Experimental and theoretical characterization of a lithium niobate photonic crystal.* Applied Physics Letters, 2005. **87**(24).

52. Roussey, M., M.P. Bernal, N. Courjal, D. Van Labeke, F.I. Baida, and R. Salut, *Electro-optic effect exaltation on lithium niobate photonic crystals due to slow photons.* Applied Physics Letters, 2006. **89**(24).

53. Diwekar, M., V. Kamaev, J. Shi, and Z.V. Vardeny, *Optical and magneto-optical studies of two-dimensional metallodielectric photonic crystals on cobalt films.* Applied Physics Letters, 2004. **84**(16): p. 3112-3114.

54. Verluise, F., V. Laude, Z. Cheng, C. Spielmann, and P. Tournois, *Amplitude and phase control of ultrashort pulses by use of an acousto-optic programmable dispersive filter: pulse compression and shaping.* Optics Letters, 2000. **25**(8): p. 575-577.

55. Courjal, N., S. Benchabane, J. Dahdah, G. Ulliac, Y. Gruson, and V. Laude, *Acousto-optically tunable lithium niobate photonic crystal.* Applied Physics Letters, 2010. **96**(13).

56. Camargo, E.A., H.M.H. Chong, and R.M. De la Rue, *2D Photonic crystal thermo-optic switch based on AlGaAs/GaAs epitaxial structure.* Optics Express, 2004. **12**(4): p. 588-592.

57. Gu, L.L., W. Jiang, X.N. Chen, L. Wang, and R.T. Chen, *High speed silicon photonic crystal waveguide modulator for low voltage operation.* Applied Physics Letters, 2007. **90**(7).

58. Psaltis, D., S.R. Quake, and C.H. Yang, *Developing optofluidic technology through the fusion of microfluidics and optics.* Nature, 2006. **442**(7101): p. 381-386.

59. Monat, C., P. Domachuk, and B.J. Eggleton, *Integrated optofluidics: A new river of light.* Nature Photonics, 2007. **1**(2): p. 106-114.

60. Wolfe, D.B., R.S. Conroy, P. Garstecki, B.T. Mayers, M.A. Fischbach, K.E. Paul, M. Prentiss, and G.M. Whitesides, *Dynamic control of liquid-core/liquid-cladding optical waveguides.* Proceedings of the National Academy of Sciences of the United States of America, 2004. **101**(34): p. 12434-12438.

61. Lim, J.M., S.H. Kim, J.H. Choi, and S.M. Yang, *Fluorescent liquid-core/air-cladding waveguides towards integrated optofluidic light sources.* Lab on a Chip, 2008. **8**(9): p. 1580-1585.

62. Tang, S.K.Y., C.A. Stan, and G.M. Whitesides, *Dynamically reconfigurable liquid-core liquid-cladding lens in a microfluidic channel.* Lab on a Chip, 2008. **8**(3): p. 395-401.

63. Mao, X.L., J.R. Waldeisen, B.K. Juluri, and T.J. Huang, *Hydrodynamically tunable optofluidic cylindrical microlens.* Lab on a Chip, 2007. **7**(10): p. 1303-1308.

64. Li, Z.Y., Z.Y. Zhang, T. Emery, A. Scherer, and D. Psaltis, *Single mode optofluidic distributed feedback dye laser.* Optics Express, 2006. **14**(2): p. 696-701.

65. Song, W.Z. and D. Psaltis, *Pneumatically tunable optofluidic dye laser.* Applied Physics Letters, 2010. **96**(8).

66. Kirby, B.J., *Micro- and Nanoscale Fluid Mechanics*. 2010: Cambridge University Press.

67. Rossmeisl, J., A. Logadottir, and J.K. Nørskov, *Electrolysis of water on (oxidized) metal surfaces.* Chemical Physics, 2005. **319**(1-3): p. 178-184.

68. Chapman, R.F., *The Insects: Structure and Function*. 4th ed. 1998, NewYork: Cambridge University Press.

69. Jung, E.E., A.J. Chung, and D. Erickson, *Analysis of liquid-to-solid coupling and other performance parameters for microfluidically reconfigurable photonic systems.* Optics Express, 2010. **18**(11): p. 10973-10984.

70. Lienhart, H.G., K.H. Lindner, and V. Wenzel, *Developing alternative strategies for the treatment of traumatic haemorrhagic shock.* Current Opinion in Critical Care, 2008. **14**(3): p. 247-253.

71. Peitzman, A.B., B.G. Harbrecht, A.O. Udekwu, T.R. Billiar, E. Kelly, and R.L. Simmons, *Hemorrhagic shock.* Curr. Probl. Surg., 1995. **32**(11): p. 925-1002.

CHAPTER 2

ELECTROKINETIC MICROFLUIDIC DEVICES FOR RAPID, LOW POWER DRUG DELIVERY IN AUTONOMOUS MICROSYSTEMS*

2.1 Abstract

In this work, a low power and robust electroactive microwell-based implantable drug delivery system, intended for use with autonomous microsystems, is presented. The device comprises of an upper silicon based structure in which the drug storage sites are defined and a lower electrically functionalized PDMS (poly-dimethylsiloxane) backing. The drug ejection mechanism developed here exploits localized electrokinetic effects to control both the release time and release rate of chemicals stored in independent well sites. It is shown how this can reduce the dosage time from hours to second over previous diffusion based approaches using as little as 20 mJ of energy per dose. This paper focuses on presenting the design and characterizing the electrokinetic transport mechanics which govern the release time and dispersal pattern of the well contents using a series of experimental and numerical techniques.

*Reproduced by permission of the Royal Society of Chemistry with permission from Aram J. Chung, Donn Kim and David Erickson, "Electrokinetic microfluidic devices for rapid, low power drug delivery in autonomous microsystems", *Lab-on-a-Chip*, **8**, 330-338 (2008) DOI: 10.1039/B713325A
The original publication is available at:
http://pubs.rsc.org/en/Content/ArticleLanding/2008/LC/b713325a

2.2 Introduction

Autonomous microsystems can be defined as "systems, enabled through microfabrication technology, that function of their own accord with the ability to interpret and interact with their environment". Recent developments in micro-electro-mechanical-systems or MEMS [1, 2] component-level technology (including power generation [3], energy storage, communications, sensing, and subcomponent assembly) have brought the development of such systems closer to a reality. While many of the initial thrusts into this field were directed towards autonomous sensor networks [4], the integration of bioMEMS [5-8] and microfluidic elements [9-12] in these types of devices is increasingly finding application to *in-vitro* and in particular *in-vivo* medical devices (mostly through various "smart-pill" type technologies) [13, 14]. While such systems are becoming increasingly functional, their primary use remains diagnostic rather than therapeutic. One of the limitations of these devices, and all autonomous microsystems, is that the power load is relatively large compared with the amount of energy available from current battery technology. This tends to significantly limit the lifetime of the device.

Oral, nasal, intravenous, pulmonary and transdermal methods represent the traditional and often preferred routes for drug delivery. Broadly speaking the advantage of the former of these is its relative simplicity, while the later methods have been developed to enable more rapid delivery and better specific organ targeting [15]. The advantages that emerging MEMS based implantable drug delivery systems offer over these conventional methods are controllability (*i.e.* the ability to autonomously deliver very precise doses either periodically or in response to a sensor event), delivery speed and microscopic localization [16, 17]. Such capabilities could have significant impact on future human health [18].

Current implantable drug delivery systems [19-21] can be categorized as either passive or active [16]. Passive systems are based on chemical release beginning immediately after implantation (either through a diffusive processes or mechanical pumping) and continuing until the "on-board" dose is depleted. Though this offers control over the total dose, neither the delivery timing nor its rate can be manipulated by the physician, patient or the system itself.[16]

One of the first experimental demonstrations of an active drug delivery was described by Santini *et al*. [22] In their system an array of individually sealed reservoirs were fabricated on a silicon microchip and filled with a series of different chemicals. The system could then be implanted and the contents of each reservoir released by applying an external electric potential (which induced electrochemical dissolution of the gold sealing membrane). This active control over the delivery timing and dosage can have a significant effect on its therapeutic efficacy in that the specific drug and its dosage can be released rapidly in consideration of the patients' current condition. Such systems have the advantage of a relatively simple construction, requiring only low voltage electrical actuation as opposed to mechanical pumping.

Drug release from self-contained reservoirs relies on a diffusive transport mechanism. This allows for continuous releases of contents over an extended period of time which could take several hours to days depending on the diffusion coefficient of the chemical [22-24]. Thus while the dose initiation time can be manipulated, the delivery rate remains fixed to this relatively slow rate. In certain cases it is desirable to possess greater control over the release rate to allow for more rapid dosage (in order to better respond to the patient's condition) or to better mimic a physiological release profile. For example insulin and other hormones are well-known to be secreted by the body in a pulsatile manner. Deficiency in hormones of the anterior pituitary gland

such as thyroid stimulating hormone, growth hormone, luteinizing hormones regulated by the hypothalamus may lead hypothyroidism (insufficient production of thyroid hormone), hypoglycemia/dwarfism (inadequate production of growth hormone) or hypogonadism (failure of gonadal function). Pulsatile administration of small volumes of thyroid releasing hormone, growth hormone releasing hormone [24] and gonadotropin releasing hormone [24] can help the severity of these deficiencies.

In this work, we present an electroactive microwell [25] based drug/chemical delivery system which provides this active chip control over the delivery rate, timing and speed without the need for significant additional on-chip architecture or large power consumption. A series of single and multiple well chips were fabricated, all of which used the two component construction. As shown in Fig. 2.1, the silicon layer contained the drug well(s) and the upper set of electrodes, while the PDMS layer served to seal the well and hold the lower electrode. The device structure is a modification of that presented by Santini *et al.* [22], exploiting the same electrochemical dissolution technique to expose the contents, but incorporating electrical functionality onto a flexible PDMS backing to enable control over the electrokinetic transport. As will be described below, the technique is based on exploiting highly localized electrokinetic transport to rapidly exchange the contents of the well with the external environment. This allows for a controlled reduction in the total dosage time to seconds rather than hours as will be demonstrated. Here we focus on presenting the overall design and construction of the device, and detailing the delivery rate and drug dispersion pattern as a function of the strength of the applied electric field. A detailed 3D finite element analysis of the transport dynamics of the system is conducted in order to better understand the governing mechanisms behind the ejection process. As alluded to above, this device is designed for use in

autonomous microfluidic systems and thus a detailed analysis of the voltage, power and energy requirements is also conducted.

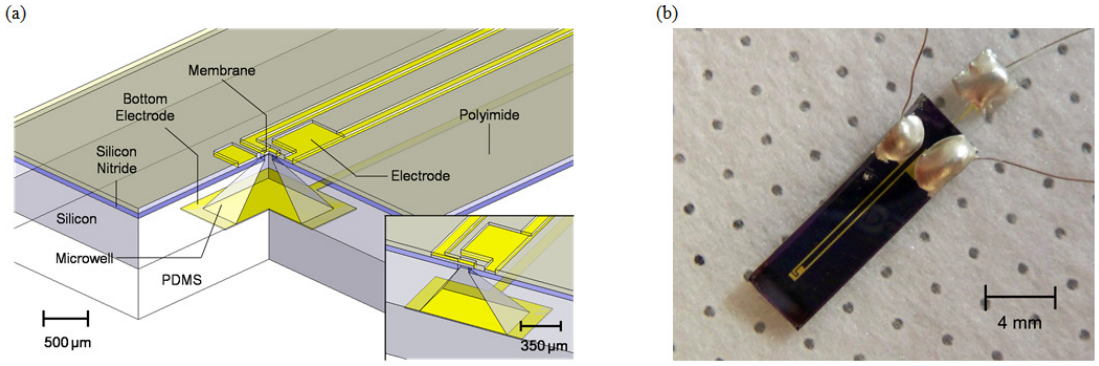

Figure 2.1. (a) Schematic representative section of an electroactive microwell drug delivery system developed here. Inset: cross sectional view of the system (b) Fabricated and assembled device with electrical leads connected to thin copper wires.

2.3 Materials and methods

In this materials and methods section we begin with a detailed description of the device fabrication and assembly procedure (A detailed process diagram of the fabrication and assembly procedure is also included as supplementary material). The final two subsections describe the device operation and experimental procedure.

2.3.1 Microfabrication

In our device we have used double side polished, (100) n-doped silicon wafers with a thickness of 500 µm. In general thicker wafers were preferred in order to maximize the well volume. To fabricate the devices we first used low pressure chemical vapour deposition (LPCVD) to deposit a 200 nm thick layer of silicon nitride on both sides of the wafer. 760 µm squares were then reactive ion etched into the back side silicon

nitride layer defining the eventual location of the wells. Following this a 300 nm layer of gold was evaporated and patterned using image reversal contact lithography process on the top surface to form the electrode leads and well membrane. A polyimide (Durimide®) passivation layer was then deposited on the topside of the wafer which served to electrically isolate the electrodes from the electrolyte solution during membrane dissolution. The passivation layer was patterned using an aluminium mask and oxygen plasma etching process so that only the eventual location of the membrane and surrounding C-shape gold features would be exposed to the solution (See Fig. 2.1c). The microwells were then defined by immersing the wafer in KOH for roughly 8 hours. During this process the exposed silicon was etched along the crystal plane resulting in the square pyramidal shape shown in Fig. 2.1a. Lastly, the remaining nitride on backside of the wafer and underneath the gold membrane were etched by reactive ion etching. The resulting drug wells were 760 μm square at the base and 52 μm square at the top resulting in a total cavity volume of approximately 100 nL.

To create the lower gold patterned PDMS layer we used a similar technique to that described by Lee *et al.* [26] 100 nm thick gold features were first patterned on a silicon substrate. After the gold features were created an MPTMS (3-mercaptopropyl-trimethoxysilane) film was deposited onto the top surface of the wafer using molecular vapour deposition (MVD). The MPTMS layer served as an organic adhesion layer aiding with the transfer of the gold features from the silicon wafer to the PDMS [27]. After surface modification, a 5:1 (base:linker) mixture of PDMS was spin coated at 100 rpm for 30 seconds onto the wafer to a final thickness of approximately 580 μm. The PDMS was then cured at 80°C for 90 minutes and the final structures were cut out of the mold (Fig. 2.2d).

2.3.2 Microchip Assembly

The microwell reservoir was filled with a phosphate buffered saline (PBS) using 36G blunt syringe (NanoFil^{TM}, World Precision Instrument). A PBS buffer solution concentrated such that it had similar chloride ion concentration to that found in human sera [28] was used here. For the flow visualization experiments, 1.9 μm fluorescent polystyrene microspheres (Duke Scientific) were added to the PBS solution. Once filled the upper (silicon) and the bottom (PDMS) substrates were placed in conformal contact with each other and bonded together.

The use of a PDMS substrate greatly facilitated robust sealing of the device. In general, as long as wells were not overfilled, the conformal contact the PDMS formed with the polished bottom of the silicon microchip was sufficient to ensure a watertight seal. Significant overfilling of the wells tended to result in bursting of the gold membrane when the PDMS backing was applied. This is a result of the liquid being largely incompressible and thus very little overfilling was required in order to increase the internal pressure above that of the membrane burst pressure. To avoid this here we slightly under filled the wells (leaving a small compressible air pocket).

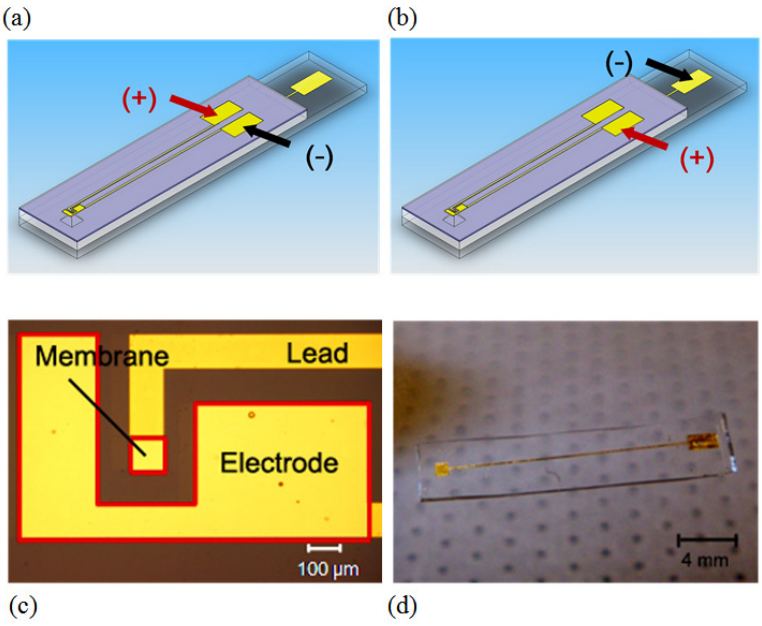

Figure 2.2. (a) Stage 1: To electrochemically dissolve the membrane a potential is applied between the two upper electrodes. (b) Stage 2: After dissolution to eject the contents, the potentials applied between the upper electrode and the lower one on the PDMS. (c) Magnified view of microchip from above looking at the region near the membrane. Pale yellow regions (membrane and C-shape gold features) are gold where the polyimide layer was etched. (d) An example of gold-PDMS bottom substrate

2.3.3 Detailed device operation

Device operation occurs in two stages. As shown in Fig. 2.2a, in the first stage the potential is applied between two electrode pads on top of the microchip serving to electrochemically dissolve the membrane [29], exposing the contents to the external environment (this was similarly demonstrated by Santini *et al.* [22]). To electrokinetically eject the contents from the well, in the second stage a potential field is applied between one of the upper electrodes and that on the PDMS at the bottom of the well, as illustrated in Fig. 2.2b. The application of this DC voltage (between 3-4 volts) over the relatively small wafer thickness results in extremely high electric field

strength (just under 10^5 V/m) localized in the well [25]. As will be characterized in detail below, the resulting electrokinetic transport dramatically reduced the amount of time required to eject the contents of the well over diffusive transport [22-24] (from hours to minutes) with very little energy consumption. In all cases a Hewlett-Packard 6234A dual output power supply was used to apply these potentials and a Keithley 236 SMU (Source-Measure Unit) was used to record the current load. The transport of the microspheres was recorded using Unibrain Fire-i^{TM} software and a Sony XCD-X710 camera.

2.3.4 Biocompatibility

Although the focus of this paper is on device design and transport analysis it is important to briefly discuss the biocompatibility of the architecture introduced here. In a recent paper, Voskerician *et al*. [30] reported on the *in vivo* biocompatibility and biofouling of many of the fabrication materials used here (*i.e.* gold, silicon nitride, silicon) in the context of similar microsystem drug delivery devices. In general it was found that of these materials silicon was the least biocompatible though it can undergo a number of simple surface passivation processes, such as silanation, to improve its performance. For the remaining materials used here, Richardson *et al*. [31] and Belanger and Marois [32] have reported polyimide and PDMS respectively as exhibiting good biocompatibility.

2.4 Results and discussions

The electroactive microwell drug delivery system described here allows the well contents to be stored indefinitely until a dose command is given, after which it can be

rapidly released. As mentioned above, the use of an electrochemical membrane dissolution technique to expose the contents of a microwell to the external environment was previously demonstrated by Santini *et al.* [22] In the following two subsections therefore we focus on characterizing the novel aspects of the device reported here, namely the electrokinetically enhanced ejection times and low power operation consumption.

For completeness however we report that for our device a 5.0 V dc bias was applied between the upper electrodes as shown in Fig. 2.2a in order to initiate membrane dissolution. At this potential the resulting electrochemical reaction required 6 to 7 seconds to release the membrane, exposing the well contents to the external environment. Lower biases resulted in much longer membrane release times. Further details on the process are available in the "Power consumption" section below.

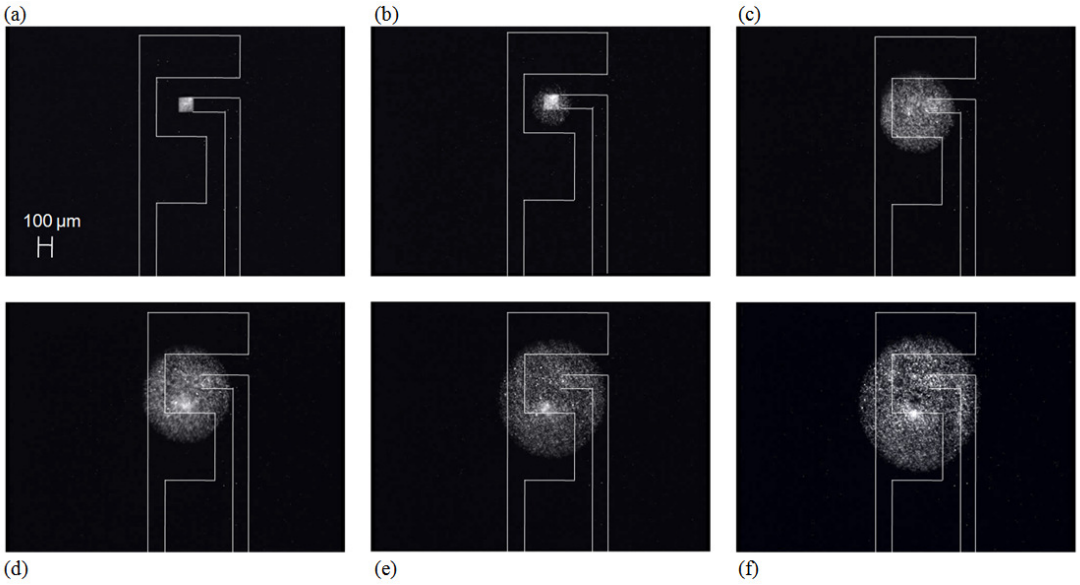

Figure 2.3. Time lapse illustrating the ejection of 1.9 µm fluorescent polystyrene microsphere particles from an electroactive microwell. (a) After dissolution of the membrane, the fluorescent particles can be seen in the well. White lines outline the gold electrodes features. (b)-(f) frames taken every two seconds (total of 10 seconds) after application of a 4.0 V potential.

2.4.1 Electrokinetic enhanced ejection

Immediately following dissolution of the membrane the applied potential field is switched to the configuration shown in Fig. 2.2b (*i.e.* between the upper and lower electrodes) and the resulting electrokinetic transport ejects the stored contents from the well to the external environment. Time lapse images in Fig. 2.3 illustrate the effect for the case of an applied potential of 4.0 V using the fluorescent flow tracers described above (see movie in supplemental material). As can be seen the process results in an approximately radial dispersal pattern. To characterize the dispersal pattern as a function of applied potential, the maximum dispersal radius was recorded as a function of time for 3.0 V, 3.5 V, 3.75 V and 4.0 V respectively. These measurements were performed using a similar sets of images to those shown in Fig. 2.3 which were processed using ImageJ (http://rsb.info.nih.gov/ij/) and a self-written MATLAB routine (Mathworks, Natick, MA). This range of applied potentials was used as they represent an optimal between expected ejection time [25] and power consumption (which will be characterized in the following section).

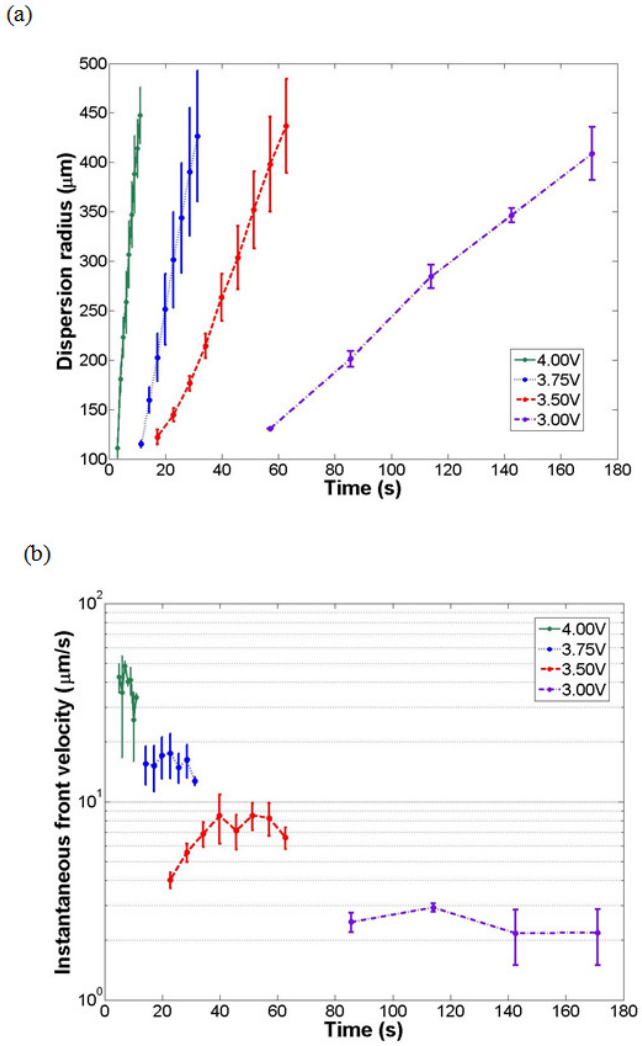

Figure 2.4. (a) Dispersion radius *vs.* time for different applied potentials (b) Instantaneous front velocity as a function of time.

The results of these experiments are presented in Figs. 2.4a and 2.4b, which show the dispersion radius and instantaneous transport front velocity as a function of time for different voltages. In all these cases the front was tracked to a distance of 500 μm, limited by the field of view of our microscope. As can be seen there exists an extremely strong dependence of the system dispersion on the applied electrokinetic potential with the 4.0 V case representing an average of a 15 fold improvement in both front velocity and dispersion radius over the 3.0 V case. A detailed analysis of the

superposition and relative importance of the electroosmotically induced convection and electrophoretic transport during the ejection process is provided in the "Characterization of electrokinetic transport" section below.

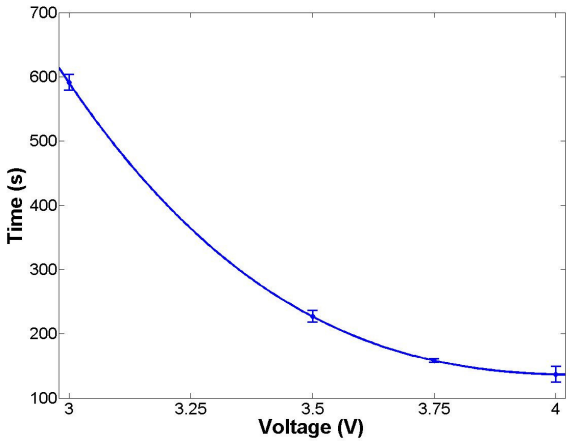

Figure 2.5. Time required to completely empty the contents of the microwell as a function of applied potential.

The time required to empty the microwell of its original contents is plotted in Fig. 2.5 again as a function of applied potential. The well was determined to be empty when fluorescent tracer particles could no longer be seen exiting the well. As can be seen at 3.0 V roughly 10 minutes was required to completely exchange the contents which was reduced to just over 2 minutes at 4.0 V. Earlier diffusion based approaches required several hours [22-24] to completely eject the contents and thus, for cases where rapid on-command chemical delivery is required, this represents an improvement on the order of approximately 130 fold.

As is apparent from the above, in addition to reducing the overall ejection time, the electrokinetic technique also provides a method for controllably modulating the delivery rate through simple adjustment of the applied potential. While some existing transdermal microneedle systems [33] also posses this capability, the simplicity of the

fabrication, assembly and operation (no fragile or moving parts nor complex or pulsatile pumping procedures) suggest that this approach may be more robust. The approach presented fuses the advantages of microwell devices, in terms of simplicity and storage stability, with the delivery flexibility afforded by microneedle systems.

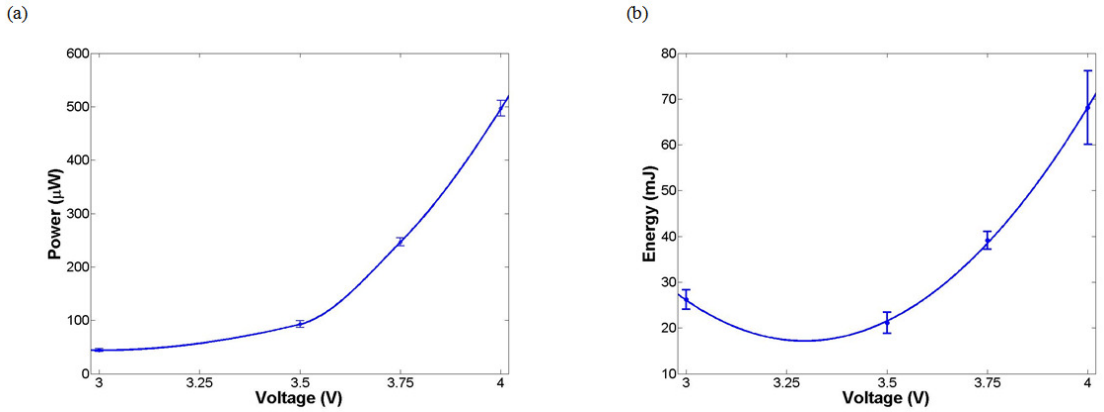

Figure 2.6. (a) Average power load during ejection process (b) Total energy consumed to completely empty the well using the times from Fig. 2.5. The line through the data points in this figure represents a quadratic best fit.

2.4.2 Power consumption

As mentioned in the introduction, one of the most significant limitations to the development of autonomous microsystems is the relatively small amount of energy which can be stored and voltage which can be generated with existing battery technology. As such minimizing voltage, power and energy requirements becomes a critical aspect of sub-component design. The small distance over which the potential is applied allows us to generate high field strengths (and therefore rapid electrokinetic transport) without the need for large applied potentials. To determine the power requirements and energy consumption of both the membrane dissolution and electrokinetic ejection stages used here a Keithley 236 Source-Measure Unit was used

to monitor the current load. Over the course of the 7 seconds required to dissolve the membrane at an applied potential of 5.0 V, an average power load of 3.70 mW was recorded resulting in 26 mJ of energy consumed. Fig. 2.6 plots the power load (6a) and energy consumption (6b) for the same ejection voltages used in Fig. 2.4. The energy consumption was obtained by multiplying the average power load (Fig. 2.6a) by the time required to completely empty the well (Fig. 2.5). As can be seen for 3.0 V an average power load of 44 μW was measured resulting in a total energy consumption of 26 mJ. By comparison at 4.0 V the average power load was 497 μW resulting in 68 mJ of energy consumed. As can be seen from Fig. 2.6b, which plots the total energy required to empty the well as a function of applied voltage, there exists a clear minimum of around 20 mJ in the region between 3.0 V and 3.5 V. Note that this minimum is based on an interpolation of the quadratic curve fit used in Fig. 2.6b. The lowest actual measured power consumption was 22 mJ at 3.5 V. Although not optimal for rapid delivery, this region would be the best operational zone for low energy consumption. As can be seen from Fig. 2.6a the power load begins the increase quite dramatically after 3.5 V. This is partially due to the fact that power should vary with the square of the applied voltage (for fixed resistance) however there is also likely additional effects which contribute like ohmic heating. Ohmic heating would serve to decrease the well's resistivity and therefore increase the current load on the system resulting in a larger than squared dependence on applied voltage. The minimum energy load region observed here represents the regime before the power load begins to spike and after the time required to empty the well has begun to drastically decrease from that observed at lower applied potentials.

For comparison representative existing drug delivery dosing actuation systems [34] are shown in Table 2.1. As can be seen they typically require on the order of 100s of mW for operation or relatively high voltage. The device presented here represents a

good combination of low voltage requirements and power draw. Based on these results the electroactive microwell system developed here appears to be a good candidate for adding drug delivery functionality to next generation autonomous microsystems.

Table 2.1. Comparison of power consumption of dosing systems

Working principle	***V*** **(V)**	**Power (mW)**
Electrostatic micropump [35]	200	1
Thermo-pneumatic [36]	15	450
Magnetohydrodynamic micropump [37]	10	18
Bubble-type planar micropump [38]	40	1000
Ionic conductive polymer film micropump [39]	1.5	180
Electroactive microwell	**4**	**0.5**

2.4.3 Characterization of electrokinetic transport

To characterize the various electrokinetic transport processes involved in the ejection stage, a three-dimensional finite element model (FEM) of the system was constructed. The computational domain used here matched exactly that shown in Fig. 2.1a, comprising of both the well and a large exterior domain selected to be large enough to mimic the external environment. For reasons that will be expanded on later, the upper electrodes were also incorporated into the model.

Details of the modelling procedures and general assumptions are available in earlier works [40] and thus here we focus on the specifics of this implementation. For the purposes of this model, we assume that the solution electrical and thermophysical properties are the same inside and outside the well and thus the applied potential field, ϕ, can be modelled with a simple Laplacian

$$\nabla^2 \phi = 0 \tag{2.1}$$

Matching the experimental conditions as closely as possible, cathodic potentials were applied along the upper electrode and a ground (0V) potential was set along the bottom of the well. With the exception of the electrode domains, electrical insulation conditions were applied along all other boundaries ($\partial\phi/\partial\mathbf{n}=0$, where $\mathbf{n}$ is the surface normal). Figure 2.7 illustrates the potential field lines obtained from these simulations. All calculations shown here and below were implemented using the COMSOL finite element package.

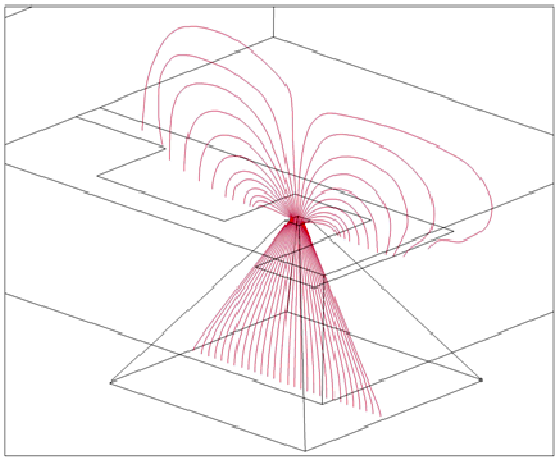

Figure 2.7. Computed electric field lines in electroactive microwell

The electroosmotic flow field, $\mathbf{v}$, was computed by solving the low Reynolds number incompressible Stokes flow equations,

$$\eta \nabla^2 \mathbf{v} - \nabla p = 0 \tag{2.2}$$

$$\nabla \cdot \mathbf{v} = 0 \tag{2.3}$$

(where η is the viscosity and p is the pressure) subject to electroosmotic slip, v_{eo}, conditions at four walls of microwell and the top surface of the device. The slip velocity was calculated using the Helmholtz-Smoluchowski equation $v_{eo} = -\varepsilon\zeta E/\eta$, where ε is the permittivity of the medium, ζ is the surface zeta potential and E is the field strength ($\boldsymbol{E} = -\nabla\phi$) evaluated tangential to the boundary. For the purposes of these simulations ζ = -60 mV was used, as has been reported for silicon dioxide surfaces under similar electrolyte conditions to those used in our experiments [40], due to the expected growth of a native oxide layer on the silicon after exposure to air. The remaining surfaces were assigned free slip ($\partial\mathbf{v}/\partial\boldsymbol{\tau}=0$, where $\boldsymbol{\tau}$ is the tangential to the surface), zero penetration ($\mathbf{v}\cdot\mathbf{n}=0$) boundary conditions.

Transient species transport was modelled using the modified convection diffusion equation,

$$\frac{\partial c}{\partial t} = D\nabla^2 c - (\mathbf{v} + \mathbf{v}_{ep})\cdot\nabla c \tag{2.4}$$

where c is the local species concentration, t is the time and D is the diffusion coefficient. The convective component from Eq. (3) comprises of both the bulk electroosmotic flow, $\mathbf{v}$ from Eq. (2a), and the electrophoretic velocity of the transported species evaluated using $\mathbf{v_{ep}} = \mu_{ep}\boldsymbol{E}$, where μ_{ep} is the electrophoretic mobility. For the polystyrene fluorescent microspheres used here the electrophoretic mobility was computed using $\mu_{ep} = \varepsilon\zeta/\eta$ with ζ = -40 mV [41].

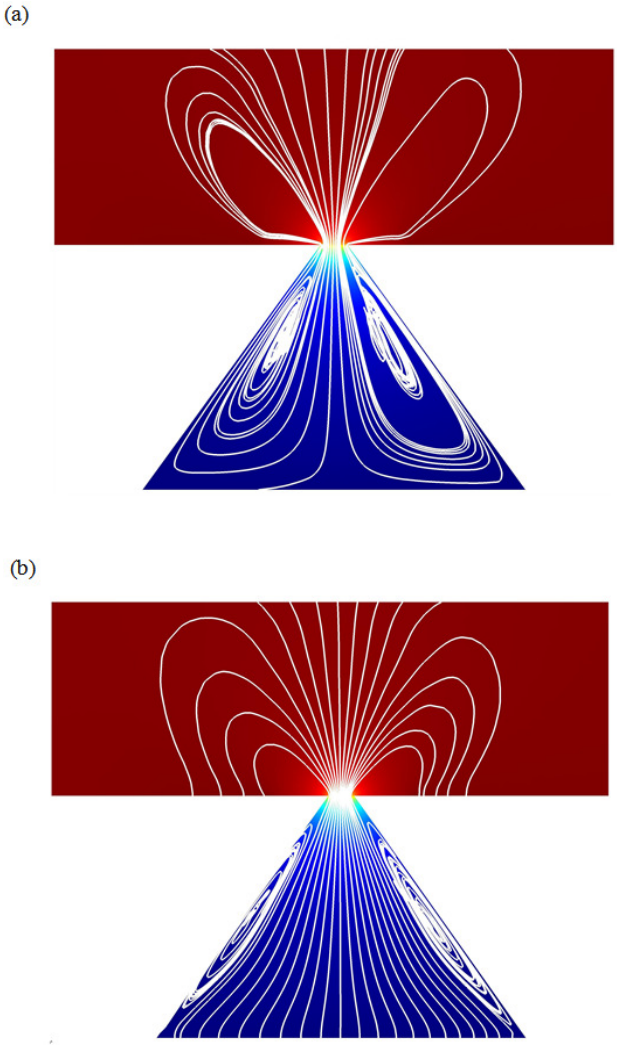

Figure 2.8. Finite element simulations of the transport process (a) Transport streamlines for pure electroosmosis (b) Streamlines when all electrokinetic effects are considered. Colour contours show applied potential ranging from blue (ground) to red (maximum potential).

Figure 2.8 shows a two dimensional cut view of the electrical potential distribution and transport streamlines ($\mathbf{v} + \mathbf{v}_{ep}$) during the ejection process. To better understand the ejection process we consider two cases: Fig. 2.8a, pure electroosmotic flow, and Fig. 2.8b, both electroosmotic and electrophoretic components. From Fig. 2.8a it can be seen that the applied potential induces a strong electroosmotic flow component very near the wall, dragging fluid from the external environment into the well. This

then displaces the contents of the well which is ejected through the middle of the outlet. The dragging of the fluid from the external environment back into the well is demonstrated experimentally in the second supplemental movie (chung_LOC_movie2.wmv). In this movie the motion of the tracer particles back into the well is clearly illustrated suggesting the flow mechanism described above is at qualitatively accurate.

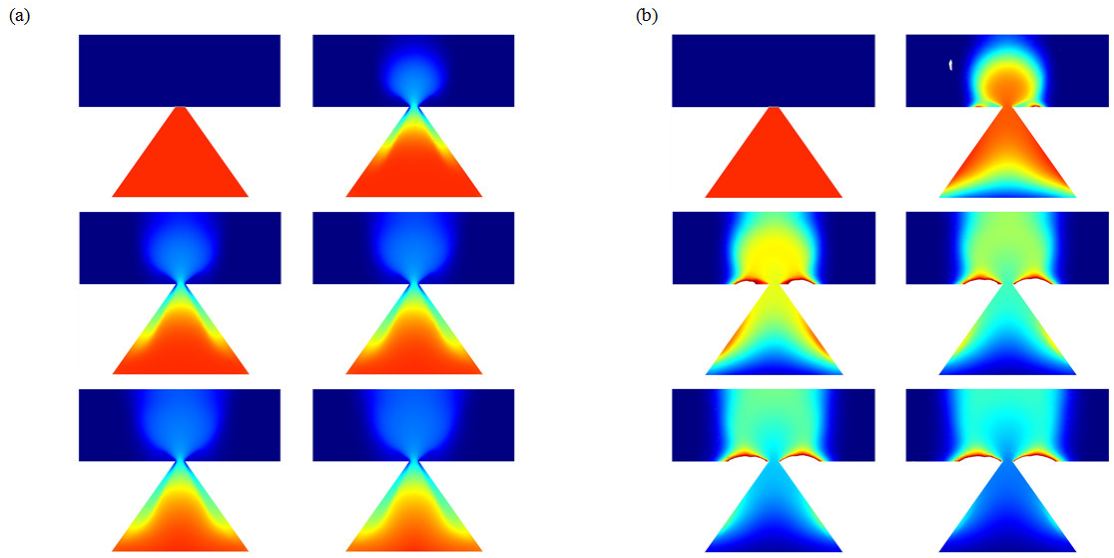

Figure 2.9. Finite element analysis of time-dependent species transport. Images show cut view of species concentration every 5 seconds up to 25 seconds after the ejection process (a) Electroosmosis only (b) Electrophoresis and electroosmosis.

This is also illustrated in Fig. 2.9a which plots the transient convection-diffusion solution, Eq. (3), in the well for a species with a diffusion coefficient equivalent to that of the polystyrene spheres used in the experiment and an applied potential of 3.5 V. When the electrophoretic component is included, Fig. 2.8b, the electroosmotic recirculation regions become confined to an area very near the wall. This is reflected in Fig. 2.9b where the much more rapid ejection of the contents is apparent since the electrophoretic ejection process dominates. Note that while the majority of the well

contents are emptied after 25 seconds, the electroosmotic flow tends to pull back into the well some of the ejected species resulting in the more concentrated regions along the wall, most evident in the final two timeframes. This accounts for the experimental observation that while the initial dispersion occurs quite rapidly (Fig. 2.3) the amount of time to completely empty the well is much longer (Fig. 2.5). Since these simulations suggest that the majority of the contents are ejected during the first 20 seconds to 25 seconds the empty times shown in Fig. 2.5 represent an upper limit.

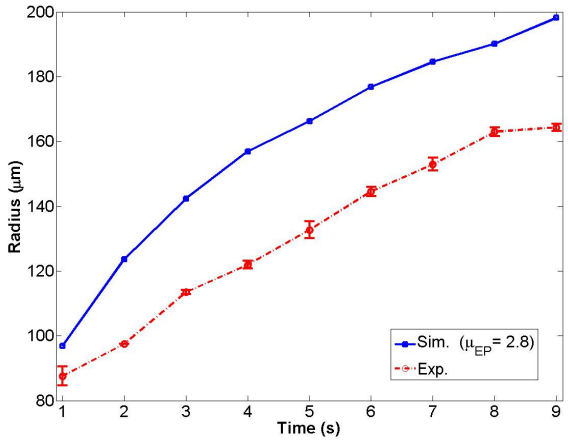

Figure 2.10. Plot comparing experimental and numerical results on the 3.5 V case.

To further validate the numerical results we compare the dispersion radius measured experimentally with that obtained from the simulations shown in Fig. 2.9b. The results are shown in Fig. 2.10 for the 3.5 V case. As can be seen the trends between the two cases are very similar with the numerical results tending to over-predict the dispersion radius over the first 8 seconds of the process. The reason for this is likely due to uncertainties in the electrophoretic mobility of the polystyrene beads in the buffer solution used here and an over estimate of the applied potential (we ignored any potential drops along the leads or at the solution/electrode interface). In

general however neither of these would affect the overall transport mechanisms described above.

2.5 Summary and conclusion

We have demonstrated here an implantable, low power and rate controllable drug delivery device incorporating an electroactive microwell structure. This approach serves to actively repel the drugs inside the well using a combination of electroosmotic and electrophoretic effects which are controlled through an electric potential applied between the top and bottom of the well. The contents dispersal rate and energetic consumption of the device were characterized experimentally. It was found that the ejection process could be completed in less than 2 minutes or using as little as 20 mJ of energy, both of which compared favourably to the state of the art. Detailed 3D numerical simulations were used to model the electrokinetic transport involved in the ejection process. In addition to providing a physical insight in to the transport mechanism, the simulations revealed that the majority of the contents are ejected early in the process.

2.6 Acknowledgement

This work was supported by the Defense Advanced Research Project Agency, Microsystems Technology Office, Hybrid Insect MEMS (HI-MEMS) program, through the Boyce Thompson Institute for Plant Research. Distribution unlimited. Fundamental research exempts from prepublication controls. We would also like to acknowledge helpful discussions from Bernardo Cordovez and Likun Chen.

REFERENCES

1. Tanaka, M., *An industrial and applied review of new MEMS devices features.* Microelectron. Eng., 2007. **84**(5-8): p. 1341-1344.
2. Gad-el-Hak, M., *MEMS : design and fabrication*. 2006, Boca Raton: CRC Press.
3. Beeby, S.P., M.J. Tudor, and N.M. White, *Energy harvesting vibration sources for microsystems applications.* Measurement Science & Technology, 2006. **17**(12): p. R175-R195.
4. Warneke, B., M. Last, B. Liebowitz, and K.S.J. Pister, *Smart dust: Communicating with a cubic-millimeter computer.* Computer, 2001. **34**(1): p. 44-+.
5. Bashir, R., D. Akin, R. Gómez, H. Li, W.-J. Chang, and A. Gupta. *From bioMEMS to bionanotechnology: Integrated biochips for the detection of cells and microorganisms*. in *Proceeding of material research society*. 2003.
6. Bhattacharya, S., J.S. Jang, L.J. Yang, D. Akin, and R. Bashir, *Biomems and nanotechnology-based approaches for rapid detection of biological entities.* Journal of Rapid Methods and Automation in Microbiology, 2007. **15**(1): p. 1-32.
7. Bhushan, B., *Nanotribology and nanomechanics of MEMS/NEMS and BioMEMS/BioNEMS materials and devices.* Microelectronic Engineering, 2007. **84**(3): p. 387-412.
8. Madou, M., J. Zoval, G.Y. Jia, H. Kido, J. Kim, and N. Kim, *Lab on a CD.* Annual Review of Biomedical Engineering, 2006. **8**: p. 601-628.

9. Dittrich, P.S. and A. Manz, *Lab-on-a-chip: microfluidics in drug discovery.* Nature Reviews Drug Discovery, 2006. **5**(3): p. 210-218.

10. Erickson, D. and D. Li, *Integrated microfluidic devices.* Analytica Chimica Acta, 2004. **507**(1): p. 11-26.

11. Abgrall, P. and A.M. Gue, *Lab-on-chip technologies: making a microfluidic network and coupling it into a complete microsystem - a review.* Journal of Micromechanics and Microengineering, 2007. **17**(5): p. R15-R49.

12. Yi, C.Q., C.W. Li, S.L. Ji, and M.S. Yang, *Microfluidics technology for manipulation and analysis of biological cells.* Analytica Chimica Acta, 2006. **560**(1-2): p. 1-23.

13. Eliakim, A.R., *Video capsule endoscopy of the small bowel (PillCam SB).* Current Opinion in Gastroenterology, 2006. **22**(2): p. 124-127.

14. Dickman, R. and R. Fass, *Ambulatory esophageal pH monitoring: New directions.* Digestive Diseases, 2006. **24**(3-4): p. 313-318.

15. Orive, G., R.M. Hernandez, A.R. Gascon, A. Dominguez-Gil, and J.L. Pedraz, *Drug delivery in biotechnology: present and future.* Current Opinion in Biotechnology, 2003. **14**(6): p. 659-664.

16. Maloney, J.M., S.A. Uhland, B.F. Polito, N.F. Sheppard, C.M. Pelta, and J.T. Santini, *Electrothermally activated microchips for implantable drug delivery and biosensing.* Journal of Controlled Release, 2005. **109**(1-3): p. 244-255.

17. Ahmed, A., C. Bonner, and T.A. Desai, *Bioadhesive microdevices with multiple reservoirs: a new platform for oral drug delivery.* J. Control. Release, 2002. **81**(3): p. 291-306.

18. Grayson, A.C.R., R.S. Shawgo, A.M. Johnson, N.T. Flynn, Y.W. Li, M.J. Cima, and R. Langer, *A BioMEMS review: MEMS technology for*

physiologically integrated devices. Proceedings of the IEEE, 2004. **92**(1): p. 6-21.

19. Kim, M.S., K.S. Seo, H. Hyun, S.K. Kim, G. Khang, and H.B. Lee, *Sustained release of bovine serum albumin using implantable wafers prepared by MPEG-PLGA diblock copolymers.* International Journal of Pharmaceutics, 2005. **304**(1-2): p. 165-177.
20. Arky, R., ed. *Physician's Desk Reference* 1998, Medical Economics Company: Montvale, NJ, USA.
21. Arky, R., ed. *Physician's Desk Reference* 1998, Medical Economics Company: Montvale, NJ, USA. 3139.
22. Santini, J.T., M.J. Cima, and R. Langer, *A controlled-release microchip.* Nature, 1999. **397**(6717): p. 335-338.
23. Scheidt, R.A., J.T. Santini, Jr., A.C. Richards, A.M. Johnson, A. Rosenberg, M.J. Cima, and R. Langer. *Microchips as implantable drug delivery devices*. in *Microtechnologies in Medicine and Biology, 1st Annual International, Conference On. 2000*. 2000.
24. Santini, J.T., A.C. Richards, R. Scheidt, M.J. Cima, and R. Langer, *Microchips as controlled drug-delivery devices.* Angewandte Chemie-International Edition, 2000. **39**(14): p. 2397-2407.
25. Cordovez, B., D. Psaltis, and D. Erickson, *Trapping and storage of particles in electroactive microwells.* Applied Physics Letters, 2007. **90**(2).
26. Lee, K.J., K.A. Tosser, and R.G. Nuzzo, *Fabrication of stable metallic patterns embedded in poly(dimethylsiloxane) and model applications in non-planar electronic and lab-on-a-chip device patterning.* Advanced Functional Materials, 2005. **15**(4): p. 557-566.

27. Ling, T.G.I., M. Beck, R. Bunk, E. Forsen, J.O. Tegenfeldt, A.A. Zakharov, and L. Montelius, *Fabrication and characterization of a molecular adhesive layer for micro- and nanofabricated electrochemical electrodes.* Microelectronic Engineering, 2003. **67-8**: p. 887-892.

28. Fitzsimons, E. and J. Sendroy, *Distribution of Electrolytes in Human Blood.* J. Biol. Chem., 1961. **236**(5): p. 1595-1601.

29. Frankenthal, R.P. and D.J. Siconolfi, *The Anodic Corrosion of Gold in Concentrated Chloride Solutions.* J. Electrochem. Soc., 1982. **129**(6): p. 1192-1196.

30. Voskerician, G., M.S. Shive, R.S. Shawgo, H.v. Recum, J.M. Anderson, M.J. Cima, and R. Langer, *Biocompatibility and biofouling of MEMS drug delivery devices.* Biomaterials, 2003. **24**(11): p. 1959-1967.

31. Richardson Jr, R.R., J.A. Miller, and W.M. Reichert, *Polyimides as biomaterials: preliminary biocompatibility testing.* Biomaterials, 1993. **14**(8): p. 627-635.

32. Belanger, M.C. and Y. Marois, *Hemocompatibility, biocompatibility, inflammatory and in vivo studies of primary reference materials low-density polyethylene and polydimethylsiloxane: A review.* Journal of Biomedical Materials Research, 2001. **58**(5): p. 467-477.

33. Henry, S., D.V. McAllister, M.G. Allen, and M.R. Prausnitz, *Microfabricated microneedles: A novel approach to transdermal drug delivery.* Journal of Pharmaceutical Sciences, 1998. **87**(8): p. 922-925.

34. Tsai, N.C. and C.Y. Sue, *Review of MEMS-based drug delivery and dosing systems.* Sensors and Actuators a-Physical, 2007. **134**(2): p. 555-564.

35. Zengerle, R., J. Ulrich, S. Kluge, M. Richter, and A. Richter, *A bidirectional silicon micropump.* Sensors and Actuators A: Physical, 1995. **50**(1-2): p. 81-86.

36. Schomburg, W.K., J. Vollmer, B. Bustgens, J. Fahrenberg, H. Hein, and W. Menz, *Microfluidic components in LIGA technique.* Journal of Micromechanics and Microengineering, 1994. **4**: p. 186-191.

37. Jang, J.S. and S.S. Lee, *Theoretical and experimental study of MHD (magnetohydrodynamic) micropump.* Sensors and Actuators a-Physical, 2000. **80**(1): p. 84-89.

38. Zahn, J.D., A. deshmukh, A.P. Pisano, and D. Liepmann, *Continuous On-Chip Micropumping for Microneedle Enhanced Drug Delivery.* Biomedical Microdevices, 2004. **6**(3): p. 183-190.

39. Guo, S., T. Nakamura, T. Fukuda, and K. Oguro. *Development of the micro pump using ICPF actuator*. in *Proc. IEEE ICRA*. 1997.

40. Erickson, D. and D. Li, *Microscale Flow and Transport Simulation for Electrokinetic and Lab-on-Chip Applications*. Biomems and Biomedical Nanotechnology, Volume IV: Biomolecular Sensing, Processing and Analysis ed. R. Bashir and S. Wereley. 2006: Kluwer Academic Publishing.

41. Kirby, B.J. and E.F. Hasselbrink, *Zeta potential of microfluidic substrates: 2. Data for polymers.* Electrophoresis, 2004. **25**(2): p. 203-213.

CHAPTER 3

ENGINEERING INSECT FLIGHT METABOLICS USING IMMATURE STAGE IMPLANTED MICROFLUIDICS*

3.1 Abstract

Small-scale insect inspired aircraft represent a promising approach to downscaling traditional aircraft designs. Despite advancements in microfabrication however it has proven difficult to fully replicate the mechanical complexities that enable these natural systems. As an alternative, recent efforts have used implanted electrical, optical or acoustic microsystems to exert direct control over insect flight. Here we demonstrate, for the first time, a method of directly and reversibly engineering insect flight metabolics using immature stage implanted microfluidics. We present our technique and device for on-command modulation of the internal levels of L-Glutamic and L-Aspartate acids and quantify the resulting changes in metabolic activity by monitoring respiratory CO_2 output. Microfluidic devices implanted 1 to 2 days prior to insects' emergence achieved survivability and flight-capable rates of 96% and 36%, respectively. Behavior ranging from retarded motion to complete, reversible paralysis, over timescales ranging from minutes to hours is demonstrated. Such a system could form the basic component of an eventual artificial insect nervous system.

*Reproduced by permission of the Royal Society of Chemistry with permission from Aram J. Chung and David Erickson, "Engineering insect flight metabolics using immature stage implanted microfluidics", *Lab-on-a-Chip*, **9**, 669-676 (2009) DOI: 10.1039/B814911A
The original publication is available at:
http://pubs.rsc.org/en/Content/ArticleLanding/2009/LC/b814911a

3.2 Introduction

Micro-air-vehicles (MAVs) are small aircraft with a maximal wingspan of approximately 15 cm and flight speed below 10 m/s [1]. Such systems are of significant interest to the military, industrial and academic communities largely as a result of their potential to perform bio-chemical sensing in hazardous locations, long-range surveillance and stealthy reconnaissance [2]. Rapid progress in micro-electro-mechanical-systems (MEMS) [3, 4] technology (including power generation, energy storage, communications, sensing, and subcomponent assembly) has enabled further miniaturization and improved performance in these systems, however to date they still suffer from small payload capacity, large size or poor flight stability, and short operational time [5-7]. The latter of these is a particularly important limitation and results from the technical challenges involved in creating a compact and lightweight high-density power source with a sufficiently long lifetime [8, 9].

As a result of the challenges in downscaling traditional aircraft designs, a number of researchers have looked to the natural world to develop bio-inspired MAVs [10]; for instance mimicking the body shapes, wing shapes and flapping patterns that are present in nature [11-16]. Emulating the vast complexity of nature however has proven to be an extremely difficult engineering problem and thus man-made systems are unlikely to outperform natural flyers (particularly in terms of flight dynamics and power efficiency) in the near future. Flying insects, for example, have evolved an aerodynamic shape that allows them to remain stable in turbulent air conditions and a complex wing flapping motion with an extremely energy efficient stroke [17]. Many insects spend the majority of their pre-adult lives constantly feeding in order to store sufficient energy (in the form of glucose) to sustain them throughout their adult lives. Additionally, large flying moths such as *Manduca sexta* or *Ascalapha odorata* are able

to carry payloads well in excess of one gram without significant degradation of their natural flight mechanics [18, 19].

The ability of flying insects to meet or exceed the performance capabilities of current MAVs has lead to recent interest in integrating MEMS technology with these living systems in order to exert some level of flight control over them. Bozkurt *et al*. [20, 21] for example reported direct electrical control over the flight of a *Manduca sexta* (*M. Sexta*) moth by implanting microfabricated electrical probes at the pupal stage. In that work the probes were used to send biphasic electrical pulses into the flight muscles enabling effective control over wing motion. They demonstrated down- and up-stroke actuation of each wing separately, which affected the flight direction of moth. Also using electrical stimulation, Sato *et al.* [22] demonstrated control over beetle flight using an implanted and tetherless microsystem and Ando and Kanzaki [23] presented longitudinal control in freely flying *hawkmoths*. Recently, Ritzmann *et al*. [24] demonstrated the possibility of controlling the locomotor activity of a cockroach using brain nerve group stimulation. With the aim of developing a technique for powering these devices, Reissman and Garcia [25] recently presented a power harvesting system aimed at extracting energy from the natural vibrations that occur during insect flight using surgically inserted piezoelectric materials and inductor-coils.

Here we demonstrate a more intimate method of exerting control over insect flight, exploiting the use of immature stage implanted microfluidics to reversibly engineer the rate of flight metabolism. In this paper we present our technique for modulating the internal levels of a series of different chemicals known to affect the insect nervous system (specifically L-Glutamic and L-Aspartate acids) and thereby demonstrate dynamic control over metabolic output using microfluidics. In this study we use *M. sexta* moths as our model species due to its large potential payload capacity and

excellent flight capability. The insect has a large body mass (~2 g), a wingspan of 10 cm and a potential flight range of kilometers. In addition to demonstrating the technique, we present here details of the implantation surgeries, injection experiments and microfluidic device. Changes in the rate of metabolic activity are quantified using a novel flight stimulation apparatus and by monitoring changes in CO_2 output. We demonstrate the ability to provide rapid chemical paralysis (from full flight activity to no motion) which lasts for several hours. Partial insect recovery is observed after 3 hours with full recover in less than 22 hours. We propose that that system is the first step towards the development of an artificial insect nervous system.

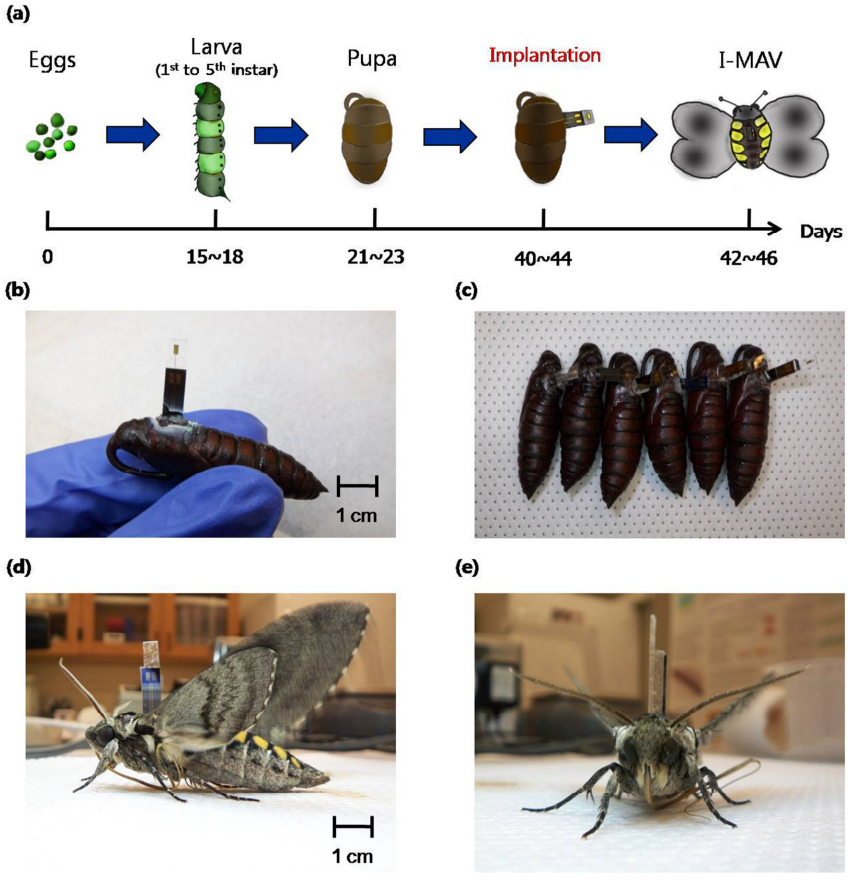

Figure 3.1. (a) A schematic view of the developmental stages of a *M. sexta* moth. Insertion of the microfluidic device is conducted at the pupal stage of development. (b and c) Device insertion surgeries are done in the dorsal thorax with the microfluidic

chip inserted approximately 5 mm into the pupa. Then wound is sealed with biocompatible glue. (d and e) *M. sexta* moth successfully emerged with an implanted device.

3.3 Materials and methods

In this materials and methods section we begin with a detailed description of the implantation, injection process, device fabrication, and assembly procedure. The final subsection describes the respirometry system used to determine resting metabolic rate.

3.3.1 Implantation process

The microfluidic devices were implanted in *M. sexta* pupae, approximately 1 or 2 days before the adult insects were scheduled to emerge. Prior to the surgery, the pupae were placed on ice for approximately 25 minutes to minimize their movement and lower the inner body pressure. Using a sterilized scalpel, the dorsal exoskeleton and body skin were cut away and the device was partially implanted into the thorax near the dorsolongitudinal flight muscles (dl muscle). During implantation the device is gently inserted into thorax to minimize the disruption to the aorta which passes nearby. To seal the wounds after surgery a viscous and fast curing biocompatible glue (Loctite® 454: ISO 10993, Henkel) was used. The rapid curing of the glue prevented penetration into body.

3.3.2 Injection process

A number of different chemicals were tested to gauge their effectiveness in generating the desired physiological response in given the limitations outlined in the

text. To gauge their performance direct injection experiments were conducted by first folding the wings then inserting a needle (700 series syringes, Hamilton) containing the test drug into different locations along the insect (specifically the dorsal/ventral thorax, the head and every segment of the abdomen). The following chemicals were tested in various different concentrations and dissolved with 10 mM phosphate buffered saline (pH 7.4): γ-aminobutyric acid (Sigma-Aldrich), Taurine (Sigma-Aldrich), β-alanine (Sigma-Aldrich), Atropine (Sigma-Aldrich), Malathion (Sigma-Aldrich), Scorpion venom (Hadrurus arizonensis, Spider Pharm), L-Aspartate acid potassium salt hemihydrates (Sigma-Aldrich), and L-Glutamic acid potassium salt monohydrate (Sigma-Aldrich). The insect response was gauged visually.

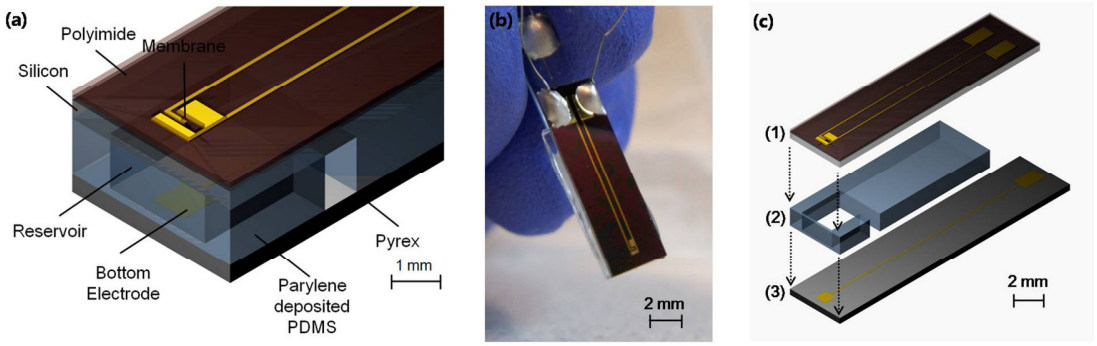

Figure 3.2. (a) Schematic of the electroactive microwell drug delivery system developed here. (b) Fabricated and assembled electrokinetic microfluidic devices used here. The devices measure 4 x 22 x 2.5 mm and weigh 250 mg. (c) Microchip assembly: (1) an upper silicon based structure, (2) Parylene deposited PDMS reservoir, and (3) electrically functionalized Pyrex bottom substrate are bonded together by the plasma treatment.

3.3.3 Microfabrication

The microfluidic device presented here consists of three layers; silicon layer contained the microwell and the upper set of electrodes, Parylene deposited PDMS

macro reservoir, and a Pyrex bottom substrate which served to seal the reservoir and hold the lower electrode. The top silicon layer was fabricated using the same methods as described previously by Chung *et al*. [26]. Briefly, silicon nitride was deposited on both sides of the (100) n-doped silicon wafer and the backside was etched to define the location of the wells. Following this, gold electrodes were evaporated and patterned, and then Polyimide dielectric layer was spun and etched. The microwells were then defined by immersing the wafer in KOH and remaining silicon nitride underneath gold membrane was removed by reactive ion etching. To create the PDMS macro reservoir, a 10:1 (base: linker) mixture of PDMS was cured at 80°C for 60 minutes, and the final structure was cut out, and then placed on the microscope slide glass. Transparent 3M scotch® tape was attached on top of the PDMS structure which allows depositing Parylene only at the sidewalls of the reservoir. The PDMS surface was modified by oxygen plasma prior to the Parylene deposition in order to improve the adhesion between Parylene and PDMS [27, 28]. Following this, 1 μm thick Parylene (Parylene C, Specialty Coating Systems) was deposited using Parylene deposition tool (PDS 2010 Labcoter, Specialty Coating Systems), and then the scotch tape was removed. Lastly, to fabricate the bottom Pyrex layer, 10 nm/100 nm layers of titanium/gold were evaporated and patterned using image reversal contact lithography process to form the electrode pads and leads.

3.3.4 Microchip assembly

The upper (silicon), the middle (PDMS), and the bottom (Pyrex) substrates were placed in conformal contact with each other and bonded together by the plasma treatment and cured in the 80°C oven for overnight. After the microchip assembly, a PEG (Poly-ethylene glycol) film was coated on the entire surface of the assembled

device using molecular vapor deposition tool (MVD 100, Applied MicroStructures) to minimize the physiological response since PEG deposition is a well known biocompatible surface molecular modification [29]. The microwell and macro reservoir were filled with different chemicals using micro-liter syringe (NanoFilTM, World Precision Instrument) through the slit, sealed with biocompatible wax (Butler GUM, Sunstar). The final full loaded device weighs approximately 0.3 g which is the 15% of the total insect's body mass and the payload capacity.

3.3.5 Respirometry to determine resting metabolic rate

Metabolic rates were measured using a flow-through respirometry chamber. The insect ventral thorax was glued onto a narrow beam and the stage was mounted inside of the chamber. Dry, CO_2 free air was went through the 3-liter respirometry chambers first for 5 minutes to set up the baseline for the resting metabolic rate, and then the insect was mechanically stimulated to initiate a flight response (which will be described more in the "Quantification of the metabolic rate" section below). To measure the continuous changes in CO_2 level reflective of the metabolic output of the insect, all the air from the jar passed through the carbon dioxide analyzer (Li-Cor 6252, Lincoln), and data were collected.

3.4 Results and discussions

3.4.1 Implantation

As shown in Fig. 3.1, the microfluidic device is partially implanted within the *M. sexta* dorsal thorax at the pupal stage of development. Consistent with the ideas

described in Bozkurt *et al*. [20, 21] and used in Paul *et al.* [30], implantation is done at an immature developmental stage. The reason for this is that wounds which occur during the implantation surgery are known to heal better during the natural molting process [31, 32]. It is expected that this results in a smaller physiological footprint, since the device has been carried through a greater portion of the insect's development. Earlier works [22-24, 33] have relied on adult stage implantations. Fig. 3.1a outlines the *M. sexta* lifecycle, illustrating the stage in its development at which the implantations done here were conducted. To determine the optimal implantation strategy that minimizes the physiological footprint and maximizes survivability, we performed a number of insertion experiments varying the timing of the implantation (see Fig. S3.1 in supplemental material) and location (see Fig. S3.2 in supplemental material). We chose to conduct implantation at two different time periods, relatively early (approximately 1 week prior to emergence) and relatively late (1-2 days prior to emergence). As shown in the supplemental material test implants were conducted at numerous different parts of the body. The impact of the implants was gauged visually post emergence by noting which insects exhibited malformed extremities (wings) or poor flight characteristics. We define a system with "poor flight capability" as one which exhibits some retarded ability to flap its wings. These problems tended to be caused by two main factors. Although most moths survived the insertion surgeries under healthy conditions, in many cases the implanted devices hindered the adult moths' ability to pull themselves out from the cuticle during emergence. The result was deformed wings clearly unable to be used for flight (see Fig. S3.3). The second causes tended to be damage to the dorsolongitudinal flight muscles during implantation. This limited the wing stroke which could be exerted during flight.

Table 3.1. Comparison of survivability rate depending on the implantation date

Survivability Data	**7-8 days**	**1-2 days**
Survivability rate	93.75%	**96.0%**
Flight-capable insect rate	12.5%	**36.0%**
Sample size	32	50

Based on these results, we found that the dorsal thorax is the best location for implantation, and 1 to 2 days prior to the insects' emergence is the best timing for our current design as indicated in Table 3.1. A movie illustrating the implantation surgery and developmental process is available as supplemental material (see chung_LOC_movie1.wmv) and Fig. 3.1d and 1e show a successfully emerged flight-capable insect. Paul *et al.* [30] presented results on inserting of silicon chips in the pupal stage with the flight-capable moths rate of 87.5%. The devices implanted here were much larger and heavier devices resulting in survivability and flight-capable insect rates of 96% and 36%, respectively (Total sample size was 50). As can be seen in Table 3.1, the survivability remains high in both cases suggesting that the implantation date does not critically affect the insects' life. The flight-capable rate however strongly depends on the insertion date with the latter implants yielding more flight ready insects. The increase in flight ready rate observed for the later implantations is likely due to the fact that since more of the insect is formed, the likelihood of damaging the flight muscles is less than in the earlier stage implants. With the more developed insect's the surgery could also be performed more precisely. At least part of the relatively low flight ready rate for the early stage implants is likely due to the relatively large size of the microfluidic device relative to that of the insect (as shown in Fig. 3.1). We are currently working on designs which reduce the physiological footprint of the device.

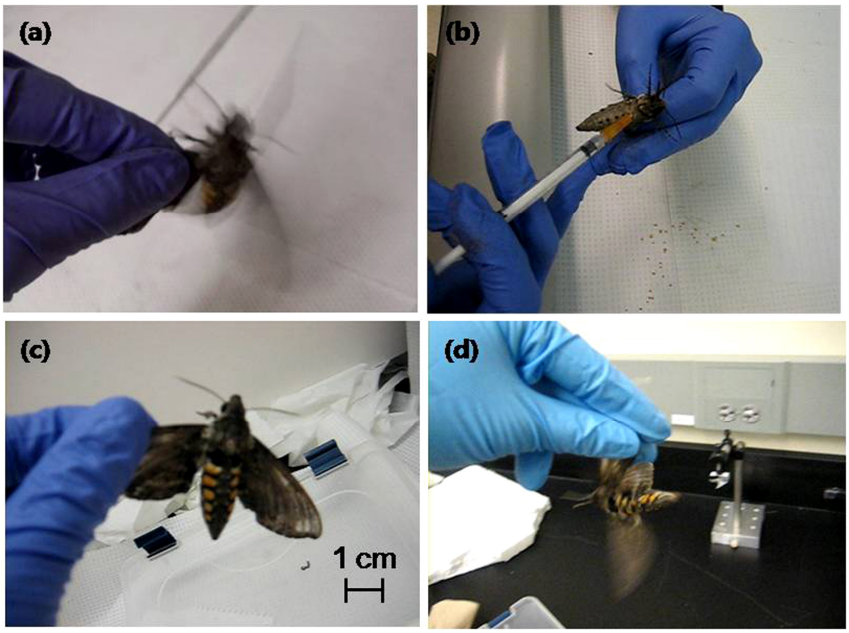

Figure 3.3. Injection procedure. (a) Prior to injection the insect was stimulated to gauge its baseline activity level. (b) Various chemicals were injected into the thorax to determine the dosage effects on the degree and length of insect temporary paralysis. (c) The moth paralyzes about a minute after injecting 5 μL of LGA. (d) In a successful test, after two to three hours, the moth recovers sufficiently to flap its wings.

3.4.2 Characterization of physiological response to chemical injection

Direct injection experiments were conducted to determine the optimal drug, dosage and delivery site for inducing the fastest physiological response and most complete but reversible impact on the level of observable insect activity. Fig. 3.3 shows the injection procedure (see also chung_LOC_movie2.wmv). The maximum capacity of our microfluidic chip was 15 μL and thus this was considered the upper limit for our injection volumes.

For the species of interest here, there are three candidate injection sites: the head, thorax and abdomen. The microfluidic device used here is larger than insect's head and thus this was removed as a candidate. Numerous injections were carried out at various positions along the abdomen. It was generally observed that physiological

response times were slower and the required dosage was higher (approximately 5 times) than for similar injections made in the thorax. We expect that the rapid response was a result of the proximity of the central nervous system (CNS) and heart (aorta) to the thorax injection site. As such the thorax was selected as the optimal injection/implantation site. Once the injection site was localized a large number of different chemicals and dosages were tested including components of spider, wasp and scorpion venom, and some insecticides.

The chemicals (L-Glutamic acid (LGA), L-Aspartate acid (LAA), γ-aminobutyric acid (GABA), Taurine and β-alanine) that were found to enable successful reanimation of the insect were the neurotransmitters that form the major/minor components of many spider and wasp venoms. We selected these chemicals because they tended to reversibly paralyze the insect by acting on the neuronal receptors, neuronal ion channels or synaptic membrane [34]. For example, GABA affects the insect's chloride ion channel to induce immobilization and LGA/LAA influences the synaptic membrane, binding site and physiologic receptors to have paralysis [34, 35]. The reversibility of the inhibition can be explained in terms of the effect of the venom on the site which does not damage or destruct the synaptic membranes (reversed by a membrane dilution-washing procedure) [35]. The excitation, therefore, decreases as time goes so that the reanimation of the activity can be found as we observed. The insecticide Malathion was found to instantly kill the insect even in small doses and thus was not considered a useful candidate for further study.

Table 3.2. List of chemicals injected into the thorax for immobilization

Chemical Type (Concentration)	**Minimum Volume**	**Remark**
LAA (11.11 M)	> 5 μL	Successful Reanimation
LGA (5.9 M)	> 5 μL	Successful Reanimation
GABA (10 M)	> 20 μL	Successful Reanimation
Taurine (0.5 M)	> 100 μL	Successful Reanimation
β-alanine (3 M)	> 100 μL	Successful Reanimation
Malathion (1.23g/L)	< 1 μL	Insect did not Survive
Atropine (N/A)	N/A	Insoluble in PBS
Hadrurus arizonensis (N/A)	N/A	Insoluble in PBS

Table 3.2 gives details of chemicals used, the minimum volume required to achieve paralysis and remarks on the ability of the insect to recover (all injections done in the thorax). As can be seen, the approach most effective at retarding insect motion was a 5 μL solutions of 5.9 M LGA and 11.1 M solution of LAA (both chemicals are excitatory transmitters at insect skeletal neuromuscular junctions [36]). These concentrations represented the saturation concentrations for these chemicals. In both cases within a minute of injection, the insect was immobilized for approximately 2 hours, after which it regained its pre-injection activity level (chung_LOC_movie2.wmv).

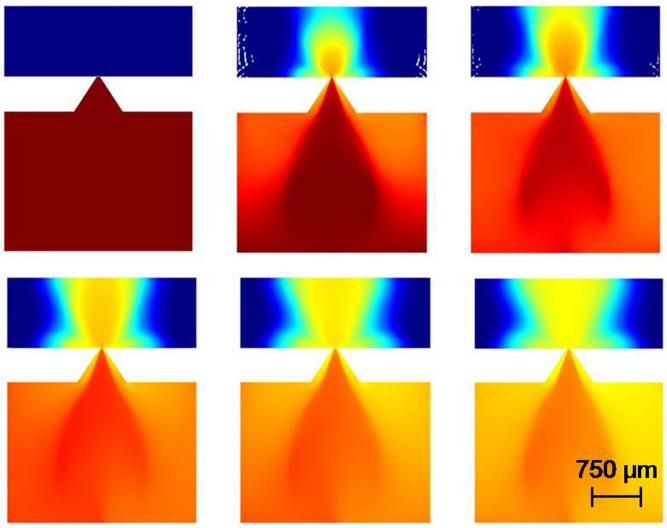

Figure 3.4. To illustrate the electrokinetic transport processes involved in the ejection stage, a finite element analysis of time-dependent species transport of the system is shown. Images show cut view of species concentration every 60 seconds up to 300 seconds after the ejection process when 15 V is applied. In the color scheme shown here, the blue contours represent lower concentrations and the red contours higher ones.Computed electric field lines in electroactive microwell

3.4.3 Electrokinetic drug delivery device

The microfluidic device structure used here is a modification of that presented by Chung *et al*. [26], which exploited the same electrochemical dissolution technique and electroactive ejection schemes. In the first stage, an electric potential is applied between two electrode pads on top of the microchip serving to electrochemically dissolve the membrane. To electrokinetically eject the contents from the reservoir, in the second stage a potential field is applied between one of the upper electrodes and that on the Pyrex bottom substrate. As described in detail in Chung *et al.* [26], the technique is based on exploiting highly localized electrokinetic transport to rapidly exchange the contents of the reservoir with the external environment. The use of electrokinetic transport allows for a significant reduction in the amount of time

required to eject the well contents over earlier diffusive transport based devices [37] (from hours to minutes), simplifies device design since only electrical components are required, and minimizes the rate amount of energy required per injection. As illustrated in Fig. 3.2, compared to our previous design [26] this device had an additional Parylene coated on-board poly(dimethylsiloxane), PDMS, reservoir to increases the injectable volume from 100 nL to approximately 15 μL. Due to water vapor permeability of the PDMS [38], Parylene was deposited on the sidewalls of the PDMS reservoir. To improve the mechanical stability of the device, Pyrex glass was used as the bottom layer (as opposed to PDMS). These latter two improvements resulted in significant improvements in device lifetime (earlier designs had a lifetime of approximately 5 days). Long term tests of the device were not conducted however it was found that in all cases they remained operable for at least the expected lifetime of the insect.

To illustrate the electrokinetic transport processes involved in the ejection stage, a finite element model of the system was constructed and simulated using the COMSOL finite element package. The computational domain used here matched exactly that shown in Fig. 3.2, comprising of both the well, PDMS reservoir and an exterior domain. Details of the modeling procedures and general assumptions are available in earlier works [26] and thus here we focus on the specifics of this implementation. Fig. 3.4 shows a two dimensional cut view of the transient convection-diffusion solution during the ejection process. To mimic the actual ejection process we consider pure electroosmotic flow. From Fig. 3.4 it can be seen that the applied potential induces a strong electroosmotic flow dragging fluid from the external environment into the reservoir. This then displaces the contents of the reservoir which is ejected through the middle of the outlet. Note that although some of it remains for the entire duration of the ejection process, much of the contents are ejected in the early stages. As we

will show in the following section the initial discharge in the first 90 seconds is sufficient to observe a response.

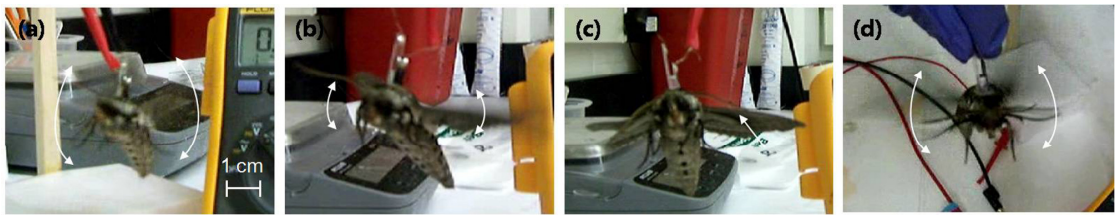

Figure 3.5. Microfluidically modulated insect activity (a) The overhanging boom supports the insect in midair allowing it to flap its wings unimpeded (b) Actuation of the drug delivery device occurs in two stages. In the first stage an electric potential is applied between two electrode pads on top of the microchip serving to electrochemically dissolve the membrane. To electrokinetically eject the contents from the reservoir, in the second stage a potential field is applied between one of the upper electrodes and that on the Pyrex bottom substrate. Due to the ejection of the drug (here LGA), the activity of the wing motion decreases. (c) Insect fully immobilized by LGA in 90 seconds after 2nd stage command is issued. (d) After one hour and 20 minutes, the moth is again able to flap its wings.

3.4.4 Demonstration of flight metabolism control using implanted microfluidics

Based on the results of the insertion experiments, the microfluidic devices were implanted in *M. sexta* pupae, approximately 1 or 2 days before the adult insects were scheduled to emerge. On-chip reservoirs were filled with one of three different chemicals, LGA, LAA, and phosphate buffered saline (PBS) buffer solution which served as a negative control. Flight metabolism control experiments and the quantification which will be described below were conducted only on moths which were capable of flight after emergence. A typical experiment is shown in Fig. 3.5, where as can be seen, the electrical leads from the device were connected to thin copper wires which lead to an overhanging boom supporting the insect in midair. All insects received only one injection (no multiple injection experiments were conducted). When a dosage command was issued, the two stage injection process (described

above) was initiated. We applied 15 V for 4 minutes and 20 V for 4 minutes for membrane dissolution and electrokinetic ejection stages, respectively. For both LGA and LAA a dramatic reduction in the wing motion (*i.e.* rate and amplitude of flapping strokes) was observed, 90 seconds after the 2nd stage command was issued. No observable difference was found for the PBS ejection experiments. In the negative control case the device was excised to visually confirm that it had been actuated. During the ejection process, the applied potentials may have lead to some ohmic heat generation which could have affected the potency of the chemicals used during the injection process. Though we have not fully characterized this, we do not expect that this is significant since the results of the device and manual ejections yielded similar results. After the discharging of the applied potential, the drug-induced immobilization lasted one hour and 20 minutes, after which the moths regained activity level (see chung_LOC_movie3.wmv). Timescale for reanimation is much larger than that of immobilization because the insect regains its previous activity by natural recovery process. To verify that the paralysis was not due to the applied potential, the same voltages were applied on a dummy chip. As expected, no immobilization was noticed.

3.4.5 Quantification of the metabolic rate

To quantify the immobilization/reanimation process, metabolic rates were inferred from the Carbon Dioxide (CO_2) output of the insects in a respirometry chamber. Details of the experiment are available elsewhere [39, 40] and here we just briefly provide an overview of the experimental procedure. The moths were glued onto a narrow beam that allowed unencumbered wing flapping and leg movements. To

stimulate a continuous flight response of the insect, a custom made mechanical agitator (chung_LOC_movie4.wmv) was placed inside of the sealed chamber. In the experiment, dry, CO_2 free air was pumped through the respirometry chamber at room temperature and all output gas passed through a carbon dioxide analyzer to measure the CO_2 output. Metabolic rate (and therefore CO_2 output) is higher during flight or attempted flight relative to periods when the animal was quiescent in the respirometry chamber.[40] To establish a baseline of the insect metabolic output at rest, the system was flushed until a stable CO_2 level was recorded. Following this the insect was mechanically stimulated as described above to initiate a flight response which was maintained until the CO_2 output again reached an equilibrium level. After 17 minutes of flight level activity, the membrane dissolution and ejection potentials were applied for approximately 10 minutes. Note that we applied the electric potential for this long of a time period here in order to be able to accurately gauge its effect on the insect activity level.

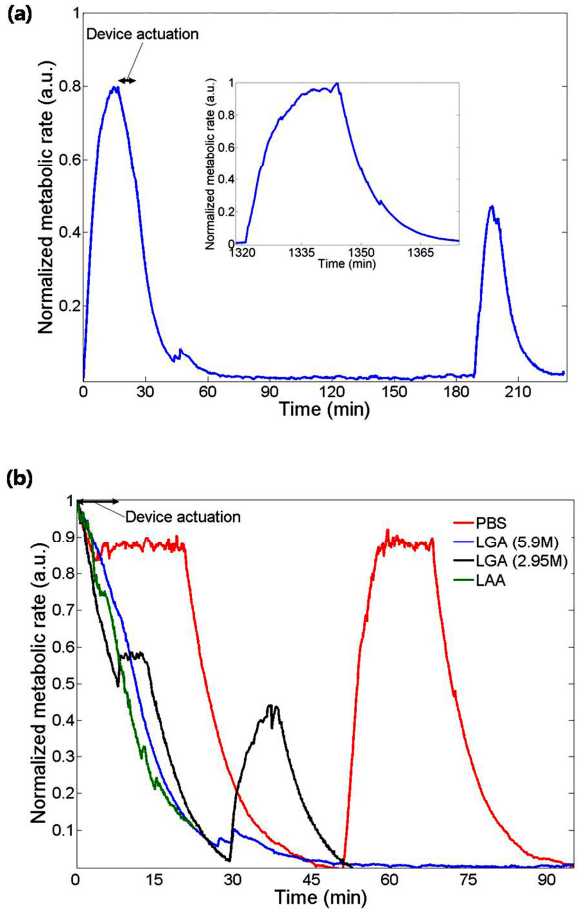

Figure 3.6. (a) Representative recording of CO_2 emission from adult moth as a function of time when an implanted microfluidic device with 15 μL of 5.9 M LGA was injected. (Inset) After 22 hours, the insect was stimulate to fly for 25 minutes and it fully recovered its previous metabolic activity rate (b) Normalized metabolic rate comparing 5.9 M LGA (blue), 2.95 M LGA (black), 11.1 M LAA (green) and PBS buffer (red).

As can be seen in Fig. 3.6a the metabolic rate drops off rapidly following the LGA (5.9 M) ejection. The insect was stimulated for 10 seconds every 5 minutes until the 2 hours mark with almost no activity observed (chung_LOC_movie5.wmv). At 45 to 47.5 minutes, to ensure the full immobilization, extremely strong perturbations were applied and the insect responded for a short time, approximately 1 minute, but returned to its quiescent state immediately afterwards. To validate the reversibility of

the process, three hours and 22 hours after the initial ejection, the insect was again stimulated. At 3 hours the insect was shown to recover 63.6% of its previous activity level (peak-to-peak value), and after 22 hours the moth fully recovered its previous level (see inset in Fig. 3.6a).

Fig. 3.6b compares the result obtained for implanted devices containing different LGA doses (5.9 M from Fig. 3.6a and 2.95 M), LAA (11.1 M) and the negative control solution (PBS). The additional experiments were conducted using the same methodology and drug volume as described above. For more accurate comparison in this figure, we set time equals zero as the time when the device was actuated. When a half concentration dose of LGA (2.95 M) was injected, the metabolic rate was dropped approximately 50%. When the agitator was reengaged, the insect resumed flight but only at this reduced activity level. The effect of LAA was similar to the full LGA dose, showing rapid immobilization and reanimation later as expected. When the negative control was ejected the insect continued to exhibit a strong flight response until the agitator was disengaged at 20 minutes. At 50 minutes the agitator was turned on again and the insect resumed full activity. This result demonstrates that the flight response of the insect can be directly manipulated through dosage control.

3.5 Summary and conclusion

We demonstrated here a method of exerting chemical control over insect flight activity, exploiting the use of immature stage implanted microfluidics to reversibly control the rate of metabolic output. Such a system could be the first step towards the development of an artificial insect nervous system where the controlled release of inhibitory or excitatory neurotransmitters could be accomplished in response to external stimuli. Extension of this work to include a multi-reservoir microfluidic

device for short timescale release control (*i.e.* off/on/off/on) would enable a new paradigm for insect flight control alongside established electrical techniques.

3.6 Acknowledgement

This work was supported by the Defense Advanced Research Project Agency, Microsystems Technology Office, Hybrid Insect MEMS (HI-MEMS) program, through the Boyce Thompson Institute for Plant Research. Distribution unlimited. Fundamental research exempt from prepublication controls. The authors would like to thank Donn Kim, Likun Chen, Doo Hyung Lee, Dr. Julie Goddard, Dr. Frank Schroeder, Prof. John Ewer, Prof. James Marden and Prof. Amit Lal for helpful discussions and technical assistances. The facilities used for this research include Nanoscale Science & Technology Facility (CNF) and Nanobiotechnology Center (NBTC) at Cornell University.

REFERENCES

1. Shyy, W., M. Berg, and D. Ljungqvist, *Flapping and flexible wings for biological and micro air vehicles.* Prog in Aero Sci, 1999. **35**(5): p. 455-505.
2. Lian, Y.S., W. Shyy, D. Viieru, and B.N. Zhang, *Membrane wing aerodynamics for micro air vehicles.* Prog. Aerosp. Sci., 2003. **39**(6-7): p. 425-465.
3. Gad-el-Hak, M., *MEMS: Design and Fabrication*. 2006, Boca Raton, FL: CRC/Taylor & Francis Group.
4. Tanaka, M., *An industrial and applied review of new MEMS devices features.* Microelectron. Eng., 2007. **84**(5-8): p. 1341-1344.
5. Wood, R.J., S. Avadhanula, E. Steltz, M. Seeman, J. Entwistle, A. Bachrach, G. Barrows, S. Sanders, and R.S. Fearing, *An autonomous palm-sized gliding micro air vehicle - design, fabrication, and results of a fully integrated centimeter-scale MAV*. IEEE Robot Automat Mag, 2007. **14**(2): p. 82-91.
6. Gad-el-Hak, M., *Micro-air-vehicles: Can they be controlled better?* J Aircraft, 2001. **38**(3): p. 419-429.
7. Pines, D.J. and F. Bohorquez, *Challenges facing future micro-air-vehicle development.* J Aircraft, 2006. **43**(2): p. 290-305.
8. Ellington, C.P., *The novel aerodynamics of insect flight: Applications to micro-air vehicles.* J Exp Biol, 1999. **202**(23): p. 3439-3448.
9. Wootton, R., *Aerodynamics: From insects to microvehicles.* Nature, 2000. **403**(6766): p. 144-145.
10. Dudley, R., *BIOMECHANICS:Enhanced: Unsteady Aerodynamics.* Science, 1999. **284**(5422): p. 1937-1939.

11. Franceschini, N., F. Ruffier, and J. Serres, *A bio-inspired flying robot sheds light on insect piloting abilities.* Curr Bio, 2007. **17**(4): p. 329-335.

12. Wood, R.J., *Liftoff of a 60mg flapping-wing MAV.* Proc IEEE/RSJ Int Conf Intelli Rob Sys, 2007: p. 1889-1894.

13. Wood, R.J., *The first takeoff of a biologically inspired at-scale robotic insect.* IEEE Trans Robotics, 2008. **24**(2): p. 341-347.

14. Wood, R.J., S. Avadhanula, R. Sahai, E. Steltz, and R.S. Fearing, *Microrobot design using fiber reinforced composites.* J Mech Design, 2008. **130**(5).

15. Tanaka, H., K. Hoshino, K. Matsumoto, and I. Shimoyama, *Flight dynamics of a butterfly-type ornithopter.* Proc IEEE/RSJ Int Conf Intelli Rob Sys, 2005: p. 2706- 2711.

16. Steltz, E., S. Avadhanula, and R.S. Fearing, *High lift force with 275 Hz wing beat in MFI.* Proc IEEE/RSJ Int Conf Intelli Rob Sys, 2007: p. 3987-3992.

17. Sane, S.P., *The aerodynamics of insect flight.* J Exp Biol, 2003. **206**(Pt 23): p. 4191-208.

18. Marden, J.H., *Maximum Lift Production during Takeoff in Flying Animals.* J Exp Biol, 1987. **130**: p. 235-258.

19. Marden, J.H., *Scaling of maximum net force output by motors used for locomotion.* J Exp Biol, 2005. **208**(9): p. 1653-1664.

20. Bozkurt, A., R. Gilmour, D. Stern, and A. Lal, *MEMS based bioelectronic neuromuscular interfaces for insect cyborg flight control.* Proc 21st IEEE Int Conf MEMS, 2008: p. 160-163.

21. Bozkurt, A., A. Paul, S. Pulla, A. Ramkumar, B. Blossey, J. Ewer, R. Gilmour, and A. Lal, *Microprobe microsystem platform inserted during early metamorphosis to actuate insect flight muscle.* Proc 20th IEEE Int Conf MEMS, 2007: p. 405-408.

22. Sato, H., C.W. Berry, B.E. Casey, G. Lavella, Y. Ying, J.M. VandenBrooks, and M.M. Maharbiz, *A cyborg beetle: Insect flight control through an implantable, tetherless microsystem.* Proc 21st IEEE Int Conf MEMS, 2008: p. 164-167.

23. Ando, N. and R. Kanzaki, *Changing motor patterns of the 3rd axillary muscle activities associated with longitudinal control in freely flying hawkmoths.* Zoolog Sci, 2004. **21**(2): p. 123-30.

24. Ritzmann, R.E., A.L. Ridgel, and A.J. Pollack, *Multi-unit recording of antennal mechano-sensitive units in the central complex of the cockroach, Blaberus discoidalis.* J Comp Physiol A Neuroethol Sens Neural Behav Physiol, 2008. **194**(4): p. 341-60.

25. Reissman, T. and E. Garcia, *Cyborg MAVs Using Power Harvesting and Behavioral Control Schemes.* Adv in Sci Technol, 2008. **58**: p. 159.

26. Chung, A.J., D. Kim, and D. Erickson, *Electrokinetic microfluidic devices for rapid, low power drug delivery in autonomous microsystems.* Lab on a Chip, 2008. **8**(2): p. 330-338.

27. Owen, M.J. and P.J. Smith, *Plasma Treatment of Polydimethylsiloxane.* J Adhesion SciTech, 1994. **8**(10): p. 1063-1075.

28. Sharma, A.K. and H. Yasuda, *Effect of Glow-Discharge Treatment of Substrates on Parylene-Substrate Adhesion.* J Vac Sci Technol, 1982. **21**(4): p. 994-998.

29. Alcantar, N.A., E.S. Aydil, and J.N. Israelachvili, *Polyethylene glycol-coated biocompatible surfaces.* J Biomed Mater Res, 2000. **51**(3): p. 343-351.

30. Paul, A., A. Bozkurt, J. Ewer, B. Blossey, and A. Lal, *Surgically Implanted Micro-Platforms in Manduca-Sexta.* Proc Solid State Sens Act Microsys Workshop, 2006: p. 209-211.

31. Chapman, R.F., *The Insects: Structure and Function*. 4th ed. 1998, NewYork: Cambridge University Press.

32. Nijhout, H.F., *Insect Hormones*. 1994, New Jersey Princeton University Press.

33. Spence, A.J., K.B. Neeves, D. Murphy, S. Sponberg, B.R. Land, R.R. Hoy, and M.S. Isaacson, *Flexible multielectrodes can resolve multiple muscles in an insect appendage.* J Neurosci Methods, 2007. **159**(1): p. 116-124.

34. Rash, L.D. and W.C. Hodgson, *Pharmacology and biochemistry of spider venoms.* Toxicon, 2002. **40**(3): p. 225-254.

35. Michaelis, E.K., N. Galton, and S.L. Early, *Spider Venoms Inhibit L-glutamate Binding to Brain Synaptic Membrance Receptors.* Proc Natl Acad Sci USA, 1984. **81**(17): p. 5571-5574.

36. Osborne, R.H., *Insect neurotransmission: Neurotransmitters and their receptors.* Pharmacol Ther, 1996. **69**(2): p. 117-142.

37. Santini, J.T., M.J. Cima, and R. Langer, *A controlled-release microchip.* Nature, 1999. **397**(6717): p. 335-338.

38. Randall, G.C. and P.S. Doyle, *Permeation-driven flow in poly(dimethylsiloxane) microfluidic devices.* Proc Natl Acad Sci USA, 2005. **102**(31): p. 10813-8.

39. Marden, J.H., B. Rogina, K.L. Montooth, and S.L. Helfand, *Conditional tradeoffs between aging and organismal performance of Indy long-lived mutant flies.* Proc Natl Acad Sci USA, 2003. **100**(6): p. 3369-3373.

40. Harrison, J.F. and J.R.B. Lighton, *Oxygen-sensitive flight metabolism in the dragonfly Erythemis simplicicollis.* J Exp Biol, 1998. **201**(11): p. 1739-1744.

CHAPTER 4

A ROBUST, ELECTROCHEMICALLY DRIVEN MICROWELL DRUG DELIVERY SYSTEM FOR CONTROLLED VASOPRESSIN RELEASE*

4.1 Abstract

Micro-electro-mechanical-system (MEMS) based implantable drug delivery devices represent a promising approach to achieving more precise dosing, faster release and better localization of therapeutic compounds than is possible with existing technology. Despite recent advancements, there remain challenges in being able to build systems that enable active control over the dose rate and release time, in a robust, low power but simple to fabricate package. Here we demonstrate an implantable microreservoir device that enables delivery of dose volumes as high as 15 μl using an electrochemically based transport mechanism. This approach allows for a significant reduction in the amount of time required for drug delivery as well as reducing the dependence on the external physiological conditions. We present the overall design, operating principle and construction of the device, and experimental results showing the volume transport rate as a function of the strength of the applied electric field. The concentration profile *vs.* time, the power consumption, and ejection efficiency are also investigated. To demonstrate the medical utility of the device we also characterize the *in-vitro* release of vasopressin.

*Re-printed by kind permission from Springer Science Business Media with permission from Aram J. Chung, Yun Suk Huh and David Erickson, "A robust, electrochemically driven microwell drug delivery system for controlled vasopressin release", *Biomedical Microdevices,* **11**, 861-867 (2010) DOI: 10.1007/s10544-009-9303-y
The original publication is available at http://www.springerlink.com/content/r48872ml55327573/

4.2 Introduction

Vasopressin (Cys-Tyr-Phe-Gln-Asn-Cys-Pro-Arg-Gly-NH_2) is a peptide hormone synthesized in the hypothalamus and stored/secreted in the posterior pituitary. Administration of vasopressin induces changes in the arterial blood pressure by increasing the resistance of the peripheral vessels [1]. In healthy individuals the effect is often negligible; however it can become a crucial compensatory mechanism for restoring blood pressure during hemorrhagic shock [1, 2]. At present, the primary treatment for hemorrhagic shock is fluid replacement; however this is sub-optimal [3], since it may worsen the patient's condition by dilution of the coagulant [4-7]. As an alternative therapy, Morales *et al.* [8] reported a set of canine experiments where vasopressin levels showed a marked increase at the onset of blood loss followed by a fall to well below the normal physiological level. Voelckel *et al.* [9] and Lindner *et al.* [10] demonstrated that the administration of vasopressin improved the survival rate in porcine cases and more recently Krismer *et al.* [11] reported for human as well. Excessive doses of vasopressin however have been known to induce injuries to the gastrointestinal tract, skin, myocardium and liver [12, 13]. Administration of vasopressin therefore represents a potential life-saving treatment for hemorrhagic shock upon its replenishment but it should be delivered rapidly and with precise timing to avoid side effects.

In this work, we present an implantable silicon micro-reservoir device that enables delivery of dose volumes as high as 15 μl using a more robust electrochemical transport mechanism. Briefly, the delivery mechanism is based on the use of an electrolytic reaction driven between the capping membrane and another electrode located inside the reservoir. When the reaction is initiated, gold dissolution causes a gradual loss of the mechanical integrity of the capping membrane which eventually

ruptures and opens. Gas released during the electrolytic reaction builds up the pressure in the reservoir which then forces the contents out of the well, independent of the external environmental conditions. We demonstrate herein that this approach also allows for a significant reduction in the amount of time required to eject well contents over earlier devices. In this paper, we present the overall design, operation principle and construction of the device, and experimental results showing the volume transport rate as a function of the strength of the applied electric field. The concentration profile *vs.* time, the power consumption, and ejection efficiency are also investigated. To demonstrate the medical utility of the device we also characterize the *in-vitro* release of vasopressin.

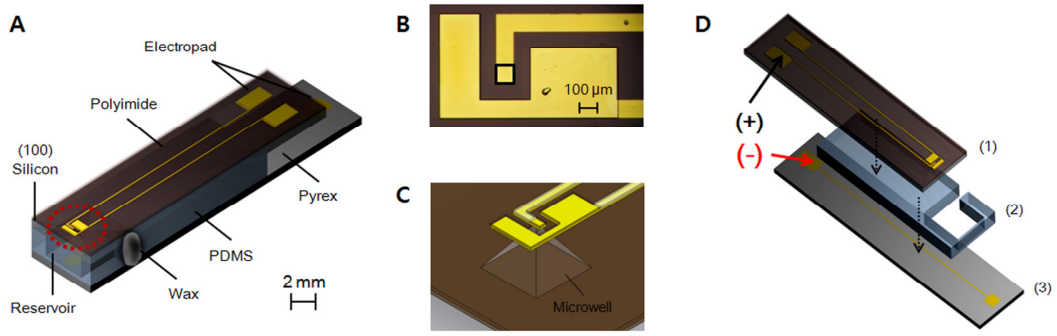

Figure 4.1. (A) Schematic representative of the electrochemically enhanced microfluidic drug delivery device developed here. The device measures 4.4 x 2.3 x 22 mm (*w* x *h* x *l*). (B) Magnified view of microchip from above looking at the region near the membrane. Black square box represents the capping gold membrane. (C) Magnified view near fabricated microwell. (D) Microchip assembly: (1) an upper silicon based structure (2) PDMS macro-reservoir (3) gold electrode on top of Pyrex substrate. All layers are bonded together by plasma oxidation.

4.3 Materials and methods

4.3.1 Device fabrication and assembly

The microfluidic device structure used here is a modification of that presented by Chung *et al.* [14] and used to control the flight metabolic output of insects in Chung and Erickson [15]. A 3D schematic of the device is shown in Fig. 4.1. All fabrication procedures described below are based on standard MEMS processes [16]. Briefly, starting with (100) silicon wafer, silicon nitride is deposited on both sides of the wafer and the backside was etched to define the bottom of a microwell reservoir. Subsequently, gold electrodes were evaporated using an image reversal contact lithography process, and then a polyimide dielectric layer was spun on and etched so as to expose the electrodes and isolate the leads. The pyramidal microwells were then defined by immersing the wafer in potassium hydroxide (Fig. 4.1C) and the remaining silicon nitride underneath the gold membrane was removed by reactive ion etching. To create the high volume macro-reservoir a scalpel patterned PDMS spacer was placed between the upper silicon chip and the lower Pyrex support. The approach is based on that developed by Li *et al.* [17] who used a similar approach to create a Pyrex macro-reservoir. The use of PDMS here however allows us to simplify device fabrication (by eliminating HF based glass etching or machining steps) and facilitate assembly (by eliminating wafer bonding steps). Finally the electrode pads and leads on the bottom Pyrex layer were fabricated through gold deposition and standard lift-off processing. Note that the biocompatibility of all the materials used here have been thoroughly investigated by others in a series of recent studies [18-21].

To assemble the device the upper (silicon), middle (PDMS), and bottom (Pyrex) substrates were air plasma treated, placed in conformal contact and then stored in an

80°C oven overnight. After this bounding process was complete, the macro-reservoir was filled with the desired chemicals using microsyringe (1705TLL, Hamilton, NV, USA) through a prefabricated side slit. The slit was then sealed with biocompatible wax (Butler GUM, Sunstar, IL, USA) as illustrated in Fig. 4.1A. After this, the electrode leads were connected to thin copper wires using silver conductive epoxy (M.G. Chemicals, Surrey, BC, Canada). As shown in our recent work [15], for long term stability the PDMS surface must be coated with Parylene (or a similar hydrophobic material [22]) in order to minimize fluid loss into the water permeable PDMS substrate. In addition, to minimize the physiological response upon implantation [18, 23], a surface modification, for example, PEG (Poly-ethylene glycol) should be applied as we have done in the past [15]. Comprehensive, long term tests of the device were not conducted here however it was found that in all cases the devices remained operable for at least a week after surface modifications.

4.3.2 Vasopressin transport: visualization and quantification

To visualize and quantify the chemical release, FITC tagged vasopressin was used. A fluorescein labeling kit and the vasopressin (Arg8-vasopressin) were purchased from Dojindo (Rockville, MD, USA) and Sigma-Aldrich (St. Louis, MO, USA), respectively. FITC was dissolved in 10 µl dimethyl sulfoxide (DMSO) and 8 µl of this solution was well mixed with 100 µl of reaction buffer. After this, the sample was incubated at 37°C for 10 minutes and 100 µl of 100 mM phosphate buffered saline (PBS) was added to a filtration tube and centrifuged. Since the molecular weight of the vasopressin is relatively small (~1kD), we used Microsep™ centrifugal devices (Pall Corporation, East Hills, NY, USA). The tube was centrifuged at 8000 rpm for 12 hours at 4°C. Lastly, 200 µl PBS was added to the FITC-vasopressin conjugation and

the final mixture was transferred to a 0.5 ml tube and stored at 4°C. The FITC-vasopressin conjugation was diluted to the appropriate concentrations described below in 100 mM PBS containing 0.145 M of chloride ions (pH 7.4) which was reasonably close to the chloride concentration in human blood (Fitzsimons and Sendroy 1961). The transport of the fluorescein was recorded using Unibrain Fire-i^{TM} software and a Sony XCD-X710 (Tokyo, Japan) camera.

The amount of vassopressin ejected from the devices was quantified via a protein assay using the BCA™ Protein Assay Kit (Pierce, Rockford, IL, USA). The assays were performed using a 96-well plate (Corning, Corning, NY, USA), and absorbance was measured at 562 nm by SPECTRAmax 384 (Molecular Devices, Sunnyvale, CA, USA). The vasopressin concentration was calculated from the bovine serum albumin (BSA) standard curve.

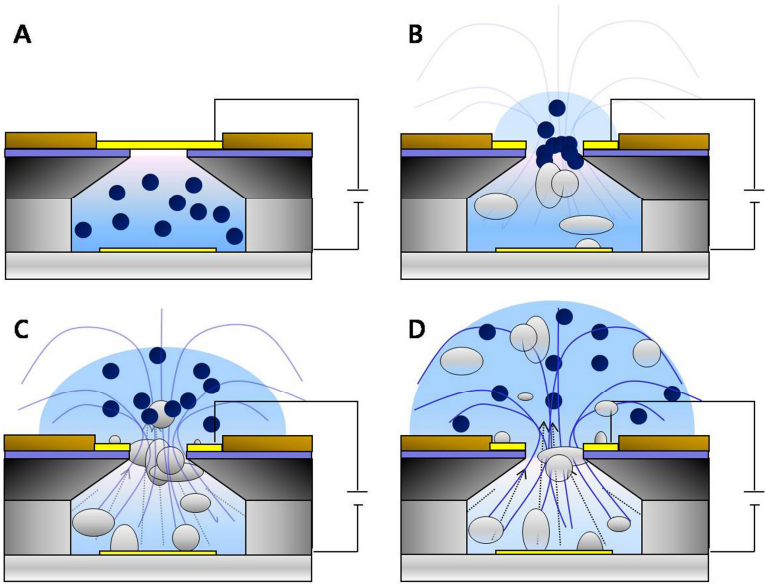

Figure 4.2. Scheme describing the operational stages of the electrochemically driven microfluidic drug delivery device (not to scale). (A) The electric potential is applied between top and bottom electrodes and current flows through the reservoir independent of the surrounding environment. (B) Two main electrochemical reactions occur: dissolution of the gold membrane and electrolysis or water resulting in gas

release. (C) The generated microbubbles propel well contents out. (D) The reaction continues until fluid transport stops.

4.3.3 Device design and operation principle

A diagram of the device operation is shown in Fig. 4.2. The PDMS reservoir and microwell contain approximately 15 μl of 0.05 g/l vasopressin for release. When drug release is desired, an electrical potential is applied between upper and lower electrodes, as shown in Fig. 4.1D, resulting in two electrochemical reactions which affect the ejection process. First, the presence of a small amount of chloride ions in the buffer solution creates a water-soluble chlorogold complex from the gold membrane [24] (this was similarly demonstrated by Santini *et al.* [25]). This results in a gradual loss of the mechanical integrity of the membrane (due to dissolution of the gold) which eventually ruptures, exposing the contents to the external environment. Simultaneously, the two electrodes also serve as an anode and cathode for electrolysis of water. Gas released during this reaction results in an increased pressure in the reservoir which pushes the liquid contents out through the dissolved membrane. More details on the electrochemical reaction are available in the supplemental material. In all cases, a Keithley 236 Source-Measure Unit (Cleveland, OH) was used to apply these potentials and to measure the current load.

4.4 Results and discussions

4.4.1 Electrochemical driven ejection

The electrochemical transport mechanism was demonstrated for two different interface conditions: the first being for the drugs ejected directly into the air and the

other is the chemicals ejects into a fluid solution surrounding the gold membrane. As mentioned in the introduction, one of the most significant limitations to the development of implantable drug delivery devices is the uncertain physiological conditions that will be faced upon implantation. Many of the passive devices discussed above are compatible with specific solution-phase environmental conditions (*e.g.* polymer based biodegradable systems) and thus suffer from significant performance degradation due to, for example, biofouling [18, 23]. One of the major advantages of the electrochemical reaction based device developed here, is that allows us to build the pressure up in the reservoir and burst into the external environment, independent of the surrounding conditions.

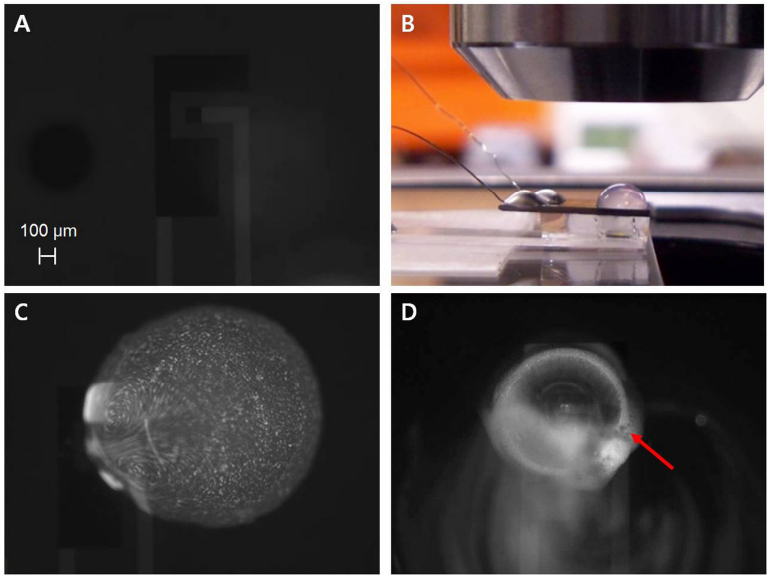

Figure 4.3. Illustration showing ejection of vasopressin with 720 nm fluorescent polystyrene microsphere particles from a reservoir. (A) Before applying potential. (B) Picture of a sample device after ejection into air for five minutes (no initial covering fluid) (C) Case 1: Ejection into the air—frame taken one minute after application of 12 V potential (D) Case 2: Ejection into PBS buffer—frame taken one minute after application of 12 V potential. The red arrow shows small bubbles release from the well during the ejection process, next to one large bubble in the center region.

Fig. 4.3 shows time lapse images illustrative of the electrochemical transport of 15 µl of 0.05 g/l vasopressin for the case of an applied potential of 12 V. In order to clearly illustrate the dispersion pattern, we added 720 nm fluorescent flow tracers to FITC-vasopressin conjugation (see supplemental Movies 4.1 and 4.2). On average approximately 23 seconds after application of the potential the stored contents begin to be ejected from the reservoir. Figure 4.3C shows when the contents are ejected into air and Fig. 4.3D shows the case for ejection into PBS buffer.

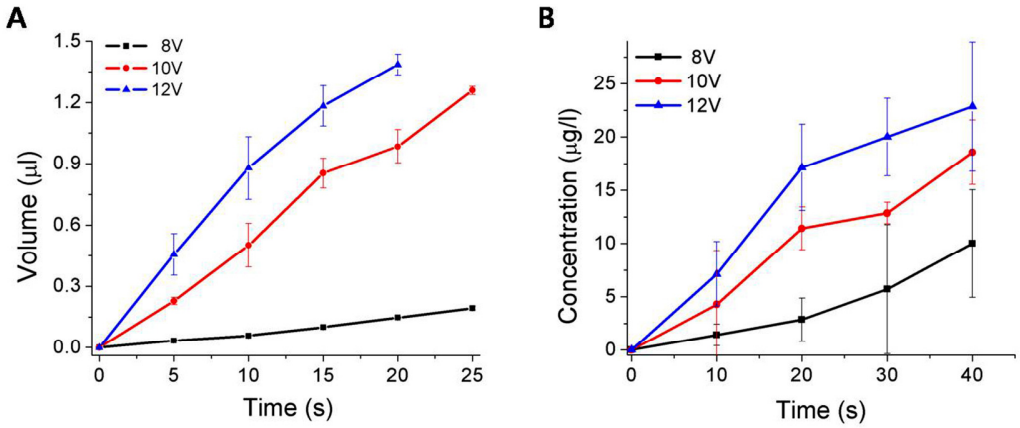

Figure 4.4. (A) Release rate of vasopressin from sample devices as a function of time for different voltages. (B) Concentration profile of vasopressin calculated from BCA protein assay. We set time equals zero as the time when the electrochemical reactions are actuated.

To characterize the ejection volume flow rate as a function applied potential, the dispersion pattern of the fluorescent microspheres was recorded as a function of time. By placing a coverslip at a controlled distance above the ejection point the area of the dispersion could be related to an ejected volume using a simple flat cylinder model. Images were then analyzed and processed using ImageJ (National Institutes of Health, http://rsb.info.nih.gov/ij/) and a self-written MATLAB routine (Mathworks, Natick, MA, USA). The results of these experiments are shown in Fig. 4.4A. In all cases the

advancing fluid front was traced to a distance of 1 mm, limited by the field of view of the microscope. As can be seen there exists a strong dependence of ejected volume on the applied potential. For the first 25 seconds, the maximum (12 V) and minimum (8 V) volumetric rates were 4.19 μl/min and 0.460 μl/min, respectively. As such in addition to reducing the overall ejection time (over passive devices), the electrochemical technique also provides a method for controllably modulating the delivery rate through simple adjustment of the applied potential. By modulating the applied voltage the device could also be adapted to pulsatile delivery [14].

4.4.2 Vasopressin release

Time dependent dose profiles were also characterized using FITC-labeled vasopressin as described above. To perform the experiments a control volume of 15 μl of 100 mM PBS was added on top of the membrane and the vasopressin ejection process was enacted for a prescribed length of time. After terminating the ejection process, 1 μl of sample was extracted from the covering drop (after gentle mixing to ensure homogeneity of the mixture) and dispensed into a 96-well plate for absorbance measurements. The concentration of vasopressin in the drop was determined using the technique described above and the results are plotted in Fig. 4.4B. For all experiments, time equals zero was set as the point when the electrochemical reaction was initiated. Analogous to the results presented earlier, Fig. 4.4B also illustrates how increasing the applied potential results in the system reaching the plateau concentration much more rapidly. Note that a relatively low concentration of vasopressin was used in this experiment in order to be compatible with the BCA protein assay. With the current volume of 15 μl, the device is able to deliver maximum of 120 IU (Arg8-vasopressin contains approximately 400 IU/mg [26] and

has a solubility of 20 mg/ml). Krismer *et al.* [11] reported a set of human cases that where dosages of 100 to 160 IU vasopressin helped to restore spontaneous circulation with sinus rhythm in 2 minutes. Importantly, the 120 IU limitation of the existing device can be circumvented by parallel integration of devices onto a single chip. This would make it possible to deliver much larger dosages.

Although the focus of this paper is on device design and transport characterization, it is important to briefly discuss the stability of the vasopressin following the electrochemical ejection process. To assess this here we have performed a number of additional mass spectroscopy experiments using MALDI-TOF/TOF (4700 Proteomics Analyzer, Applied Biosystems, Foster City, CA, USA). Samples were tested after different electrolytic ejection times using 12 V as the driving voltage, since this represented the harshest conditions we considered in this paper. The details and results of these experiments are presented in the supplemental material (Fig. S4.1 and associated text) however strong vasopressin peaks (at ~1.085kD) were still observed in the ejected contents after continuous application of the driving potential for 5 minutes. When compared with the control sample however two additional smaller peaks were also observed at 1.101 kD and 1.117 kD. These two extra peaks are likely oxidation products, suggesting that the electrochemical reaction did cause some degree of degradation to the vasopressin. We are continuing to investigate this observation and hope to better quantify the degradation in the future.

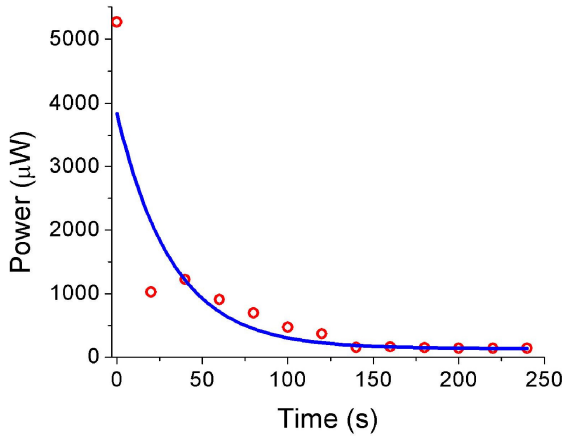

Figure 4.5. Representative power load during ejection process for the 12 V case. The line through the data points in this figure represents an exponential best fit. Error bars are not shown since they were smaller than the data marks.

4.4.3 Power consumption

To determine the power requirements for both the membrane dissolution and electrochemical ejection stages a Keithley 236 Source-Measure Unit was used to monitor the current load. Figure 4.5 plots a representative case at 12 V where the instantaneous total power consumption was obtained by multiplying the measured current by the applied potential. As can be seen, the power consumption decreases with time, reaching a plateau of around 0.130 mW after 240 seconds. For the 12 V case the maximum power load was approximately 5 mW, however this dropped to around 0.9 mW for the 8 V case. This could be further reduced by decreasing the thickness of the PDMS layer, thereby decreasing the distance over which fluid transport must occur and with that the required voltage. Previous studies on similar dose control systems have shown that the electrostatic micropump [27], thermo-pneumatic [28], bubble-type planar micropump [29], and ionic conductive polymer film micropump [30] techniques require 1 mW with 200 V, 450 mW with 15 V, 18 mW with 10 V, 1000 mW with 40 V and 180 mW with 1.5 V, respectively. In

comparison the method represent a good combination of both low voltage requirements and low power consumption.

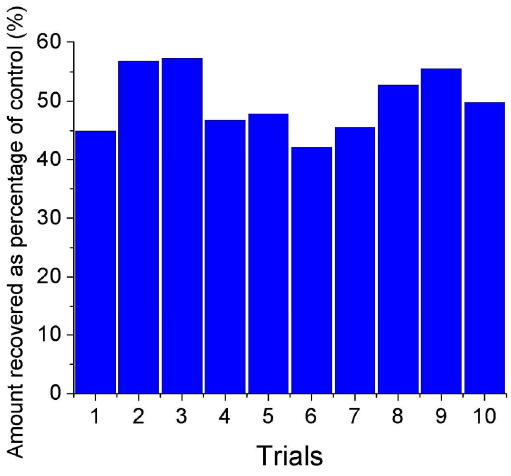

Figure 4.6. Release results: total amount of vasopressin recovered over 5 minute from each reservoir when 20 V is applied.

4.4.4 Ejection efficiency

The efficiency with which the contents were ejected from the well was quantified by comparing the ratio of the volume loaded into the reservoir with that recovered after the ejection process. In these experiments the recovered volume was calculated in the same manner described in section 3.2. The cumulative amounts of FITC-vasopressin recovered per release for each trial are shown in Fig. 4.6. The average amount recovered from 10 reservoirs over 5 minutes when 20 V was applied was 50.3%. The standard deviation among the 10 trials was 6.6%. We expect that this ejection efficiency could be increased by decreasing the thickness of the PDMS layer. This would however result in a lower total dose volume.

4.5 Conclusion

We have demonstrated here an electrochemically driven, implantable, low power and rate controllable drug delivery device. This approach serves to actively propel the drugs from within a sealed reservoir to the external environment using a combination of electrolytic and gold dissolution reactions induced by the application of a voltage between the top and bottom of the device. The contents dispense rate, concentration profile and power consumption of the device were characterized experimentally. An ejection rate as high as 4.19 μl/min was recorded at a maximum power consumption of roughly 5 mW.

4.6 Acknowledgement

This work was supported by the Defense Advanced Research Project Agency, Microsystems Technology Office, Hybrid Insect MEMS (HI-MEMS) program, through the Boyce Thompson Institute for Plant Research. Distribution unlimited. Fundamental research exempt from prepublication controls. The authors would like to thank Donn Kim and Bernardo Cordovez for helpful discussions and technical assistances. The facilities used for this research include Nanoscale Science & Technology Facility (CNF) and Nanobiotechnology Center (NBTC) at Cornell University.

REFERENCES

1. Lienhart, H.G., K.H. Lindner, and V. Wenzel, *Developing alternative strategies for the treatment of traumatic haemorrhagic shock.* Current Opinion in Critical Care, 2008. **14**(3): p. 247-253.
2. Peitzman, A.B., B.G. Harbrecht, A.O. Udekwu, T.R. Billiar, E. Kelly, and R.L. Simmons, *Hemorrhagic shock.* Curr. Probl. Surg., 1995. **32**(11): p. 925-1002.
3. Roberts, I., P. Evans, F. Bunn, I. Kwan, and E. Crowhurst, *Is the formalisation of blood pressure in bleeding trauma patients harmful?* Lancet, 2001. **357**(9253): p. 385-387.
4. Bickell, W.H., S.P. Bruttig, G.A. Millnamow, J. Obenar, and C.E. Wade, *The detrimental effects of intravenous crystalloid after aortotomy in swine.* Surgery, 1991. **110**(3): p. 529-536.
5. Milles, G., C.J. Kouchk, and H.G. Zacheis, *Experimental uncontrolled arterial hemorrhage.* Surgery, 1966. **60**(2): p. 434-442.
6. Shaftan, G.W., C.J. Chiu, C. Dennis, and C.S. Grosz, *The effect of transfusion and of certain hemodynamic factors on the spontaneous control of arterial hemorrhage.* J. Cardiovasc. Surg., 1964. **5**(3): p. 251-256.
7. Stern, S.A., S.C. Dronen, P. Birrer, and X. Wang, *Effect of blood pressure on hemorrhage volume and survival in a near-fatal hemorrhage model incorporating a vascular injury.* Ann. Emerg. Med., 1993. **22**(2): p. 155-163.
8. Morales, D., J. Madigan, S. Cullinane, J. Chen, M. Heath, M. Oz, J.A. Oliver, and D.W. Landry, *Reversal by vasopressin of intractable hypotension in the late phase of hemorrhagic shock.* Circulation, 1999. **100**(3): p. 226-229.

9. Voelckel, W.G., K.G. Lurie, K.H. Lindner, T. Zielinski, S. McKnite, A.C. Krismer, and V. Wenzel, *Vasopressin improves survival after cardiac arrest in hypovolemic shock.* Anesth. Analg., 2000. **91**(3): p. 627-634.

10. Lindner, K.H., A.W. Prengel, E.G. Pfenninger, I.M. Lindner, H.U. Strohmenger, M. Georgieff, and K.G. Lurie, *Vasopressin improves vital organ blood flow during closed-chest cardiopulmonary resuscitation in pigs.* Circulation, 1995. **91**(1): p. 215-221.

11. Krismer, A.C., V. Wenzel, W.G. Voelckel, P. Innerhofer, K.H. Stadlbauer, T. Haas, M. Pavlic, H.J. Sparr, K.H. Lindner, and A. Koenigsrainer, *Employing vasopressin as an adjunct vasopressor in uncontrolled traumatic hemorrhagic shock - Three cases and a brief analysis of the literature.* Anaesthesist, 2005. **54**(3): p. 220-224.

12. Malay, M.B., J.L. Ashton, K. Dahl, S.A. Burchell, R.C. Ashton, R.R. Sciacca, J.A. Oliver, and D.W. Landry, *Heterogeneity of the vasoconstrictor effect of vasopressin in septic shock.* Critical Care Medicine, 2004. **32**(6): p. 1327-1331.

13. Yoo, J.H., C. Park, D.H. Hahm, H.J. Lee, and H.M. Park, *Determination of optimal dose of arginine vasopressin in hemorrhagic shock in dogs.* Journal of Veterinary Medical Science, 2007. **69**(7): p. 755-758.

14. Chung, A.J., D. Kim, and D. Erickson, *Electrokinetic microfluidic devices for rapid, low power drug delivery in autonomous microsystems.* Lab on a Chip, 2008. **8**(2): p. 330-338.

15. Chung, A.J. and D. Erickson, *Engineering insect flight metabolics using immature stage implanted microfluidics.* Lab on a Chip, 2009. **9**(5): p. 669-676.

16. Judy, J.W., *Microelectromechanical systems (MEMS): fabrication, design and applications.* Smart Mat. Struct., 2001. **10**(6): p. 1115-1134.

17. Li, Y.W., H.L.H. Duc, B. Tyler, T. Williams, M. Tupper, R. Langer, H. Brem, and M.J. Cima, *In vivo delivery of BCNU from a MEMS device to a tumor model.* Journal of Controlled Release, 2005. **106**(1-2): p. 138-145.

18. Voskerician, G., M.S. Shive, R.S. Shawgo, H.v. Recum, J.M. Anderson, M.J. Cima, and R. Langer, *Biocompatibility and biofouling of MEMS drug delivery devices.* Biomaterials, 2003. **24**(11): p. 1959-1967.

19. Richardson, R.R., J.A. Miller, and W.M. Reichert, *Polyimides as biomaterials: preliminary biocompatibility testing.* Biomaterials, 1993. **14**(8): p. 627-635.

20. Dokmeci, M.R., J.A. von Arx, and K. Najafi. *Accelerated testing of anodically bonded glass-silicon packages insalt water*. 1997.

21. Belanger, M.C. and Y. Marois, *Hemocompatibility, biocompatibility, inflammatory and in vivo studies of primary reference materials low-density polyethylene and polydimethylsiloxane: A review.* Journal of Biomedical Materials Research, 2001. **58**(5): p. 467-477.

22. Shin, Y.S., K. Cho, S.H. Lim, S. Chung, S.J. Park, C. Chung, D.C. Han, and J.K. Chang, *PDMS-based micro PCR chip with Parylene coating.* Journal of Micromechanics and Microengineering, 2003. **13**(5): p. 768-774.

23. Ratner, B.D., A.S. Hoffman, F.J. Schoen, and J.E. Lemons, *Biomaterials science: An Introduction to Materials in Medicine*. 2004, San-Diego: Academic Press.

24. Frankenthal, R.P. and D.J. Siconolfi, *The Anodic Corrosion of Gold in Concentrated Chloride Solutions.* J. Electrochem. Soc., 1982. **129**(6): p. 1192-1196.

25. Santini, J.T., M.J. Cima, and R. Langer, *A controlled-release microchip.* Nature, 1999. **397**(6717): p. 335-338.

26. Dawson, R.M.C., D.C. Elliott, W.H. Elliott, and K.M. Jones, *Data for Biochemical Research, Clarendon*. 1986, Oxford.

27. Zengerle, R., J. Ulrich, S. Kluge, M. Richter, and A. Richter, *A bidirectional silicon micropump.* Sensors and Actuators a-Physical, 1995. **50**(1-2): p. 81-86.

28. Schomburg, W.K., J. Vollmer, B. Bustgens, J. Fahrenberg, H. Hein, and W. Menz, *Microfluidic Components in Liga Technique.* Journal of Micromechanics and Microengineering, 1994. **4**(4): p. 186-191.

29. Zahn, J.D., A. Deshmukh, A.P. Pisano, and D. Liepmann, *Continuous on-chip micropumping for microneedle enhanced drug delivery.* Biomedical Microdevices, 2004. **6**(3): p. 183-190.

30. Guo, S., T. Nakamura, T. Fukuda, and K. Oguro. *Development of the micro pump using ICPF actuator*. in *Robotics and Automation, 1997. Proceedings., 1997 IEEE International Conference on*. 1997.

CHAPTER 5

HYBRID TECHNIQUES FOR MODULATING INSECT FLIGHT ACTIVITY AND LONGEVITY*

5.1 Abstract

Insect microairvehicles represent a promising alternative to traditional small scale aircraft because they combine the enhanced energy storage and maneuverability of living insects with the controllability offered by microelectromechanical systems. These systems have been previously demonstrated, usually using either electrical (with implanted electrodes) or chemical (with implanted microfluidics) control schemes, but to date little work has been done on the creation of hybrid systems that use both these two methods simultaneously. In this paper we develop an integrated microsystem that uses both chemical and electrical methods to modulate the flight activity of *Manduca sexta* moths. The electrical component of the system initiates and maintains flight by applying electrical pulses to an antenna lobe and an implanted drug delivery component modulates flight output power by administering a neurotransmitter dose to the central nervous system. Flight longevity results acquired with this system are compared with those obtained from direct mechanical stimulation. We demonstrate that the electrical stimulation provides as much as 35-fold enhancement in flight duration with respect to mechanical agitation and that a 50% mean flight power output reduction can be achieved with the proper neurotransmitter dose.

*Submitted to *Lab-on-a-Chip*, and reproduced by permission of the Royal Society of Chemistry with permission from Aram J. Chung‡, Bernardo Cordovez‡, Nipun Jasuja, Daniel Lee, Xinyu Huang and David Erickson, "Hybrid techniques for modulating insect flight activity and longevity"
‡ Contributed equally to this work

5.2 Introduction

The downscaling of traditional air vehicles [1] presents severe challenges. Most prominently, wing size reduction compromises vehicle aerodynamics and makes a flapping type motion necessary in order to lift an aircraft body. One way this problem has been addressed in the past is by using microelectromechanical system (MEMS) technology [2] to generate small flying robotic systems with biomimetic [3] characteristics. An example of this is the flapping *Diptera* robots reported by Wood *et al.* [4]. Such systems experience long term power constrains since storage capacity scales with the volume of the carrier. Living insects, on the other hand, are aerodynamically efficient and can offer superior long term flight endurance [5, 6] with flight times reaching as long as several days. Attempts to directly train insects to perform useful flight maneuvers have proved extremely challenging [7].

One way to address this dichotomy is through the development of systems that take advantage of the energy storage and flight capabilities of living insects with the precise control enabled by modern MEMS technology. These systems are of significant technological interest [8] due to their applicability to remote surveillance [9] and power harvesting [10, 11]. The dominant paradigm for insect flight manipulation is based on electrical control of neuromuscular activity [12]. Aerodynamic operations including liftoff, yaw control and landing have been demonstrated by Bozkurt *et al.* [13] in *Manduca sexta* moths. Similar operations were performed by Sato *et al.* [14, 15] with *Cotinis texana* beetles using wireless DC pulses applied to neuromuscular centers. Tsang *et al.* [16] demonstrated flight steering in *Manduca sextae* by controlling their abdominal orientation using a flexible electrode ring attached to the nerve cord. Microsystems which use chemical control have also been used. For example, Chung and Erickson [17] induced a reversible chemical

paralysis in a tethered *Manduca sexta* moth via an implantable microfluidic chip that released various neurotransmitter solutions.

A system that harnesses the maneuverability offered by the electrical approach with the speed control and physiological access enabled by chemistry could increase the number of achievable flight routines. Towards this end, in this paper we demonstrate the integration of chemical and electrical methods for modulating the flight activity of *Manduca sexta* moths. To analyze the flight behavior we performed a series of tethered experiments which measure changes in flight output power for different neurotransmitter doses subject to continuous electrical pulse stimulation. The results are used to create a wireless hybrid system that enables tetherless hybrid flight control and compared with direct mechanical stimulation which is used as a baseline. We focus here on developing the hybrid flight mechanism rather than device miniaturization as this has already been demonstrated [13, 14, 16].

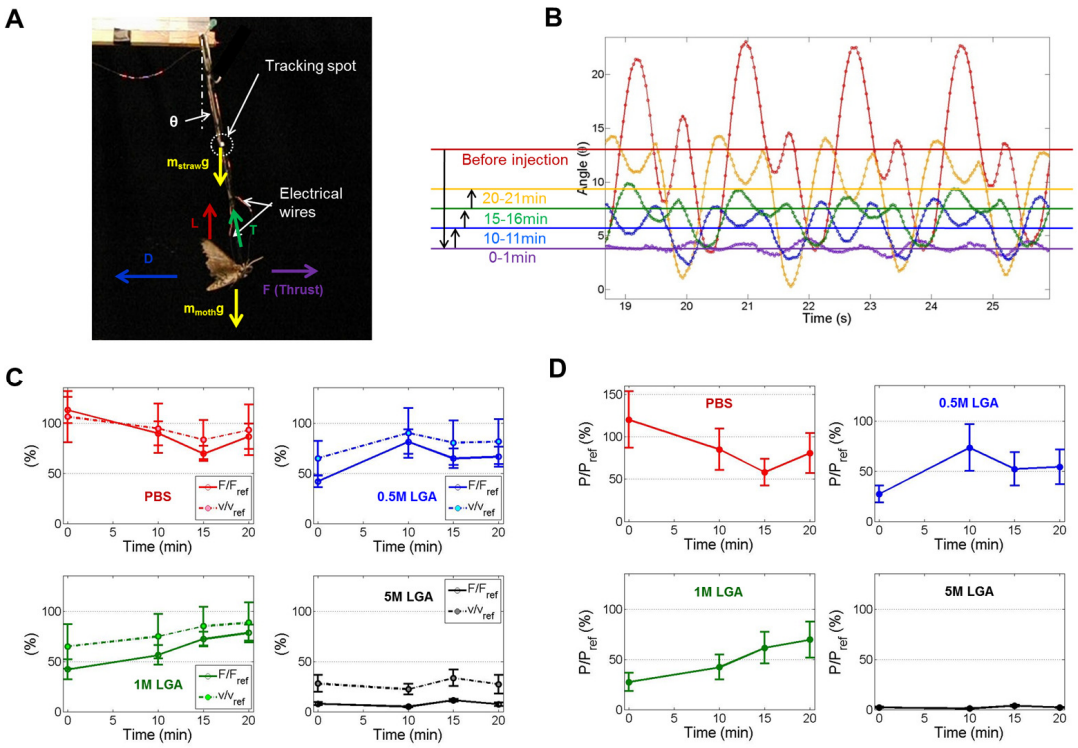

Figure 5.1. Combined electrical and chemical modulation of insect flight power and speed. (A) Experimental setup showing moth attached to hinged solid beam (see Movie S5.1). (B) Flight angle before (red) and after 0.5 M L-Glutamic Acid (LGA) injection. (C) Flight velocity and thrust response following injection of different concentrations of LGA. (D) Flight power output following injection of different concentrations of LGA

5.3 Results and discussion

5.3.1 Flight power/speed analysis of combined chemical and electrical modalities

In this first section we analyze the flight response of *Manduca sextae* to simultaneous chemical and electrical stimulation. To characterize thrust, speed and flight power moths were tethered to a hinged beam as shown in Fig. 5.1A. The

displacement angle (θ) was measured and analyzed[18] for moths that had been injected with solutions containing different concentrations of L-Glutamic acid (LGA) neurotransmitters (refer to Materials and Methods section below for more details). After injection, insects are stimulated into flight by supplying a sequence of 3 V, 25 Hz DC pulses with a 50% duty cycle for 0.5 seconds followed by a one second pause. These pulses are applied between an electrode implanted near the antennal lobe and a common ground implanted in the dorsal thorax (Fig. 5.1A). These electrical pulses tended to stun the moth when initially applied, but resulted in strong flight behavior during the off cycle (see Movie S5.1). The electrical stimulation can maintain continuous flight activity and the role of the injected chemical is to throttle flight speed by overstimulating the moth's central nervous system[19]. Figure 5.1B shows a sample experiment following manual injection of 10 µl of 0.5 M LGA solution.

To translate angle data into flight thrust, the simple moment balance model shown below was used, the details of which are provided in the supplementary information.

$$F = g \tan\theta (m_{straw}/2 + m_{moth}) \tag{2.1}$$

The supplementary information also explains how the thrust data can also be converted to velocity and power output differences. The thrust and velocity characteristics of moths subjected to different concentrations of LGA are shown in Fig. 5.1C. For the phosphate buffered saline (PBS) injection (negative control, 0% LGA) one minute after injection the thrust and velocity values are greater than those obtained prior to injection (denoted with the subscript "ref" in Figs. 5.1C and D). This is because inserting and withdrawing of the needle irritates the insects, and PBS does not drastically reduce flight capacity. For 1 M and 0.5 M LGA solutions, moths fly on average at 22% below their pre-injection flight speed (Fig.5.1C) for the first twenty minutes, with a gradual speed increase as the solution is metabolized. The flight power

output is shown in Fig. 5.1D. 0.5 M and 1 M LGA solutions result in rapid drop in output power which is regained to approximately 50% of the reference value within 10 minutes. Those subjected to 5 M doses regain half of their activity 1.5 hours later. Long-term reduction in flight speed can be useful for applications such as remote surveillance [9]. It is worth noting that the recovery time is approximately 2-fold quicker compared to our previous work [17] where no electrical stimulation was used. In addition to the functions demonstrated here, chemical injection could also offer additional capabilities. For example, different chemicals have been used to promote growth [20, 21] or to induce characteristic flight patterns [22, 23] in *Manduca sexta* moths.

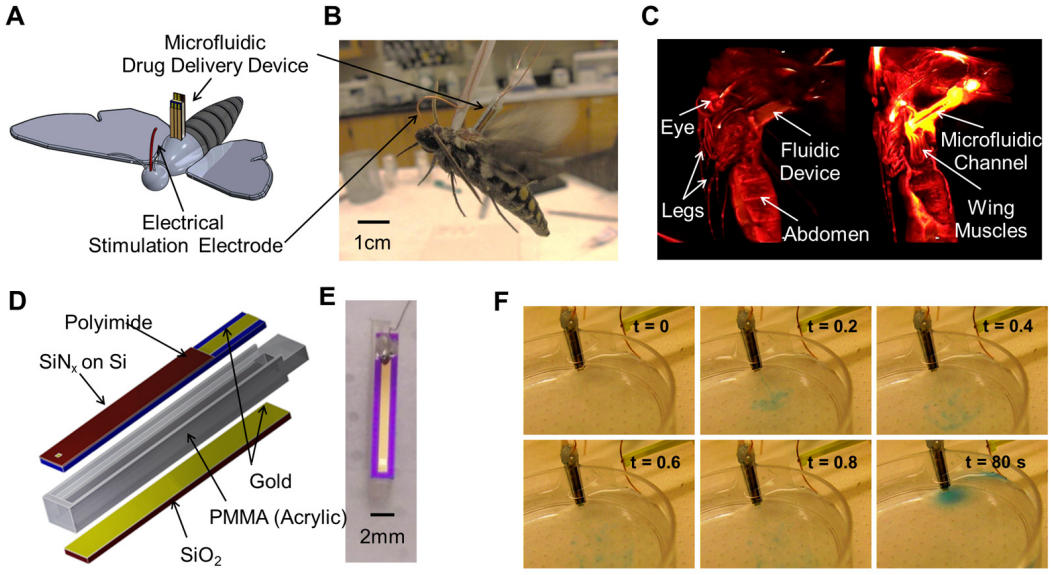

Figure 5.2. Wireless hybrid system for *Manduca sexta* flight control. (A) Schematic of moth showing both microfluidic chip, which is implanted in dorsal thorax, and the copper wire used for electrical stimulation, implanted in the antennal lobe (see Movie S5.2 for interactive version). (B) Insect showing implanted microfluidic chip and electrode. (C) 3D Computed Tomography (CT) image of fluidic chip implanted into dorsal thorax (also available as Movie S5.4). (D) Fluidic chip subcomponent assembly in exploded view and (E) actual fluidic chip. (F) Time lapse of images showing sample ejection sequence of 5 M L-Glutamic acid (LGA) solution into 10 mM PBS solution (see Movie S5.3).

5.3.2 Wireless hybrid system for insect flight modulation

We now construct and test a wireless system based on the electrical and chemical hybrid technique demonstrated above. The full scale system is shown in Fig. 5.2B and illustrated schematically in Fig. 5.2A for clarity. Movie S5.2 is an animated video that illustrates the hybrid stimulation process. For the integrated system, a commercial wireless microcontroller (TI eZ430) with multiple independent electrical output ports is used to trigger both the electrical stimuli and the actuation of the microfluidic chip (see Fig. S5.1). The microfluidic chip (Figs. 5.2D-F) is implanted in the moth's dorsal thorax and uses an electrochemical pumping procedure that was previously demonstrated by Chung *et al.* [24] Briefly, chlorine ions in the buffer react with the capping gold membrane on top of the fluidic chip thereby dissolving it. In addition, water electrolysis releases gas which builds up the pressure in the enclosed chamber, leading to mechanical failure of the capping membrane and release of the contents. The microcontroller has a standard output of 3 V, so the anode of the microfluidic chip was connected to a custom designed 34 V DC to DC converter to increase the reaction rate. The bottom electrode of the fluidic chip is connected to the universal ground. This version of the chip is 4 times smaller than its predecessor[24] while still capable of carrying the same volumetric payload. This was achieved by reducing the lithographic pattern dimensions as well as implementing a custom 3D printed acrylic channel to hold the chemical payload (see the Materials and Methods for more details on fabrication). Figure 5.2F is a time-lapse image showing the fluidic ejection of 5 M LGA solution (also see Movie S5.3). The enclosed solution bursts out of the device at a speed of nearly 10 cm/s and the majority of the fluidic contents are ejected by the 80 second mark. Electrical stimulation was achieved by implanting a thin wire electrode in the moth's antennal lobe (Fig. 5.2A and 2B) and connecting it to a secondary output

port of the wireless microcontroller. To facilitate our experiments, we use a helium balloon to support the additional weight of the electronics, but further miniaturization of the electrical system is possible and has been already demonstrated [14, 16, 25]. To assess the invasiveness of our microfluidic and electrical implants, Fig. 5.2C and Movie S5.4 show a 3D CT scan following implantation. We note that the chip penetrated about 3 mm into the thorax, bringing the chemical payload close to both the central nervous system and the main circulatory system for effective drug dispersal.

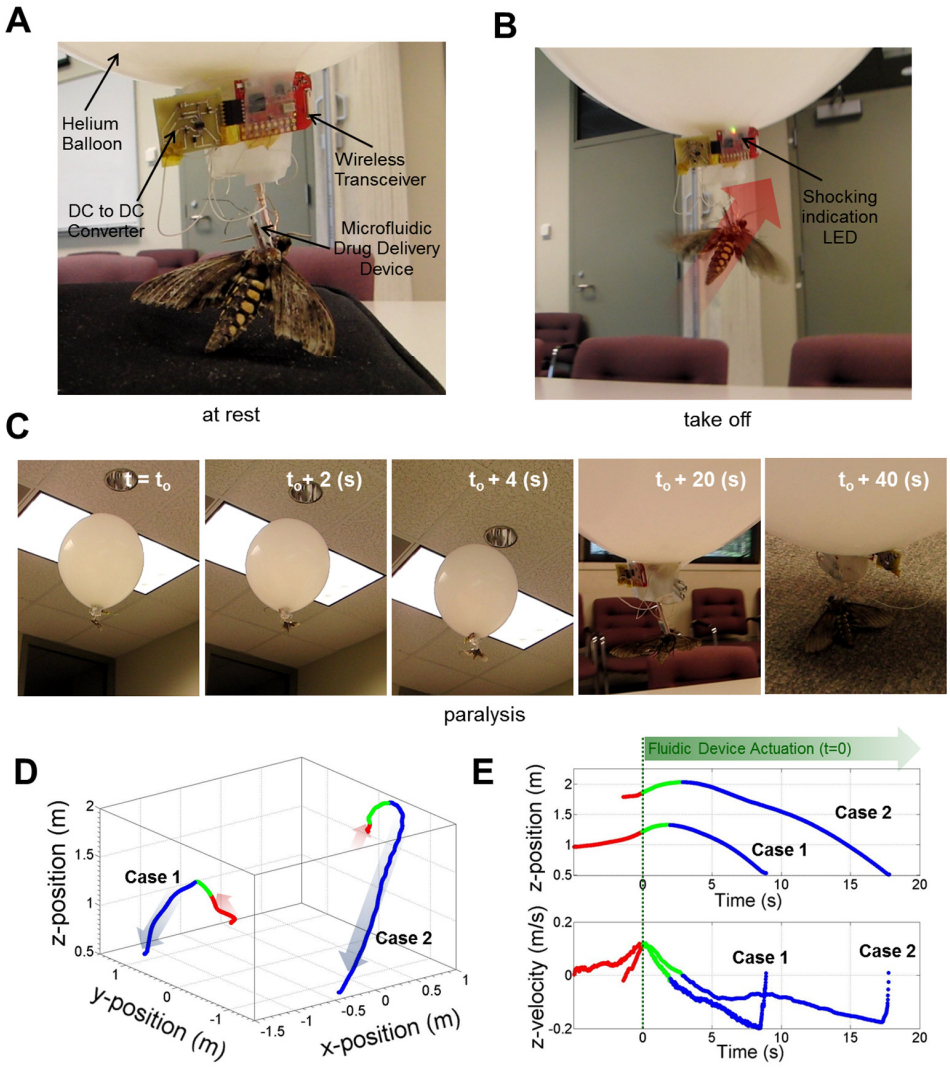

Figure 5.3. Wireless hybrid flight operation and flight tracking. (A) Moth at rest. (B) Electrically stimulated take-off. (C) Time lapse images showing moth subjected to electrical stimulation followed by chemically induced paralysis (D) Two representative cases of insect trajectories where the red bands denote flight under electrical stimulation, green during the drug delivery stage and blue during the deceleration due to chemical overstimulation. (E) Vertical displacement and speed as a function of time. Insects speed up during electrical stimulation (red), are subjected to the chemical release (green) and decelerate (blue) due to chemical overstimulation (see Movie S5.5).

The operation and characterization of the system is shown in Fig. 5.3 and in Movie S5.5. The insect is brought from rest (Fig. 5.3A) into take-off (Fig. 5.3B) by supplying the same pulse sequence used in Figs. 5.1 and 2 and in Movie S5.1. After 30 seconds of sustained flight (Fig. 5.3C), the microfluidic chip was actuated, releasing the 5 M solution of LGA. The insect responds by first decelerating for about 20 seconds until it reaches full paralysis (Fig. 5.3C). The DC pulse routine was suspended during chemical release to prohibit interference between the two signals but resumed immediately after dosing was complete. To track the moth's displacement and flight speed changes during flight, we used an in-door VICON tracking system. Two representative flight trajectories of full hybrid tests are presented in Fig. 5.3D, illustrating the three stages of flight: The red region denotes sustained flight under electrical stimulation (average flight speed 10 cm/s), followed by the drug delivery stage shown in green which captures the transition from stimulation to deceleration, and finally deceleration (blue) due to chemical overstimulation. The time to reach the onset of paralysis from the chemical ejection is within 5 seconds for both cases. Fig. 5.3E shows the vertical displacement and its corresponding speed as a function of time. Both trends in Fig. 5.3E also show how the moths reach a standstill once they hit the ground.

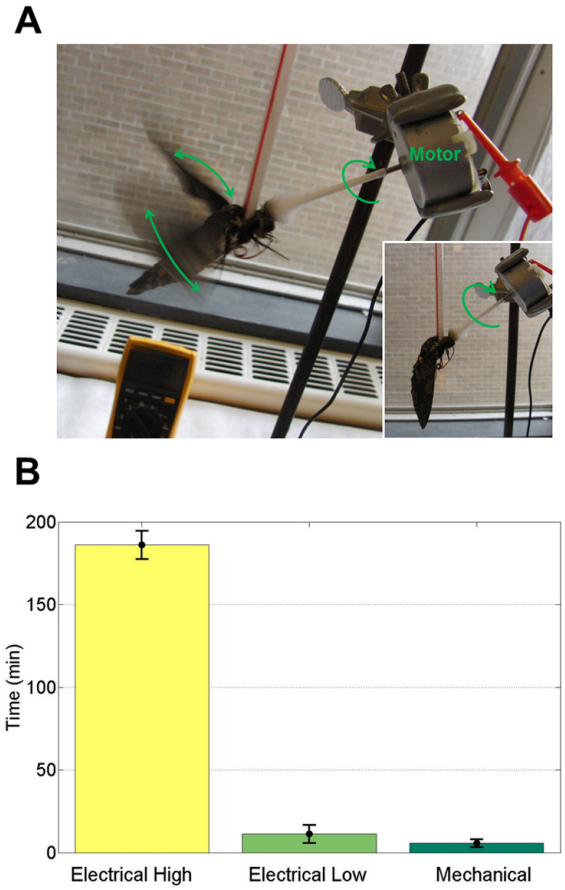

Figure 5.4. Comparison of mechanical and electrical flight duration enhancement techniques. (see Movies S5.1 and S5.6 for electrical and mechanical stimulation respectively) (A) Mechanical stimulation setup showing the moth prompted into flight by spinning a cotton swab on its head. (Inset) Moth unresponsive to long period of mechanical stimulation. (B) Comparison of electrical and mechanical enhancements in flight endurance showing both high and low electrical response groups.

5.3.3 Comparison of electrical and mechanical flight longevity enhancement modalities

In nature *Manduca sexta* moths tend to fly sporadically, a few times a day and in a manner that is very sensitive to the environmental conditions [26]. In practice it becomes necessary then to override their native behavior to achieve predictable flight

duration. Previously we demonstrated that direct mechanical stimulation can also be used to enhance flight longevity [17]. Although it is more difficult to construct an insect portable mechanical stimulation system, than it is for the electrical and chemical techniques demonstrated above, it is worthwhile to quantitatively determine which stimulation technique is better at promoting flight longevity.

The results of our experiments comparing flight longevity for these modalities are shown in Fig. 5.4 and Movies S5.1 and S5.6. Mechanical stimulation experiments were conducted without tampering with moth internal physiology (which does occur with both electrical and chemical implants), by rubbing a spinning cotton swab on the moth's head as shown in Fig. 5.4A and Movie S5.6. The cotton swab is attached to a pulsed DC motor and operates at the same frequency and duty cycle as that of the electrical stimulation experiments described above. The criterion used in these experiments is that 10 seconds of no flapping activity is considered as a full stop and the end of a test. Moths subjected to mechanical stimulation flew for an average of 5 minutes as shown in Fig. 5.4B. For electrical stimulation, data was collected using a similar apparatus to that shown in Fig. 5.1. It was observed that these insects responded in a bimodal way with one group tending to fly continuously for close to 3 hours on average and the other which flew for 17 minutes on average. The reason for this bimodal response is not known however it was clear that the low flight endurance group were much more rapid to adapt to the presence of electrical stimulation. When compared to the mechanically stimulated group, the high flight endurance group exhibited a 35-fold enhancement in flight duration.

5.4 Materials and methods

5.4.1 Microfabrication

The drug delivery system consists of three subcomponents. The first is a silicon layer containing a microwell with a suspended upper electrode through which fluids are ejected, a 3D printed acrylic channel coated with Parylene which contains the dose, and a bottom gold coated Pyrex substrate which serves as the counter electrode. The top silicon component was devised using the method established by Chung and Erickson [24], in which LPCVD silicon nitride is deposited on both sides of a <100> n-doped silicon wafer. The backside was patterned to define the well location, followed by gold deposition on the top side. The wells were then etched by immersing the wafer in KOH overnight and the remaining silicon nitride underneath the gold membrane was removed through reactive ion etching. This left a 100 μm by 100 μm square suspended gold membrane. A photoactive polyimide layer was spun and patterned on the top of the device to reduce electrical contact outside of the suspended gold membrane. One millimeter tall acrylic channels were defined and cleaned with a NaOH solution, followed by a Parylene deposition to ensure impermeability to water. The three subcomponents were then assembled and sealed using Loctite 454. The assembled device was then subjected to oxygen plasma cleaning, followed by fluidic loading from the backside and sealing using wax.

5.4.2 Implantation process

The microfluidic chips were implanted in adult moths 2 days after emerging from the pupal stage. Prior to the surgery, the moths were placed on an ice platform for

approximately 10 minutes to lower their internal body temperature and to minimize movement. With a sterilized scalpel, a portion of the dorsal exoskeleton and body skin were removed and the chip was placed 3 mm into the thorax near the dorso-longitudinal flight muscles. After gently inserting the device into the thorax, the wound was sealed using Loctite 454. This step was followed by the thin electrode implantation, which is gently inserted next to antennal lobe and sealed with the same biocompatible glue.

5.4.3 Displacement angle measurement and analysis

A thin wire leash was used to tether the moths head and thorax to the swinging arm during the image tracking experiments. 10 µl solution volumes were used for all injections. The displacement angle was evaluated using a customized MATLAB code based on Hedrick *et al.*'s [18] previous work. To track the insects' displacement in 3D tetherless flight, a reverse GPS system employing 24 VICON cameras was used to track IR reflecting balls attached to the helium balloon. All relevant animal care and use guidelines were followed in this study.

5.5 Conclusion

In summary, here we have demonstrated the use of simultaneous chemical and electrical modalities for modulating the flight activity of *Manduca sexta* moths. The optimal hybrid stimulation conditions were determined through series of tethered experiments and implemented on a wireless insect-borne system. The results were quantitatively analyzed by comparing them with baseline measurements using mechanical stimulation. It was shown that electrical stimulation can result in as much

as 35-fold improvement (on average 3 hours continuous flight) in flight longevity and chemically induced neurotransmitters overdose could result in a recoverable 50% mean flight speed reduction. This combined modality could allow for a broader range of flight operations to be performed.

5.6 Acknowledgement

The authors would like to thank J. Atchison for his contributions towards the boost converter design, Prof. M. Campbell and Prof. H. Kress-Gazit for access to the VICON system, M. Kalontarov for helpful discussions, Prof. H. Lipson for access to the 3D Acrylic Printer and Dr. M. Ozgur at MEMS Exchange. This work was supported by the DARPA Defense Sciences Office under the HI-MEMS program through the BTI for Plant Research. Distribution unlimited. The facilities used for this research include Cornell Nanoscale Science & Technology Facility (CNF), Nanobiotechnology Center (NBTC) at Cornell University.

REFERENCES

1. Wootton, R., *Aerodynamics: From insects to microvehicles.* Nature, 2000. **403**(6766): p. 144-145.
2. Tanaka, M., *An industrial and applied review of new MEMS devices features.* Microelectron. Eng., 2007. **84**(5-8): p. 1341-1344.
3. Franz, M.O. and H.A. Mallot, *Biomimetic robot navigation.* Robotics and Autonomous Systems, 2000. **30**(1-2): p. 133-153.
4. Wood, R.J., *The first takeoff of a biologically inspired at-scale robotic insect.* Ieee Transactions on Robotics, 2008. **24**(2): p. 341-347.
5. Ellington, C.P., *The Aerodynamics of Hovering Insect Flight .1. the Quasi-Steady Analysis.* Philosophical Transactions of the Royal Society of London Series B-Biological Sciences, 1984. **305**(1122): p. 1-15.
6. Pesavento, U. and Z.J. Wang, *Flapping Wing Flight Can Save Aerodynamic Power Compared to Steady Flight.* Phys. Rev. Lett., 2009. **103**(11).
7. Helm, B., *Finding Land Mines by Following a Bee*, in *Business Week*. 2005.
8. Weinberger, S., *Defence research: Still in the lead?* Nature, 2008. **451**: p. 390-393.
9. Lian, Y.S., W. Shyy, D. Viieru, and B.N. Zhang, *Membrane wing aerodynamics for micro air vehicles.* Prog. Aerosp. Sci., 2003. **39**(6-7): p. 425-465.
10. Jeon, Y.B., R. Sood, J.h. Jeong, and S.G. Kim, *MEMS power generator with transverse mode thin film PZT.* Sensor. Actuat. A, 2005. **122**(1): p. 16-22.
11. Wickenheiser, A.M., T. Reissman, W.J. Wu, and E. Garcia, *Modeling the Effects of Electromechanical Coupling on Energy Storage Through*

Piezoelectric Energy Harvesting. Ieee-Asme Transactions on Mechatronics, 2010. **15**(3): p. 400-411.

12. Bozkurt, A., R.F. Gilmour, A. Sinha, D. Stern, and A. Lal, *Insect-Machine Interface Based Neurocybernetics.* Ieee Transactions on Biomedical Engineering, 2009. **56**(6): p. 1727-1733.
13. Bozkurt, A., A. Lal, and R. Gilmour, *Aerial and terrestrial locomotion control of lift assisted insect biobots.* Conf. Proc. IEEE. Eng. Med. Biol. Soc., 2009. **2009**: p. 2058-61.
14. Sato, H., C.W. Berry, Y. Peeri, E. Baghoomian, B.E. Casey, G. Lavella, J.M. Vandenbrooks, J.F. Harrison, and M.M. Maharbiz, *Remote radio control of insect flight.* Front. Integr. Neurosci., 2009. **3**: p. 24.
15. Daly, D.C., P.P. Mercier, M. Bhardwaj, A.L. Stone, Z.N. Aldworth, T.L. Daniel, J. Voldman, J.G. Hildebrand, and A.P. Chandrakasan, *A Pulsed UWB Receiver SoC for Insect Motion Control.* Ieee Journal of Solid-State Circuits, 2010. **45**(1): p. 153-166.
16. Tsang, W.M., A.L. Stone, Z.N. Aldworth, J.G. Hildebrand, T.L. Daniel, A.I. Akinwande, and J. Voldman, *Flexible Split-Ring Electrode for Insect Flight Biasing Using Multisite Neural Stimulation.* Ieee Transactions on Biomedical Engineering, 2010. **57**(7): p. 1757-1764.
17. Chung, A.J. and D. Erickson, *Engineering insect flight metabolics using immature stage implanted microfluidics.* Lab on a Chip, 2009. **9**(5): p. 669-676.
18. Hedrick, T.L., *Software techniques for two- and three-dimensional kinematic measurements of biological and biomimetic systems.* Bioinspiration & Biomimetics, 2008. **3**(3).

19. Skinner, W.S., P.A. Dennis, J.P. Li, R.M. Summerfelt, R.L. Carney, and G.B. Quistad, *Isolation and Identification of Paralytic Peptides from Hemolymph of the Lepidopteran Insects Manduca-Sexta, Spodoptera-Exigua, and Heliothis-Virescens.* J. Biol. Chem., 1991. **266**(20): p. 12873-12877.

20. Ziegler, R. and M. Schulz, *Regulation of Carbohydrate-Metabolism During Flight in Manduca-Sexta.* Journal of Insect Physiology, 1986. **32**(12): p. 997-1001.

21. Ziegler, R., *Changes in Lipid and Carbohydrate-Metabolism During Starvation in Adult Manduca-Sexta.* Journal of Comparative Physiology B-Biochemical Systemic and Environmental Physiology, 1991. **161**(2): p. 125-131.

22. Claassen, D.E. and A.E. Kammer, *Effects of Octopamine, Dopamine, and Serotonin on Production of Flight Motor Output by Thoracic Ganglia of Manduca-Sexta.* Journal of Neurobiology, 1986. **17**(1): p. 1-14.

23. Johnston, R.M. and R.B. Levine, *Crawling motor patterns induced by pilocarpine in isolated larval nerve cords of Manduca sexta.* Journal of Neurophysiology, 1996. **76**(5): p. 3178-3195.

24. Chung, A.J., Y. Huh, and D. Erickson, *A robust, electrochemically driven microwell drug delivery system for controlled vasopressin release.* Biomed. Microdevices, 2009. **11**(4): p. 861-867.

25. Bozkurt, A., R.F. Gilmour, and A. Lal, *Balloon-Assisted Flight of Radio-Controlled Insect Biobots.* Ieee Transactions on Biomedical Engineering, 2009. **56**(9): p. 2304-2307.

26. McCrea, M.J. and J.E. Heath, *Dependence of Flight on Temperature Regulation in the Moth, Manduca Sexta.* J. Exp. Biol., 1971. **54**(2): p. 415-435.

CHAPTER 6

OPTOFLUIDIC WAVEGUIDES FOR RECONFIGURABLE PHOTONIC SYSTEMS*

6.1 Abstract

We report the development of two liquid waveguide based photonic elements for use in reconfigurable photonic systems. This work demonstrates the ability to couple light from a conventional optical fiber to an adaptable liquid-core/liquid-cladding waveguide and back again to an optical fiber(s) enabling us to take advantage of both liquid- and solid-state photonic modalities. We demonstrate and characterize the use of this fiber-in and fiber-out system as either an optical switch or signal attenuator. Microscale flow control enables the adaptive morphology and tunable position of the liquid waveguide yielding an attenuation range of 3.1-10.7 dB, operability over a broad bandwidth spanning the range of wavelengths from visible to telecommunication, and a 1x2 sub-second switching system with a cross-talk as low as 20 dB and maximum coupling efficiency of 3.87 dB.

*Reprinted by permission of the Optical Society of America (OSA) with permission from Aram J. Chung and David Erickson, "Optofluidic waveguides for reconfigurable photonic systems", *Optics Express*, **19** (9), 8602-8609 (2011), DOI: 10.1364/OE.19.008602 © OSA

6.2 Introduction

A reconfigurable system is one that can dynamically adapt its properties or function in response to an externally issued command or autonomously in response to changes in operational conditions. In electronics, the FPGA (Field Programmable Gate Array) [1] is the ubiquitous example of such a system in that it can provide "on-the-fly" reconfigurability by reprogramming the hierarchy of interconnections between different logic blocks. Despite the advantages, there are very few other microsystem based fields which have demonstrated technologies that exhibit anywhere near the level of reconfiguration possible through FPGAs.

A key factor for the development of an analogous high-performance reconfigurable photonic system would be the capability to dynamically control either (1) the physical layout or (2) the refractive indices of the optical components. Recent advancements in optical MEMS technology [2-4] has provided significant functionality and flexibility to the former of these techniques. With regards to the latter, traditional techniques for manipulating the refractive index through electro-optic [5, 6], magneto-optic [7], acousto-optic [8, 9], thermo-optic [10], and carrier injection [11] techniques are limited by the achievable $\Delta n/n$ (see Erickson *et al.* [12] for details and a tabulated comparison). The practical implication of a smaller $\Delta n/n$ is that either a longer interaction length is required (occupying more on-chip space) or resonant elements must be incorporated (reducing the bandwidth).

Recent developments in optofluidics [13, 14] have demonstrated how incorporating microfluidic elements into photonic systems can yield much higher $\Delta n/n$. For example, Erickson *et al.* [15], reported high refractive index modulation of the photonic crystal circuits using nanofluidics. The disadvantage of these approaches is that while broad tunability can be obtained, the base optical elements (*e.g.* photonic

crystals [15, 16] and ring resonators [17, 18]) must be incorporated at the fabrication stage. Although a number of pure fluid state photonic elements, like waveguides [19, 20], microlenses [21, 22], and dye lasers [23, 24] have been demonstrated, they are not often used to directly physically reconfigure elements within a solid-state photonic system. The advantage of using fluidics in comparison with the MEMS based reconfigurability approaches listed above is that the physical displacement of the optical elements can be much larger.

In this paper, we demonstrate the use of high performance liquid-core/liquid-cladding waveguides to achieve optical attenuation and 1x2 switching in a fiber-in and fiber-out system. Previously we reported a numerical study [25] on a hybrid system for coupling light between liquid- and solid-state waveguides, demonstrating the potential to achieve high coupling efficiencies using a fluid enveloping "end-fire" type technique. Here we implement this technique experimentally demonstrate coupling efficiencies as high as 48.98% (including all losses from the input fiber to the output detector). Recently, Seow *et al.* [26] and Lim *et al.* [27] also reported liquid-core based switching systems, with the latter demonstrating a high-speed 2x3 fiber-in and fiber-out switch. Here we demonstrate analogous switching but also introduce: the ability to perform controlled the attenuation, a single layer fabrication technique optimized for achieving low cross-talk (less than 20 dB), and characterize the system over the broader bandwidth including visible and telecommunication wavelengths. By integrating liquid- and solid-state photonic modalities on a single chip, we hope this hybrid system can become an element of a new type of photonic element for use in reconfigurable photonic and optical communication systems.

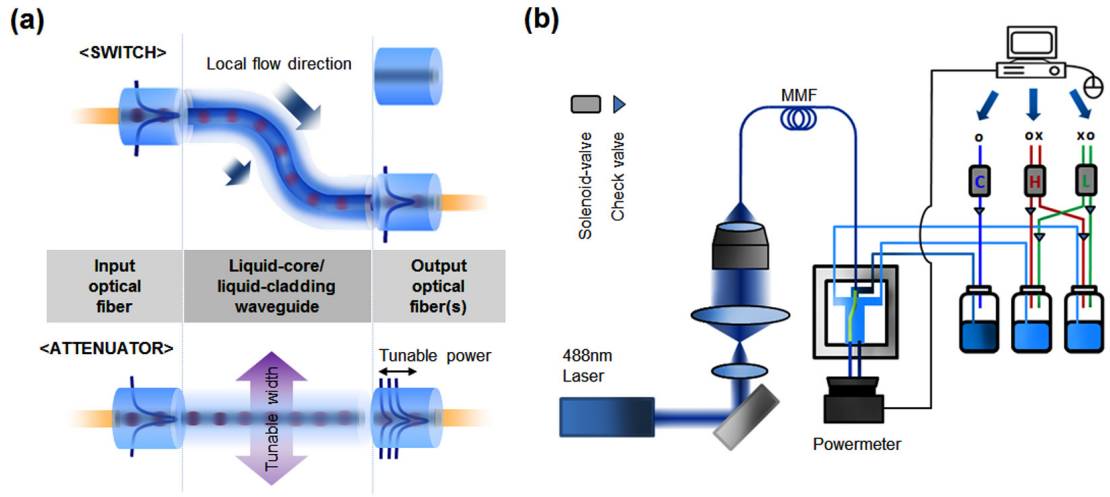

Figure 6.1. Schematic views of (a) the optofluidic system showing the principle of operation for the optical switch (upper image) and the tunable modulator (lower image) (b) Experimental setup showing the coupling of the optical and flow control systems to the chip.

6.3 Principles of operation, device design and experimental setup

We demonstrate here two hybrid fiber-in and fiber-out reconfigurable optofluidic systems: (1) a 1x2 optical switch and (2) a tunable attenuator. The operating principle of both these devices is shown schematically in Fig. 6.1(a). Briefly, in both cases light is first coupled from the input optical fiber to the adaptable liquid-core/liquid-cladding waveguide. In the case of the switch the liquid waveguide is then directed to one of the two output fibers by changing the input pressure of one of the cladding flows. For the attenuator we modulate the power transferred from the input to the output optical fiber by adjusting the width of the liquid-core waveguide. This is done by increasing or decreasing the pressure of both cladding flows equally.

To form the liquid-core/liquid-cladding waveguide [19], a solution of 5.0 M Calcium Chloride ($CaCl_2$, n~1.44) is introduced as the core solution and two low refractive index streams of DI water (n~1.33) are used as the cladding. For the

waveguide visualization experiments shown below, the core fluid was also doped with FITC (fluorescein isothiocyanate) dye. For all excitation wavelengths multi-mode fiber (MMF, outer diameter = 125 μm, core diameter = 105 μm, and nominal numerical aperture NA = 0.22) was used for both the input and output channels. We used MMF here since they are often preferred to single mode fibers in optical communication due to their lower cost and relative ease of in-coupling. Unless otherwise noted below, all experiments were conducted with a 488 nm laser with the output power fixed at 4.3 mW. As illustrated in Fig. 6.1(b) the fiber is directly inserted into a poly(dimethylsiloxane)(PDMS) chip whose channel height was matched with that of the optical fiber outer diameter. The PDMS-microchannel was fabricated using a conventional soft photolithography method [28]. Flows are pumped into the PDMS microfluidic chip using off-chip solenoid-valves and all fluid flow manipulation which was controlled via a customized LabVIEW program as can be seen in Fig 6.1(b).

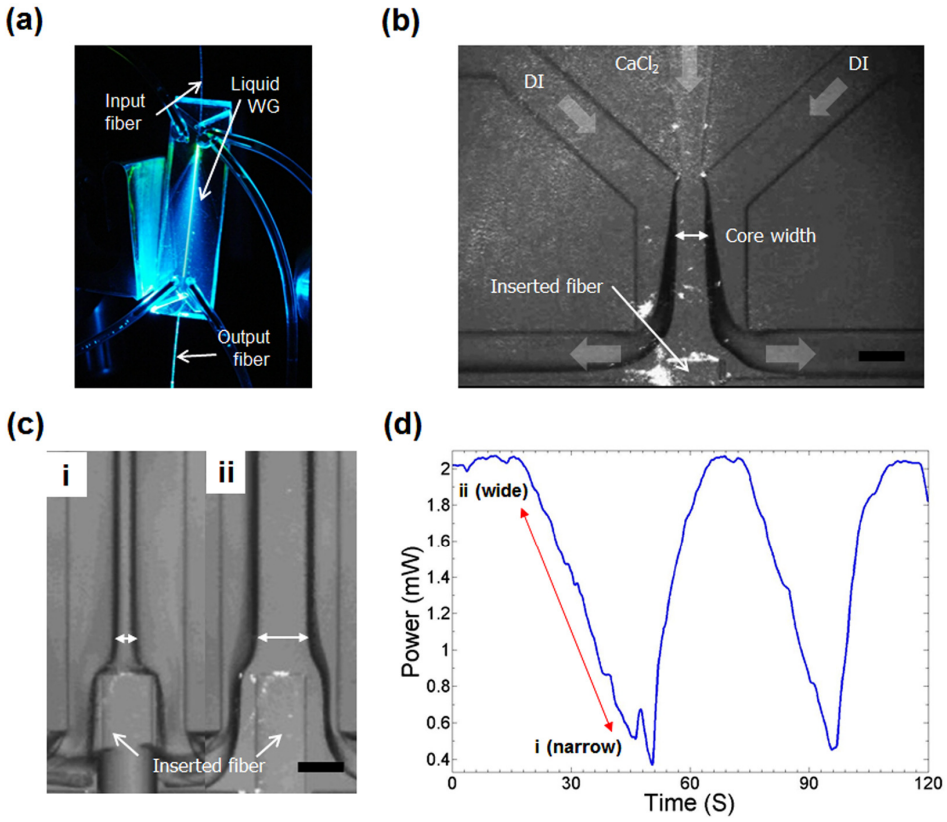

Figure 6.2. Optofluidic tunable attenuator (a) PDMS chip showing liquid-core/liquid-cladding waveguide and light propagation along it. (b) Magnified view from above looking at the region near liquid waveguide. (c) Minimum and maximum transmitted power states for the liquid waveguide. (d) Output power measurements for the 1.25 mm liquid waveguide length: output (see supplemental Movie S1). In all cases, scale bar represents 125 μm.

6.4 Results and discussions

6.4.1 Optofluidic attenuator

For the optofluidic attenuator, the input and output optical fibers are directly coupled by the liquid waveguide. By changing the width of the liquid core (by modulating the relative flow rates of the core and cladding fluids) the amount of power transmitted to the output fiber can be dynamically modulated. The mode

profile in the liquid waveguide can be also reconfigured simply by adjusting the local flow conditions. Single mode operation is possible, as demonstrated by Wolfe *et al*. [19]. As mentioned above however, here we focus primarily on multimode operation. The optofluidically tunable attenuator and a magnified view of the microfluidic arrangement at the region near liquid waveguide are showed in Fig. 6.2 (a) and (b) respectively. Figure 6.2(c) and (d) illustrate the transmitted power changes as the core is adjusted from its maximum to minimum width (see supplemental Movie S6.1 for more details). Based on the power output for the 1.25 mm waveguide length shown here, the observed attenuation power range was between 3.1 to 10.7 dB.

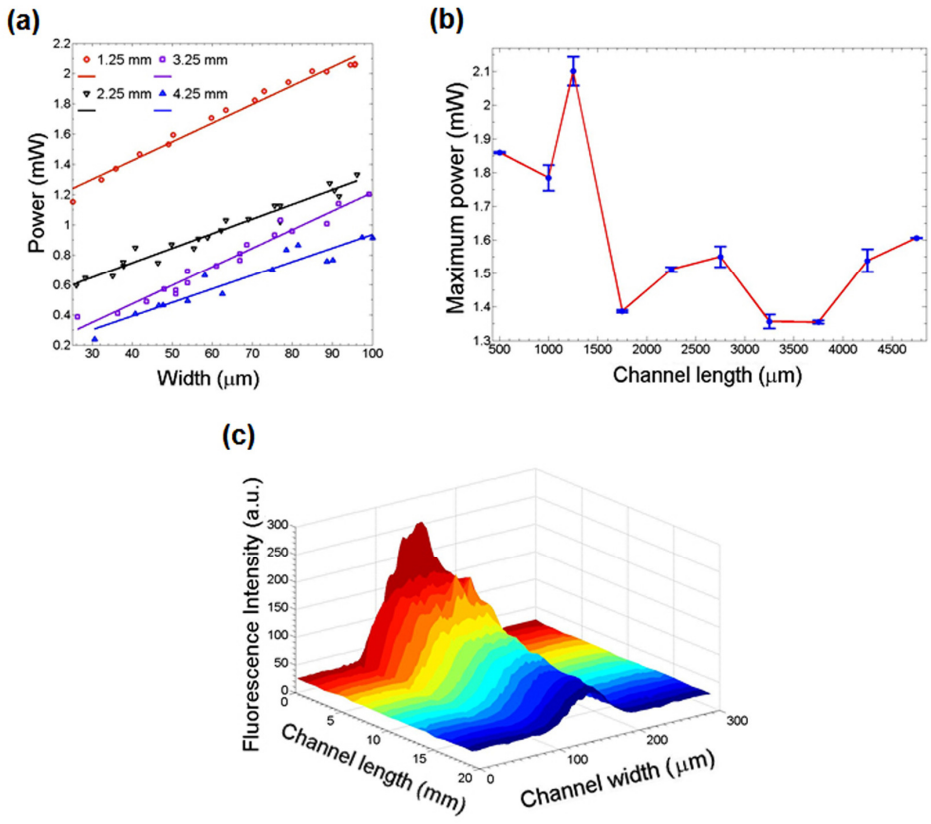

Figure 6.3. (a) Output power as a function of the waveguide width for different channel lengths (equivalent to liquid waveguide length). (b) Maximum power as a function of the liquid waveguide length ranging from 0.5 mm to 4.75 mm. The error

bars represents standard error of the mean. (c) Emitted fluorescence intensity from the liquid waveguide as a function of downstream distance.

In order to further characterize the optofluidic attenuator, a series of experiments were performed to measure the transmitted power as a function of the width and length of the liquid core waveguide. Figure 6.3(a) shows results for four different channel lengths: 1.25, 2.25, 3.25 and 4.25 mm. The method of least squares was used to fit the data points. Figure 6.3(b) shows the maximum transmitted power trend for all the waveguide lengths tested here. As can be seen in Fig. 6.3(a), regardless of the length of the liquid waveguide a linear response of the output power was observed as a function of the core width. It was however also observed that when the core size became much larger than that of the optical fiber, the transmitted power was also reduced. As expected, the maximum transmitted power tended to decrease for longer liquid waveguides. The inconsistency in the slope and variability in the maximum coupled power with waveguide length, seen in Figs. 6.3(a) and (b), was a repeatable effect and likely the result of irregular reflections off the waveguide surface and mode mismatching between the liquid waveguide and the output optical fiber. Commercially available tunable attenuators have a higher variable attenuation range but tend to have much higher power insertion loss. In addition, the material costs for manufacturing fluid based attenuators such as this one could be much lower, given that only 6 g of PDMS are required at an approximate cost of 50 cents.

To characterize the loss in the liquid waveguide itself we performed an experiment where the liquid waveguide was doped with a florescent dye and the change in emitted intensity was measured as a function of the downstream distance. Figure 6.3(c) shows the intensity profile for a 120 μm wide waveguide for two centimeters of propagation distance. With these results, we calculate the waveguide loss is 0.451 dB/mm. Note that the waveguide loss calculated here includes the loss due to the florescent dye

absorption. We expect that major cause for this loss was diffusive broadening of the core and cladding interface (see Jung *et al.* [25] for a numerical analysis of the relationship between light propagation and diffusion as a function of Peclet number). Reduction of this loss could be achieved through the use of immiscible fluids [29].

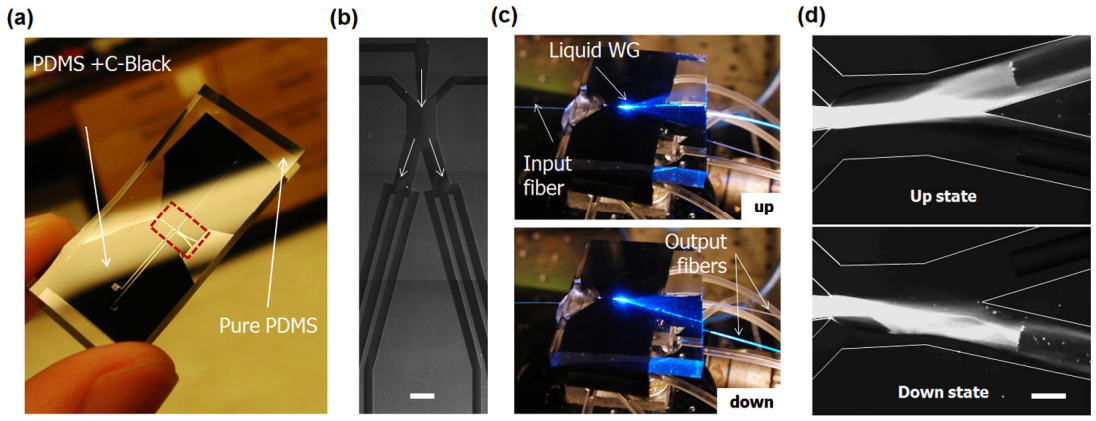

Figure 6.4. (a) Optofluidic switch showing carbon black added to the bottom substrate in order to reduce cross-talk between the two output optical fibers. (b) Optical micrograph view of the red dashed zone in (a). (c) Photographic image of the 1x2 optofluidic switch in both states. (d) Magnified view of the switching states. In all cases, scale bar represents 125 μm.

6.4.2 Optofluidic switch

As briefly mentioned above, the optofluidic switching element operates through pressure manipulation of the core and cladding fluids, directing the position of the liquid waveguide so that it out couples to one of the output optical fibers. Figure 6.4(a) shows the optofluidic chip and Fig. 6.4(b) shows a magnified view of the microfluidic channel layout. To reduce cross-talk between the two output channels, carbon black was introduced during the PDMS polymerization process (2.4 % wt/wt with a 5:1 mass ratio of the base to the curing agent for the PDMA). Optofluidic

switching between the two states of a 1x2 switch is shown in Figs. 6.4(c) and (d) (see supplemental Movie S6.2 for more details). In both these figures the liquid waveguide was doped with fluorescent dye to facilitate visualization. Note that the presence of the carbon black significantly interferes with fluorescent imaging, resulting relative poor quality of the images. In this paper, we demonstrate a 1x2 switching system however we note that it could be expanded to a 1xN system for higher performance applications.

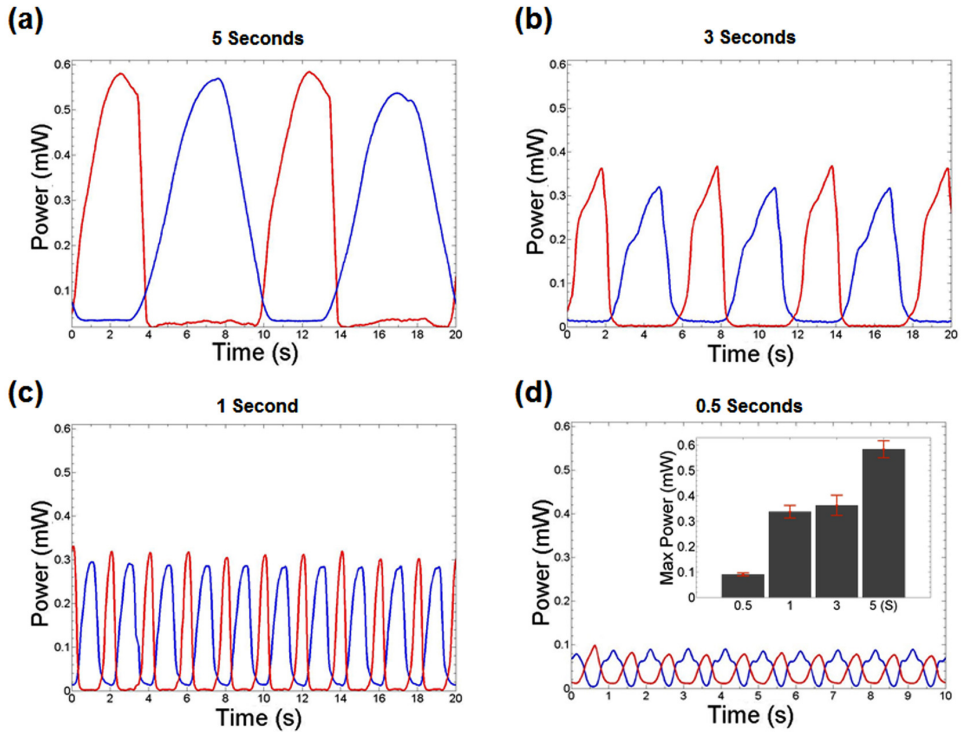

Figure 6.5. Output power *vs.* switching period for (a) 5 seconds, (b) 3 seconds, (c) 1 second, and (d) 0.5 seconds. (Inset) Maximum power plot for each switching period. The error bars represents standard error of mean.

Figure 6.5 shows the relationship between the measured output power and the switching period. The two output channels are represented by blue and red lines. As expected, when the switching period is decreased from 5 seconds to 0.5 seconds, the

maximum output power is also decreased from 0.584 mW to 0.0907 mW. The maximum coupled power for all switching periods is plotted in the inset of Fig. 6.5(d). For these experiments, cross-talk is defined as the ratio of the power coupled into the on fiber to that coupled into the off fiber. Without carbon black doping of the PDMS, the cross-talk was on the order of 10 dB. Introducing carbon black into the chip served to absorb the vast majority of the truant scattered light in the system, reducing the cross-talk down to the 20 dB levels shown in Fig. 6.5. As can be seen, the quality of the switching also decreased for quicker switching periods placing an upper limit on the rate at which this technique could be used to reconfigure a photonic system. Higher performance may be able to be obtained either by introducing immiscible fluids or using pneumatically actuated PDMS membrane microvalves as has been demonstrated previously [27]. Commercially available MEMS (Microelectromechanical systems) or prism based optical switching devices have shown lower cross-talk (50-80 dB) and faster switching (milliseconds) however the optofluidic switch has advantages including: low insertion coupling loss (3.1 dB) and potential cost advantages as mentioned above.

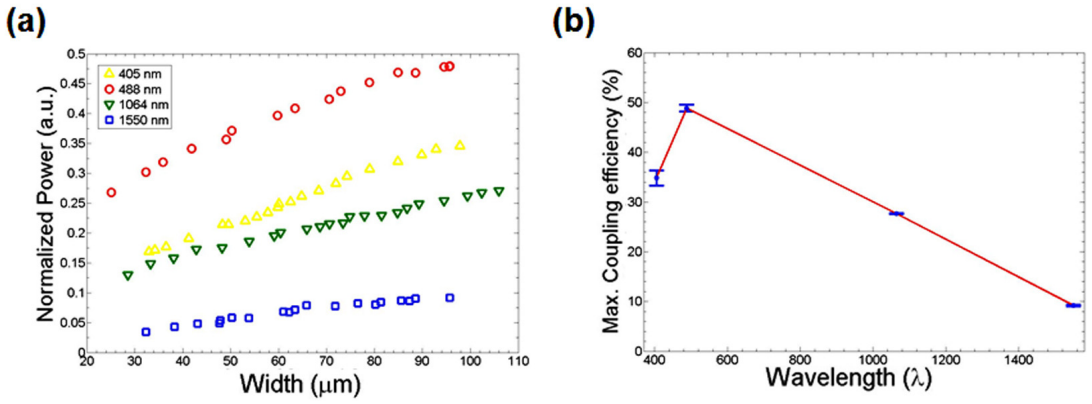

Figure 6.6. (a) Coupled power into the output waveguide as a function of core width for 4 different laser wavelengths. (b) Maximum coupling efficiency for all wavelengths tested here. The error bars represents standard error of the mean.

6.4.3 Bandwidth

To characterize the optical bandwidth of the system the attenuated power *vs.* core width experiments described above were repeated for four different lasers with wavelengths of 405 nm, 488 nm, 1064 nm, and 1550 nm. All experiments were done using a 1.25 mm liquid waveguide as it showed the maximum transmitted power in the earlier experiments (see Fig. 6.3(b)). Since each test laser had a different input power value, the output power of the chip was normalized against the input power to the chip from the waveguide. As illustrated in Fig. 6.6(a), the output power for all wavelengths showed a linear response to waveguide width for both visible and telecommunication wavelengths. Figure 6.6(b) shows the maximum output power as a function of wavelength. These results show a peak at the blue end of the visible spectrum and match well with the water absorption spectrum suggesting that this is the limiting factor in the bandwidth of our system. Higher performance can be obtained by using waveguiding fluids whose absorption spectrum are better matched to the wavelength range of interest. For example, at 1550 nm, heavy water would be preferable as a waveguiding fluid for lower optical absorption [30].

6.5 Conclusion

We present here a new approach to reconfigurable photonics which couples the physical adaptability of microfluidic waveguides to fiber-in and fiber-out optical systems. Our efforts focused on the development of two components that could form the basis of a more complex reconfigurable photonic system: a signal attenuator and a 1x2 optical switch. By integrating liquid- and solid-state photonic modalities onto a single chip, we have demonstrated high coupling efficiency (3.1 dB), low cross-talk

(less than 20 dB), and demonstrated good performance over a broad range of wavelengths from visible and telecommunication.

6.6 Acknowledgement

The authors would like to thank Y-F. Chen for his contribution to the LabVIEW program used to run the experiments, and E. Jung and B. Romero for helpful discussion. The facilities used for this research include the Nanoscale Science & Technology Facility (CNF) and the Nanobiotechnology Center (NBTC) at Cornell University. This work was supported by the Air Force Office of Scientific Research through an STTR grant under the Reconfigurable Materials for Cellular Electronic and Photonic Systems discovery challenge thrust.

REFERENCES

1. Strukov, D.B. and K.K. Likharev, *CMOL FPGA: a reconfigurable architecture for hybrid digital circuits with two-terminal nanodevices.* Nanotechnology, 2005. **16**(6): p. 888-900.
2. Lin, L.Y. and E.L. Goldstein, *Opportunities and challenges for MEMS in lightwave communications.* IEEE Journal of Selected Topics in Quantum Electronics, 2002. **8**(1): p. 163-172.
3. Lyshevski, S.E., *MEMS and NEMS : systems, devices, and structures*, ed. C. Press. 2002, Boca Raton, Fl.
4. Gad-el-Hak, M., *MEMS : design and fabrication*. 2006, Boca Raton: CRC Press.
5. Roussey, M., M.P. Bernal, N. Courjal, and F.I. Baida, *Experimental and theoretical characterization of a lithium niobate photonic crystal.* Applied Physics Letters, 2005. **87**(24).
6. Roussey, M., M.P. Bernal, N. Courjal, D. Van Labeke, F.I. Baida, and R. Salut, *Electro-optic effect exaltation on lithium niobate photonic crystals due to slow photons.* Applied Physics Letters, 2006. **89**(24).
7. Diwekar, M., V. Kamaev, J. Shi, and Z.V. Vardeny, *Optical and magneto-optical studies of two-dimensional metallodielectric photonic crystals on cobalt films.* Applied Physics Letters, 2004. **84**(16): p. 3112-3114.
8. Verluise, F., V. Laude, Z. Cheng, C. Spielmann, and P. Tournois, *Amplitude and phase control of ultrashort pulses by use of an acousto-optic programmable dispersive filter: pulse compression and shaping.* Optics Letters, 2000. **25**(8): p. 575-577.

9. Courjal, N., S. Benchabane, J. Dahdah, G. Ulliac, Y. Gruson, and V. Laude, *Acousto-optically tunable lithium niobate photonic crystal.* Applied Physics Letters, 2010. **96**(13).

10. Camargo, E.A., H.M.H. Chong, and R.M. De la Rue, *2D Photonic crystal thermo-optic switch based on AlGaAs/GaAs epitaxial structure.* Optics Express, 2004. **12**(4): p. 588-592.

11. Gu, L.L., W. Jiang, X.N. Chen, L. Wang, and R.T. Chen, *High speed silicon photonic crystal waveguide modulator for low voltage operation.* Applied Physics Letters, 2007. **90**(7).

12. Erickson, D., C.H. Yang, and D. Psaltis, *Optofluidics emerges from the laboratory.* Photonics Spectra, 2008. **42**(2): p. 74-78.

13. Psaltis, D., S.R. Quake, and C.H. Yang, *Developing optofluidic technology through the fusion of microfluidics and optics.* Nature, 2006. **442**(7101): p. 381-386.

14. Monat, C., P. Domachuk, and B.J. Eggleton, *Integrated optofluidics: A new river of light.* Nature Photonics, 2007. **1**(2): p. 106-114.

15. Erickson, D., T. Rockwood, T. Emery, A. Scherer, and D. Psaltis, *Nanofluidic tuning of photonic crystal circuits.* Optics Letters, 2006. **31**(1): p. 59-61.

16. Smith, C.L.C., U. Bog, S. Tomljenovic-Hanic, M.W. Lee, D.K.C. Wu, L. O'Faolain, C. Monat, C. Grillet, T.F. Krauss, C. Karnutsch, R.C. McPhedran, and B.J. Eggleton, *Reconfigurable microfluidic photonic crystal slab cavities.* Optics Express, 2008. **16**(20): p. 15887-15896.

17. Levy, U., K. Campbell, A. Groisman, S. Mookherjea, and Y. Fainman, *On-chip microfluidic tuning of an optical microring resonator.* Applied Physics Letters, 2006. **88**(11).

18. Galas, J.C., J. Torres, M. Belotti, Q. Kou, and Y. Chen, *Microfluidic tunable dye laser with integrated mixer and ring resonator.* Applied Physics Letters, 2005. **86**(26).

19. Wolfe, D.B., R.S. Conroy, P. Garstecki, B.T. Mayers, M.A. Fischbach, K.E. Paul, M. Prentiss, and G.M. Whitesides, *Dynamic control of liquid-core/liquid-cladding optical waveguides.* Proceedings of the National Academy of Sciences of the United States of America, 2004. **101**(34): p. 12434-12438.

20. Lim, J.M., S.H. Kim, J.H. Choi, and S.M. Yang, *Fluorescent liquid-core/air-cladding waveguides towards integrated optofluidic light sources.* Lab on a Chip, 2008. **8**(9): p. 1580-1585.

21. Tang, S.K.Y., C.A. Stan, and G.M. Whitesides, *Dynamically reconfigurable liquid-core liquid-cladding lens in a microfluidic channel.* Lab on a Chip, 2008. **8**(3): p. 395-401.

22. Mao, X.L., J.R. Waldeisen, B.K. Juluri, and T.J. Huang, *Hydrodynamically tunable optofluidic cylindrical microlens.* Lab on a Chip, 2007. **7**(10): p. 1303-1308.

23. Li, Z.Y., Z.Y. Zhang, T. Emery, A. Scherer, and D. Psaltis, *Single mode optofluidic distributed feedback dye laser.* Optics Express, 2006. **14**(2): p. 696-701.

24. Song, W.Z. and D. Psaltis, *Pneumatically tunable optofluidic dye laser.* Applied Physics Letters, 2010. **96**(8).

25. Jung, E.E., A.J. Chung, and D. Erickson, *Analysis of liquid-to-solid coupling and other performance parameters for microfluidically reconfigurable photonic systems.* Optics Express, 2010. **18**(11): p. 10973-10984.

26. Seow, Y.C., S.P. Lim, and H.P. Lee, *Tunable optofluidic switch via hydrodynamic control of laminar flow rate.* Applied Physics Letters, 2009. **95**(11).

27. Lim, J.M., J.P. Urbanski, T. Thorsen, and S.M. Yang, *Pneumatic control of a liquid-core/liquid-cladding waveguide as the basis for an optofluidic switch.* Applied Physics Letters, 2011. **98**(4): p. In press.

28. Whitesides, G.M., E. Ostuni, S. Takayama, X.Y. Jiang, and D.E. Ingber, *Soft lithography in biology and biochemistry.* Annual Review of Biomedical Engineering, 2001. **3**: p. 335-373.

29. Jung, E.E., A.J. Chung, and D. Erickson. *Advancements in microfluidically reconfigurable photonics* in *European Optical Society Conference on Optofluidics*. 2011.

30. Bayly, J.G., V.B. Kartha, and W.H. Stevens, *The absorption spectra of liquid phase H_2O, HDO and D_2O from 0.7µm to 10µm.* Infrared Physics, 1963. **3**(4): p. 211-222.

CHAPTER 7

CONCLUSIONS

I was able to develop (1) rapid, low power drug delivery devices for insect biorobots and (2) optofluidic reconfigurable photonic systems. Below, I present the summary of my research accomplishments and contributions by project:

7.1. Summary of Individual Accomplishments by Project

7.1.1. Electrokinetic microfluidic devices for rapid, low power drug delivery in autonomous microsystems

- Implantable, low power and rate controllable drug delivery systems designed for autonomous microsystems as little as 20 mJ of energy consumption.
- Using a combination of electroosmotic and electrophoretic effects controlled through an electric potential, rapid drug delivery with an improvement on the order of approximately 130-fold compared to the diffusion based system [1].
- Detailed three dimensional numerical simulations to model the electrokinetic transport involved in the electrokinetic ejection process.
- Providing a physical insight in to the transport mechanism, the simulations revealed that the majority of the contents are ejected early in the process.

7.1.2. Engineering insect flight metabolics using immature stage implanted microfluidics

- A method of exerting chemical control over insect flight activity, exploiting the use of immature stage implanted microfluidics to reversibly control the rate of metabolic output.

- First step towards the development of an artificial insect nervous system where the controlled release of inhibitory or excitatory neurotransmitters could be accomplished in response to external stimuli.

- Behavior controls ranging from retarded motion to complete, reversible paralysis, over timescales ranging from minutes to hours.

- A new paradigm for insect flight control alongside established electrical techniques and for basic component of an eventual artificial insect nervous system.

7.1.3. A robust, electrochemically driven microwell drug delivery system for controlled vasopressin release

- Implantable microreservoir device that enables delivery of dose volumes as high as 15 μl using an electrochemically based transport mechanism.
    - Significant reduction in the amount of time required for drug delivery as well as reducing the dependence on the external physiological conditions
    - Potential usage for the medical use for hemorrhagic shock through release of vasopressin
- Actively propel the drugs using a combination of electrolytic and gold dissolution reactions induced by the application of a voltage.

- An ejection rate as high as 4.19 μl/min with a maximum power consumption of approximately 5 mW.

7.1.4. Hybrid techniques for modulating insect flight activity and longevity

- An integrated microsystem that uses both chemical and electrical methods to modulate the flight activity of *Manduca sexta* moths.
- Characterization of performance, recovery and endurance times of insects subjected to hybrid chemical and electrical stimulations.
- 35-fold improvement (on average 3 hours continuous flight) in flight longevity compared to mechanical stimulation.
- 50% mean flight power output reduction achieved with the proper neurotransmitter dose.

7.1.5. Optofluidic waveguides for reconfigurable photonic systems

- New approach to reconfigurable photonics which couples the physical adaptability of microfluidic waveguides to fiber-in and fiber-out optical systems.
- Two components that could form the basis of a more complex reconfigurable photonic system: a signal attenuator and a 1x2 optical switch.
- High coupling efficiency (3.1 dB) and low cross-talk (less than 20 dB).
- Performance over a broad range of wavelengths from visible and telecommunication.

7.2. Major challenges

This section states the major problems that I faced over the course of my Ph.D. Following challenges have been set to investigate more in detail and all solutions have described in Chap. 2-6.

7.2.1. Electrokinetic microfluidic devices for rapid, low power drug delivery in autonomous microsystems

- Granting proper robustness of the suspending gold membrane (100 nm).
- Avoiding the rupture of the pyramidal reservoir (~100 nL) during the filling up procedure.

7.2.2. Engineering insect flight metabolics using immature stage implanted microfluidics

- Determination of the optimal location and timing to implant of the microdevices.
- Determination of the effective chemicals that could modulate moths' flight capability including full paralysis, deceleration and stimulation.
- Developing a mechanical stimulation apparatus in a closed gas measurement system to gauge the change in the carbon dioxide level.

7.2.3. A robust, electrochemically driven microwell drug delivery system for controlled vasopressin release

- Sampling a small volume of the ejected vasopressin into phosphate buffered saline solution to obtain the concentration profile as a function of time.

7.2.4. Hybrid techniques for modulating insect flight activity and longevity

- Flight power quantifications of the effectiveness of the chemicals via the angle measurements setup.
- Insertion of the electrical stimulation electrode while marinating minimized impairment of the central nerve system.
- Designing multi-output wireless transceivers to actuate multi-reservoir micro-fluidic drug delivery system.
- Eliminating the electrical cross-talk between electrical shocking mode and chemical ejection mode.
- Quantification of the moths' flying trajectory under VICON system without being affected by the local current in the room.

7.2.5. Optofluidic waveguides for reconfigurable photonic systems

- Minimizing the cross-talk between two on/off states that degrades the quality of switching performance.

7.3. Concluding Remarks

I believe my work has shown how microfluidics can be integrated with other two fields: biology and optics. Demonstration of the fusing a living system with an implanted microfluidics has shown a new way of the interfacing living creatures with MEMS based robotic control components. With regards to the optofluidics, I have presented how liquid based photonic components can be integrated into conventional optical components to form a reconfigurable photonics. In conclusion, the idea of combining microfluidics with other modalities enables to create novel tools to solve problems at the interface between life and physical sciences. My hope is that other researchers will adopt and expand this concept further into other areas to solve complex multidisciplinary problems.

REFERENCES

1. Santini, J.T., M.J. Cima, and R. Langer, *A controlled-release microchip.* Nature, 1999. **397**(6717): p. 335-338.